

# Development of an SDD-based Gamma Camera

Alberto Gola  
Politecnico di Milano

# Outline

## The Silicon Drift Detector

- Concept.
- Optimized structure.

## The SDD as a photodetector

- Signal Generation.
- Ballistic Deficit.
- $\text{LaBr}_3$  measurements.

## The SDD-based Anger Camera

- Dead areas.
- Energy Correction.
- Position reconstruction.
- Geometric correction.
- Optimal position reconstruction.

## Readout Electronics (hints)

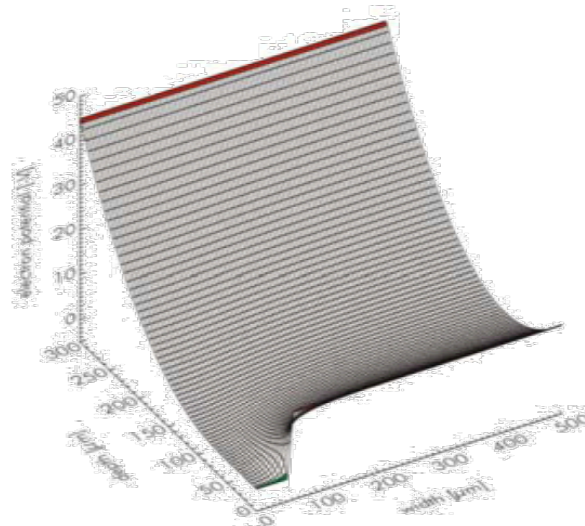
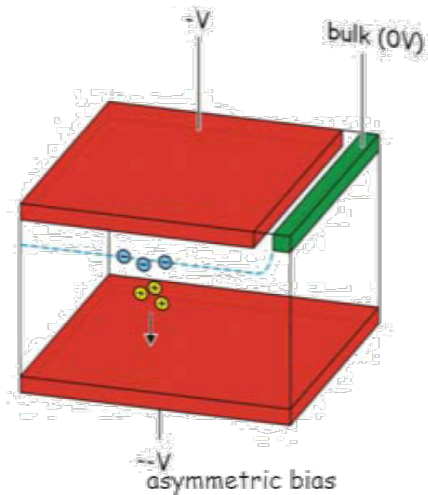
## Final Measurements

# The Silicon Drift Detector – SDD

The SDD was introduced in 1984 by E. Gatti and P. Rehak

→ improvement of detector performance – electronic noise (position sensitive).

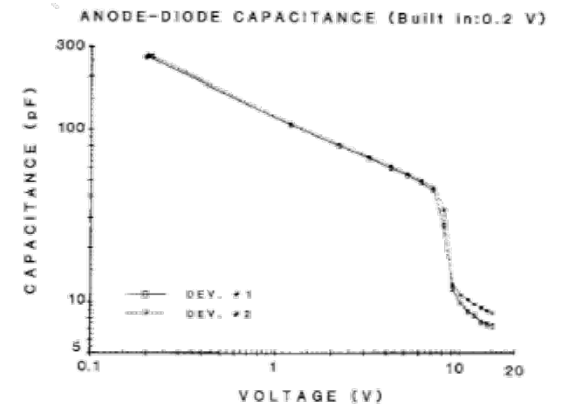
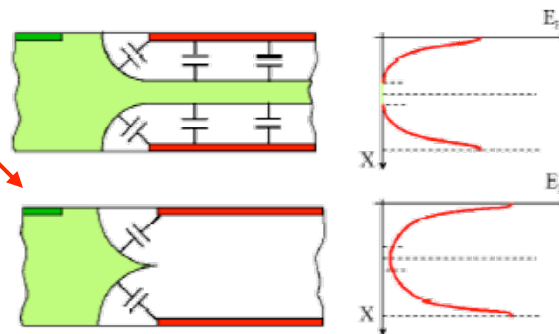
Based on the Sideward Depletion Structure:



E. Gatti and P. Rehak

Step decrease of the anode capacitance at full depletion

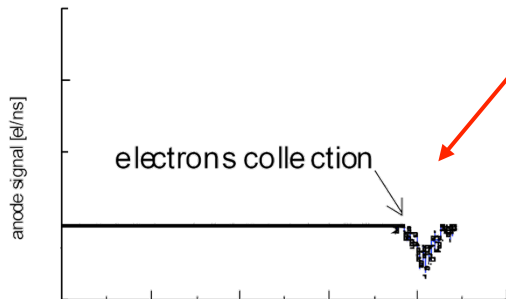
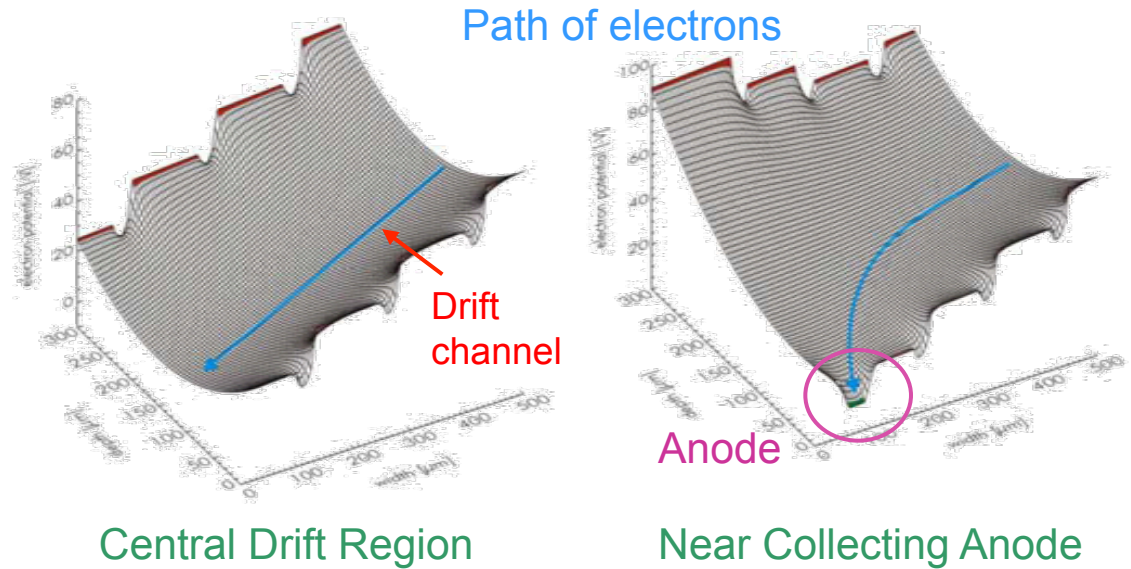
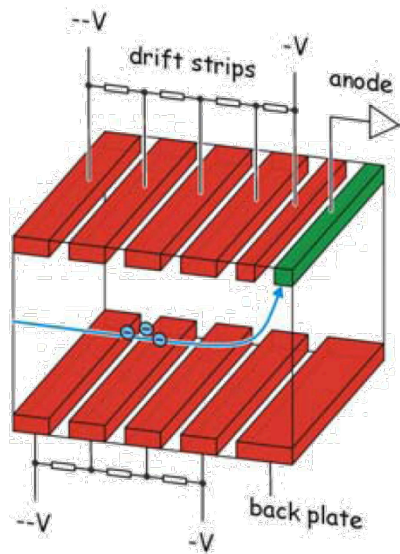
Small capacitance of readout anode, dependent on anode size and not on active area



# The Silicon Drift Detector – SDD

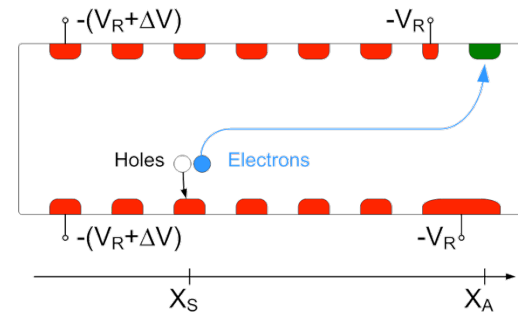
The charge is collected at the anode thanks to an electric field parallel to the surface, generated by p<sup>+</sup> strips with increasing potential on both sides.

The signal electrons are focused in the middle of the wafer, drift parallel to surface towards the anode.



Fast signal pulse, since the anode is shielded by the surrounding contacts, until the charge packet is in close proximity.

(see Ramo's Theorem – small pixel effect)

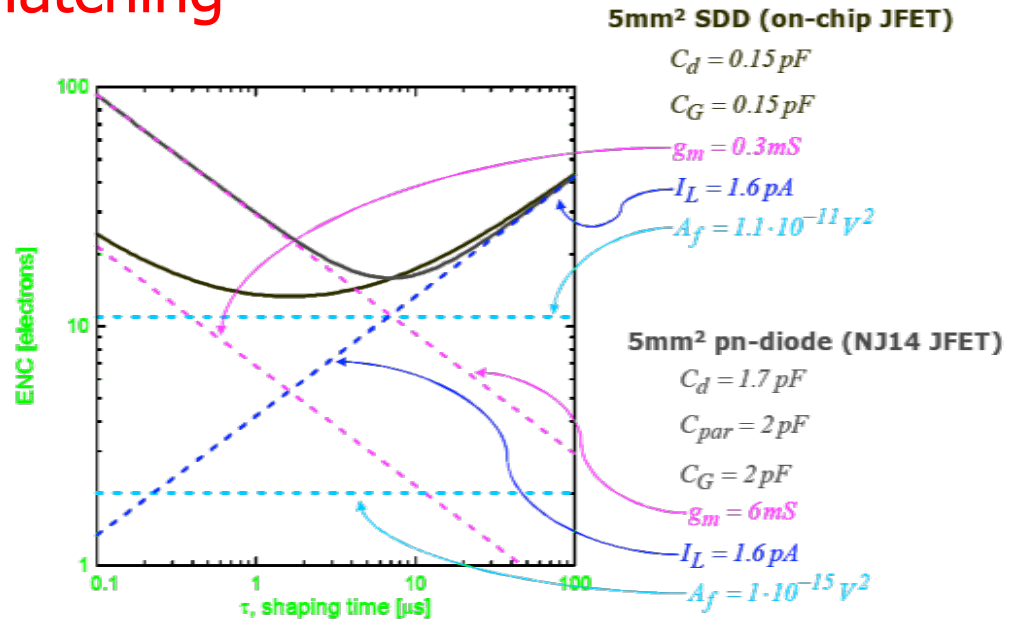
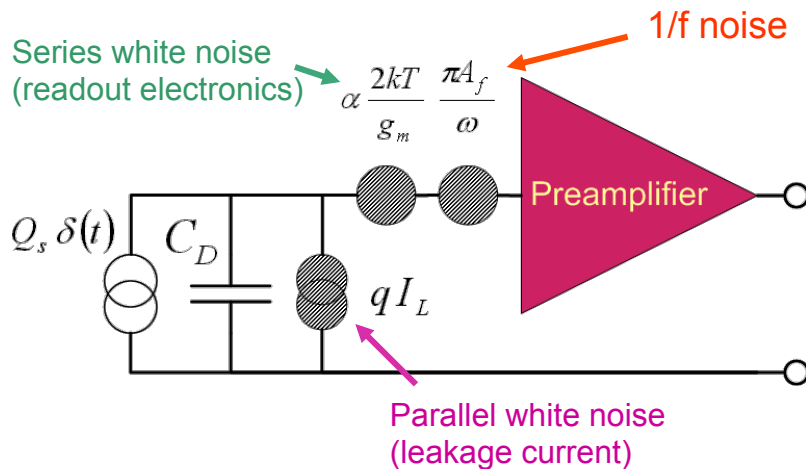


Drift Time

$$\tau_d = \frac{x_S - x_A}{\mu_e \frac{\Delta V}{L}}$$

# ENC and Capacitive Matching

Considering the Equivalent Noise Charge model, the reduction of the anode Capacitance allows a reduction of the optimal ENC, obtained at shorter shaping times.



Comparison of the ENC curve of a standard pn-diode and a SDD with the same active area.

$$ENC^2 = \underbrace{A_1 \frac{2kT\alpha}{\omega_t} C_D \left( \sqrt{\frac{C_G}{C_D}} + \sqrt{\frac{C_D}{C_G}} \right)^2 \frac{1}{\tau_s}}_{\text{Series noise}} + \underbrace{A_2 (\pi A_f) C_G C_D \left( \sqrt{\frac{C_G}{C_D}} + \sqrt{\frac{C_D}{C_G}} \right)^2}_{\text{1/f noise}} + \underbrace{A_3 (qI_L) \tau_s}_{\text{Parallel noise}}$$

$A_i \rightarrow$  coefficients related to the type of filtering done by the readout electronics.

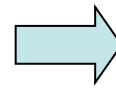
$\tau_s \rightarrow$  time constant proportional to the pulse response duration of the filter applied.

# SDD – Optimized structure

Considering the ENC equation, it is possible to optimize the size of the first transistor of the readout electronics, which is a design parameter.

$$ENC^2 = A_1 \frac{2kT\alpha}{\omega_t} C_D \left( \sqrt{\frac{C_G}{C_D}} + \sqrt{\frac{C_D}{C_G}} \right)^2 \frac{1}{\tau_s} + A_2 (\pi A_f) C_G C_D \left( \sqrt{\frac{C_G}{C_D}} + \sqrt{\frac{C_D}{C_G}} \right)^2 + A_3 (qI_L) \tau_s$$

Under the hypothesis of fixed current density in the first transistor, i.e. constant  $\omega_t$ , the ENC is minimized by the capacitive matching condition.

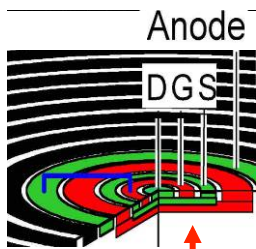


$$C_G = C_D$$

If MOS:

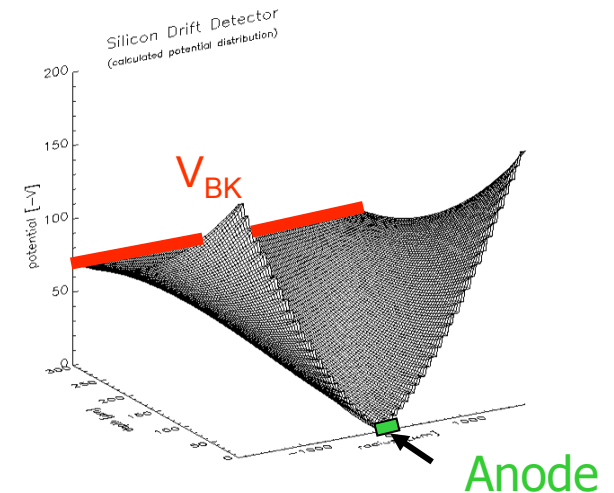
$$W_{opt} = \frac{C_{Det}}{C_{ox}L}$$

Optimized SDD structure:



The on-chip integration of the first transistor allows an effective capacitive matching and the reduction of connection capacitance.

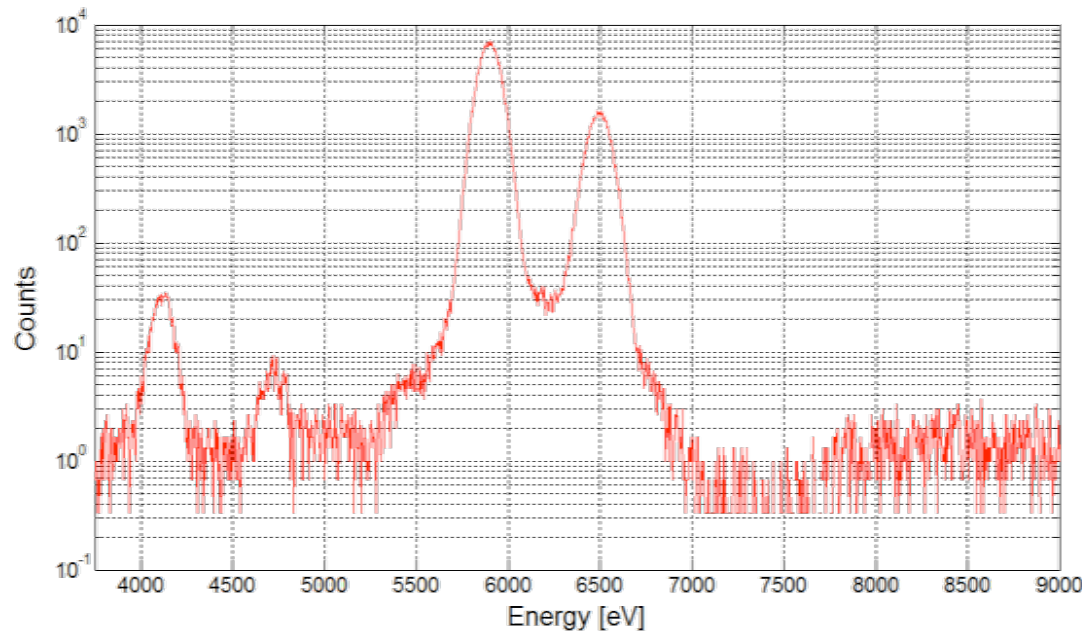
Uniform entrance window for efficient detection of low-energy photons – visible light → soft X-rays



$$\tau_d^{\max} \propto \frac{A}{\mu_e V_{DEP}}$$

# SDD – X-ray spectroscopy performance

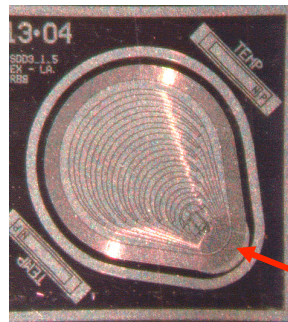
The SDD offers very good spectroscopic performance at near room temperature.



<sup>55</sup>Fe X-ray spectrum, recorded with a SDD droplet at -10°C.

Further optimization: SDD droplet, with a modified geometry.

- Further reduction of anode capacitance.
- Easier shielding of integrated transistor for improved Peak/Background.



Anode + First FET

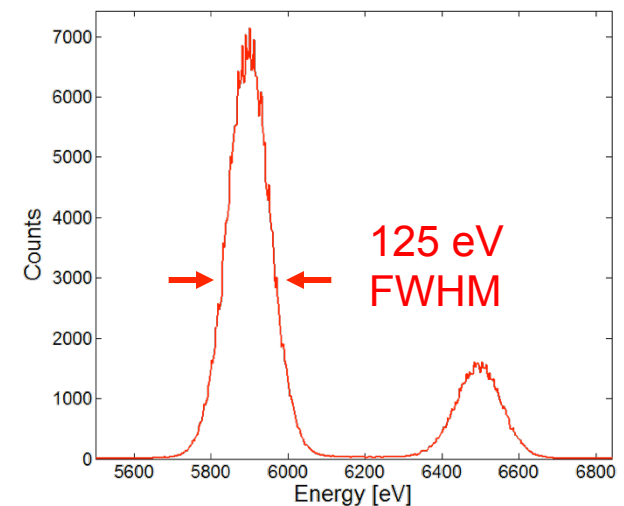
Energy resolution  $\Delta E_{FWHM} = 125 \text{ eV}$   
(equivalent to  $ENC = 4 \text{ e}^- \text{ r.m.s.}$ ).

Count rate up to  $10^6 \text{ cps}$ , thanks to the short optimum shaping time.

Peak/Background  $\sim 10.000 : 1$ .

Quantum Efficiency:  $> 90\%$  @ 0.3-10 keV

Operating Temperature =  $-10^\circ\text{C}$



Same <sup>55</sup>Fe X-ray spectrum, in linear scale.

# SDD as a photodetector

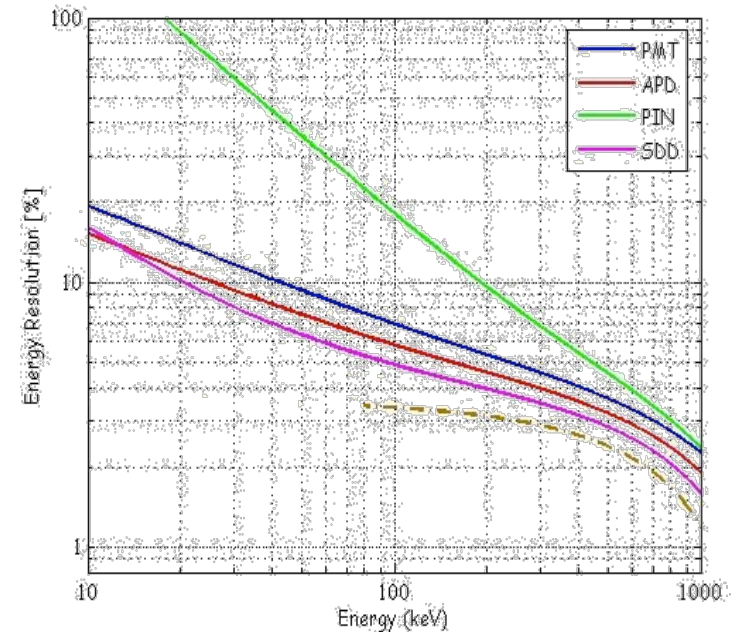
Considering its good noise properties, is it possible to use the SDD as the photodetector in indirect-conversion measurements of Gamma-ray with a scintillator crystal?

Possible advantages, over the reference detector for scintillation light readout, which is the PMT:

- Better energy resolution.
- Solid state: compactness, ruggedness, (cost)
- Lower bias voltage, Less sensitivity to bias and temperature variations.
- Reduced sensitivity to magnetic fields → Integration with MRI.

$$\frac{\Delta E}{E} = 2.35 \sqrt{\underbrace{\frac{ENC^2}{(QE N_{ph})^2 M^2}}_{\text{Electronic noise}} + \underbrace{\frac{\alpha}{QE N_{ph}}}_{\text{Light Statistic}} + \underbrace{\left(\frac{\Delta E}{E}\right)_{np,inh}^2}_{\text{Intrinsic (crystal)}}$$

	PMT	PIN	APD	SDD
QE	30%	80%	80%	80%
$\alpha$	1.25	1	2	1
M	$10^5$	1	200	1
ENC/M	$\sim 0$	370	20	25

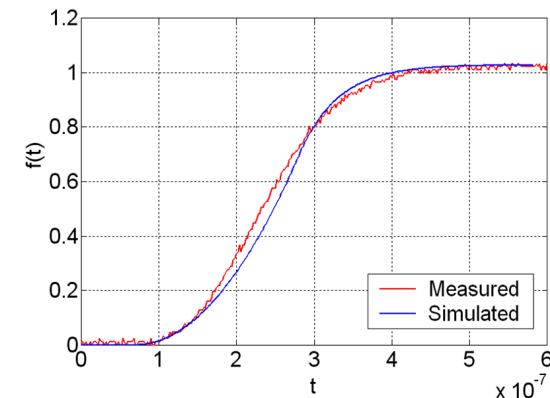
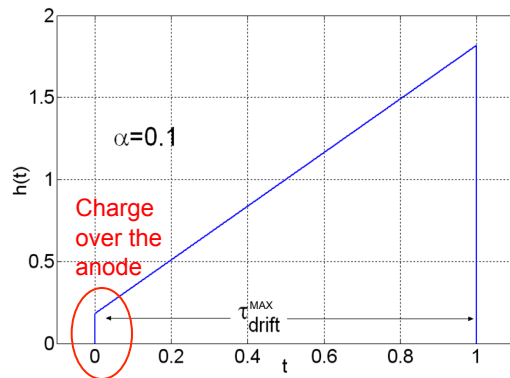
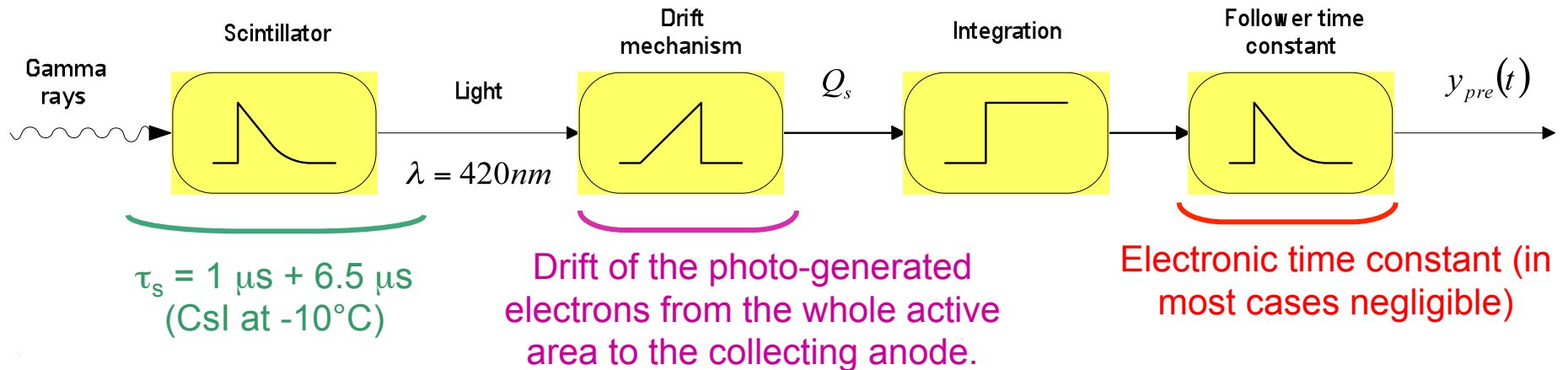


Data collected in 2006:

- PMT model R960 from Hamamatsu Corporation
  - Standard PIN from Scionix Scintillation Detectors
  - Large-Area APD developed by Advanced Photonics, Inc.
  - Large-Area SDD developed by MPI, PNSensor, POLIMI-INFN
- Both PMT and SDD technologies have improved.

# SDD as a photodetector

In order to use the SDD as a photodetector, however, we must consider carefully the signal shape, when coupled to a scintillator.



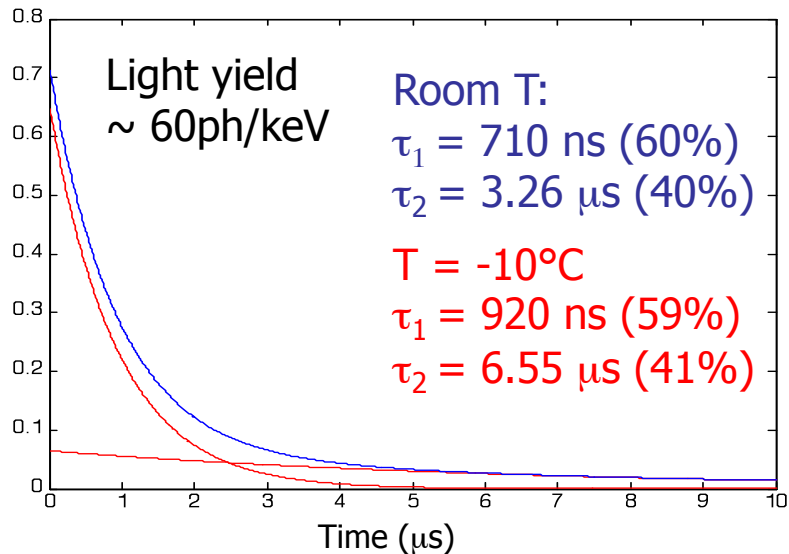
In the case of a circular SDD, the charge collected at the anode increases linearly with time, since it comes from rings with increasing radius.

The anode current is modeled with a ramp starting from a non-zero value, due to the charge generated above the First FET and the anode region.

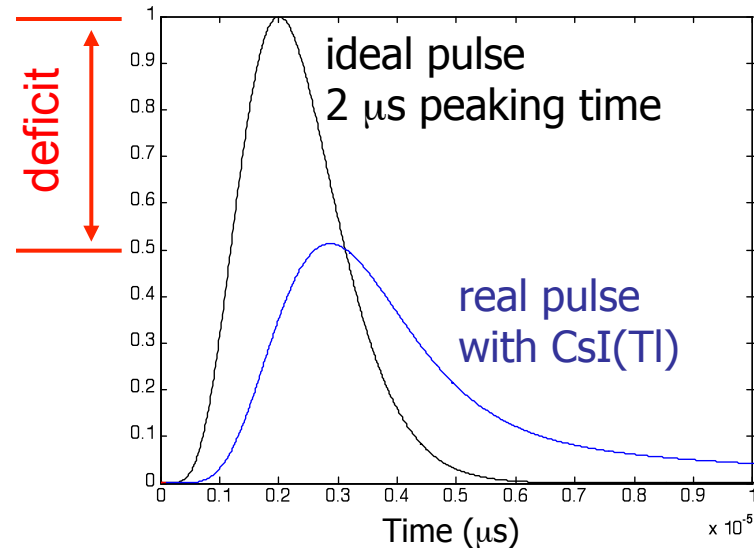
Good agreement with the simulated data from the model and the measured data, obtained illuminating the entrance window of a  $5 \text{ mm}^2$  SDD with a pulsed laser source.

# Ballistic Deficit - Scintillator

The first reason for the ballistic deficit is the scintillation time constant: the output waveform is the convolution between the pulse response of the scintillator and of the shaping amplifier.



The CsI(Tl) has two emission time constants, which become longer for colder operating temperatures.

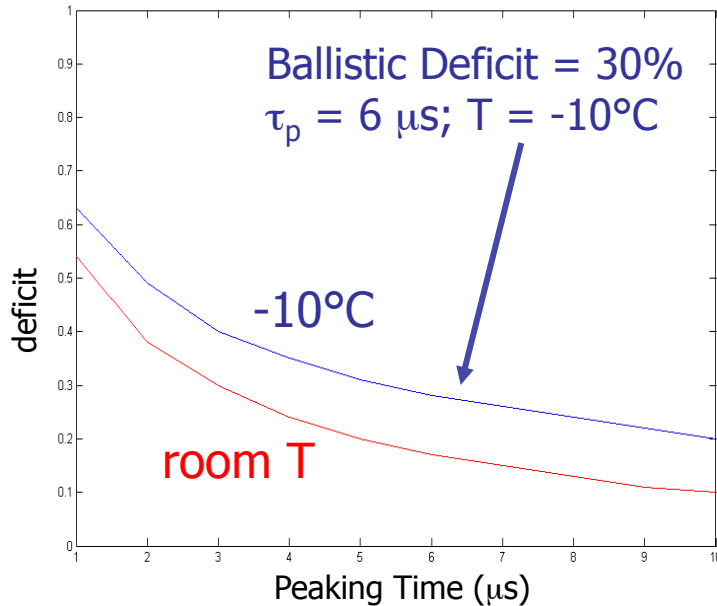


Comparison of the pulse response of the system in the case of an infinitely fast scintillator and a real one, with a 6<sup>th</sup> order shaping amplifier.

As a result, the signal amplitude is attenuated. The noise, however is not affected by this process and keeps its amplitude, so that the SNR is degraded. The phenomenon can be seen, alternatively, as an increase of the effective ENC.

$$ENC_{eff} = \frac{ENC}{(1 - deficit)}$$

# Ballistic Deficit - Scintillator

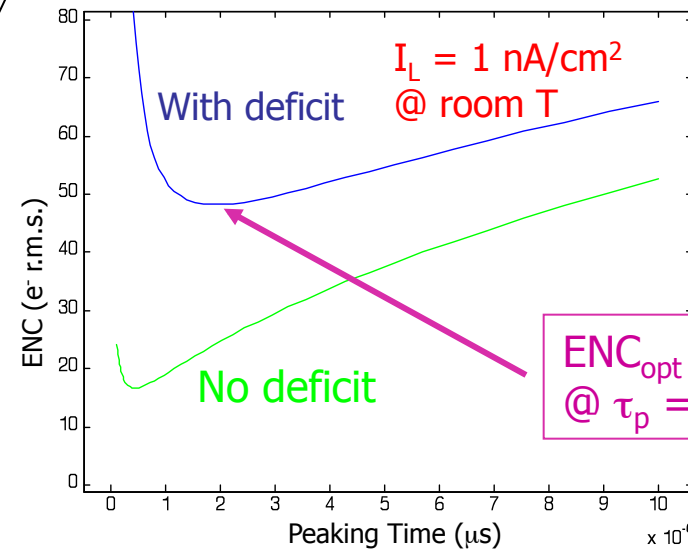
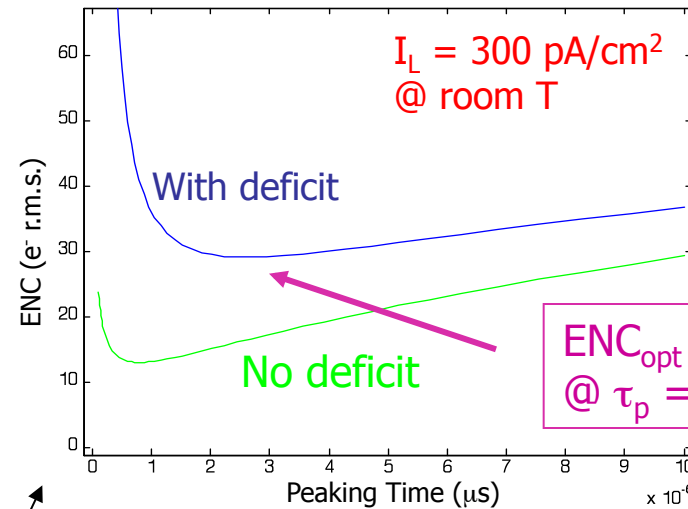


Simulation of the Ballistic Deficit due to the CsI scintillator with a 6<sup>th</sup> order, complex-poles shaping amplifier at two different temperatures.

Simulation of the effective ENC at -10°C for a 1 cm<sup>2</sup> SDD coupled to the CsI, for two different values of the leakage current → process related.

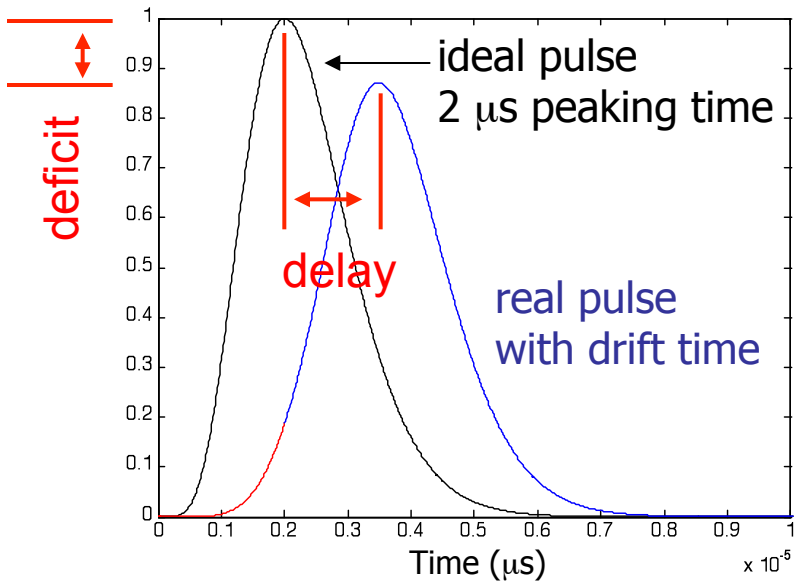


- Reducing the operating temperature would reduce the leakage exponentially but would also increase deficit, forcing the use of longer shaping times.
- Cooling limited due to practical limits of the Peltier cooling.

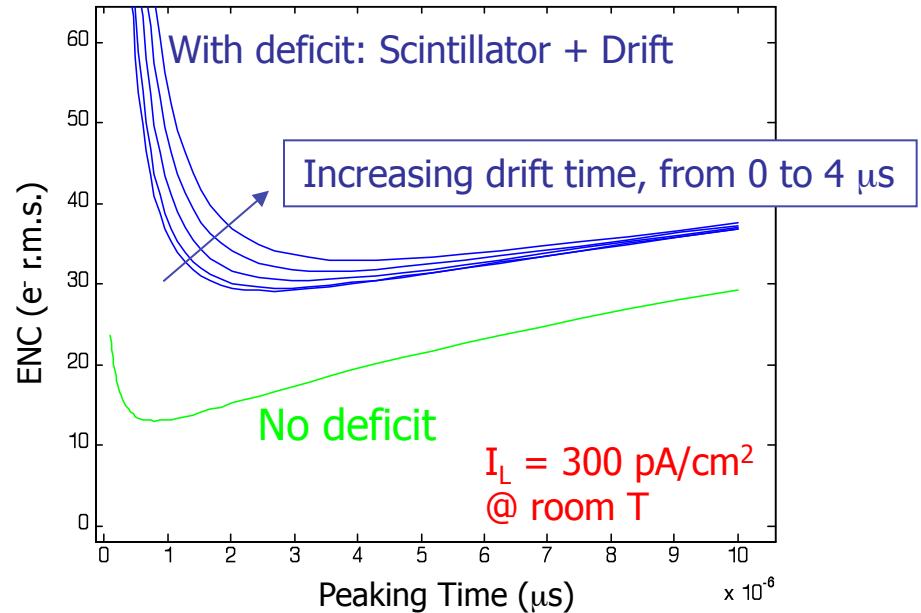


# Ballistic Deficit – Drift Time

In addition to the scintillation time constant, which is common to all photodetectors, the SDD adds also the Drift time constant.



Simulation of the Ballistic Deficit due to the SDD drift time with a 6<sup>th</sup> order, complex-poles shaping amplifier at two different temperatures.



Simulation of the effective ENC at -10°C for a 1 cm<sup>2</sup> SDD coupled to the CsI, for different values of the drift time, which is also dependent on the operating temperature..

$$\tau_d^{\max} \propto \frac{A}{\mu_e V_{DEP}}$$

**SDD**

Summing up, it is increasingly more difficult to achieve good electronic noise with increasing active areas, because both  $I_L$  and  $\tau_d$  increase proportionally to  $A$ .  
 On the other hand, bigger active area are needed for systems of practical use → astrophysics, medical imaging..

# LaBr<sub>3</sub> Scintillator

The reason of the large ENC loss with the CsI(Tl) scintillator is that the SDD optimum shaping time is short, thanks to the reduced series noise because of the small anode capacitance.

→ In order to fully exploit the good noise performances of the SDD a faster scintillator is needed, of course with the same high light yield as the CsI(Tl).

→ LaBr<sub>3</sub>(Ce) scintillator.

Pros of the LaBr<sub>3</sub>:

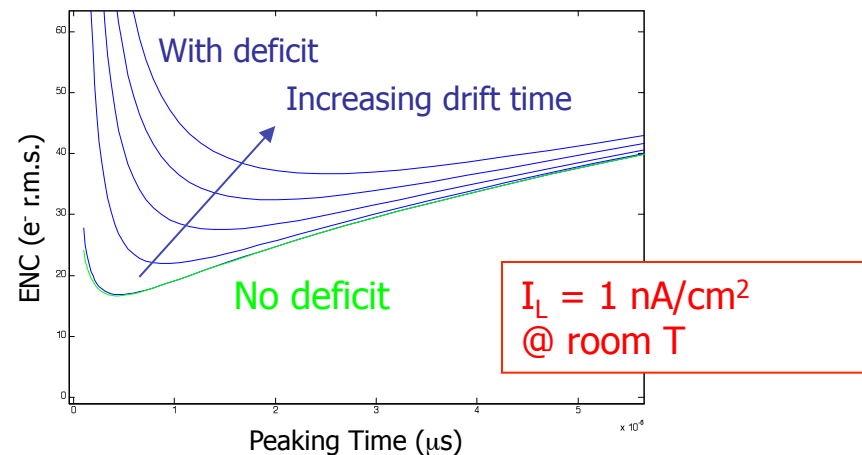
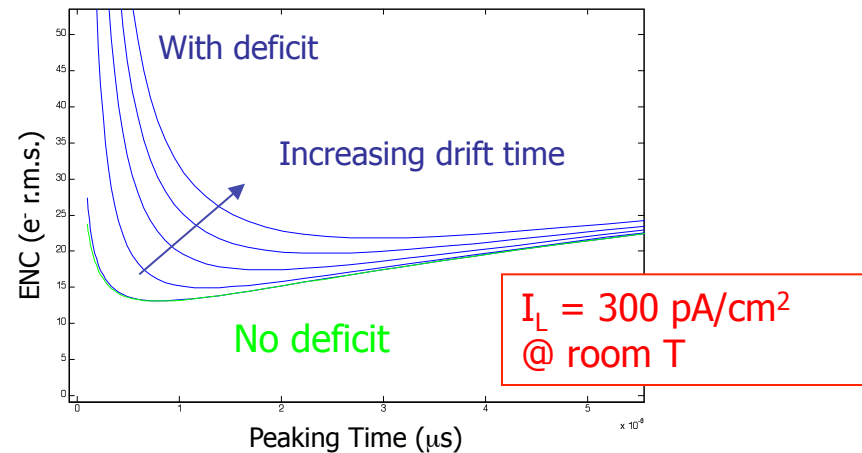
- Short decay time
- A shorter shaping time is better also for higher rate applications.
- High light yield
- High proportionality → reduced intrinsic component of the energy resolution.

Cons:

- hygroscopic → sealing necessary
- shorter emission wavelength → new ARCs may be necessary
- More expensive and difficult to obtain in larger sizes (needed e.g. for Gamma Cameras)

The benefits are more important with higher leakage currents:

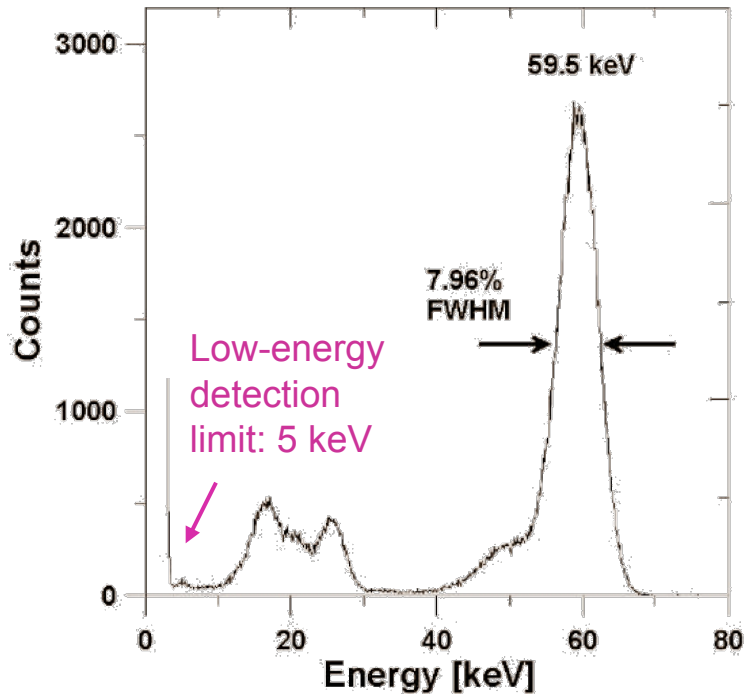
- “looser” requirements on the detector technology
- Higher operation temperature possible.





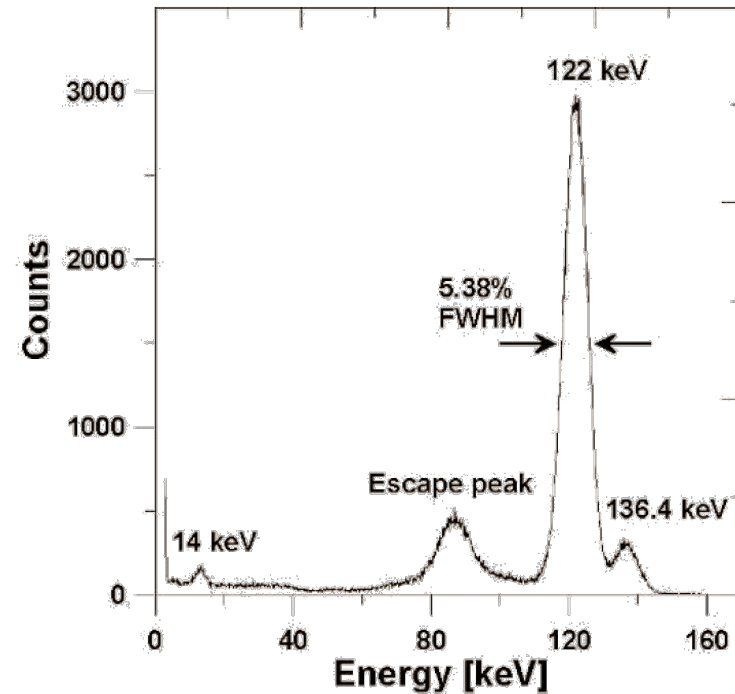
# LaBr<sub>3</sub> Spectroscopy Measurements

At lower Gamma-ray energies, there is an important contribution of the electronic noise of the SDD, consequently a moderate cooling is necessary → Peltier cooling at 0 °C.



<sup>241</sup>Am spectrum

For comparison, a PMT with QE = 30% and the same crystal would have measured a resolution of 11.4% FWHM (simulated).



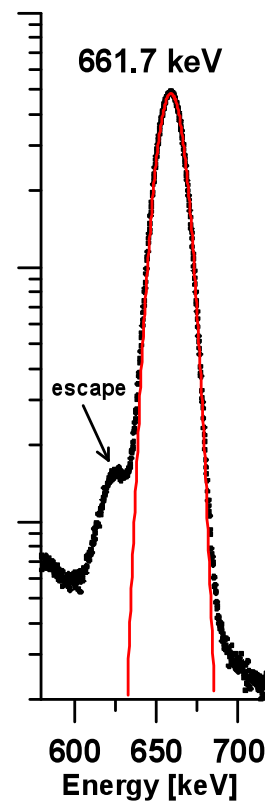
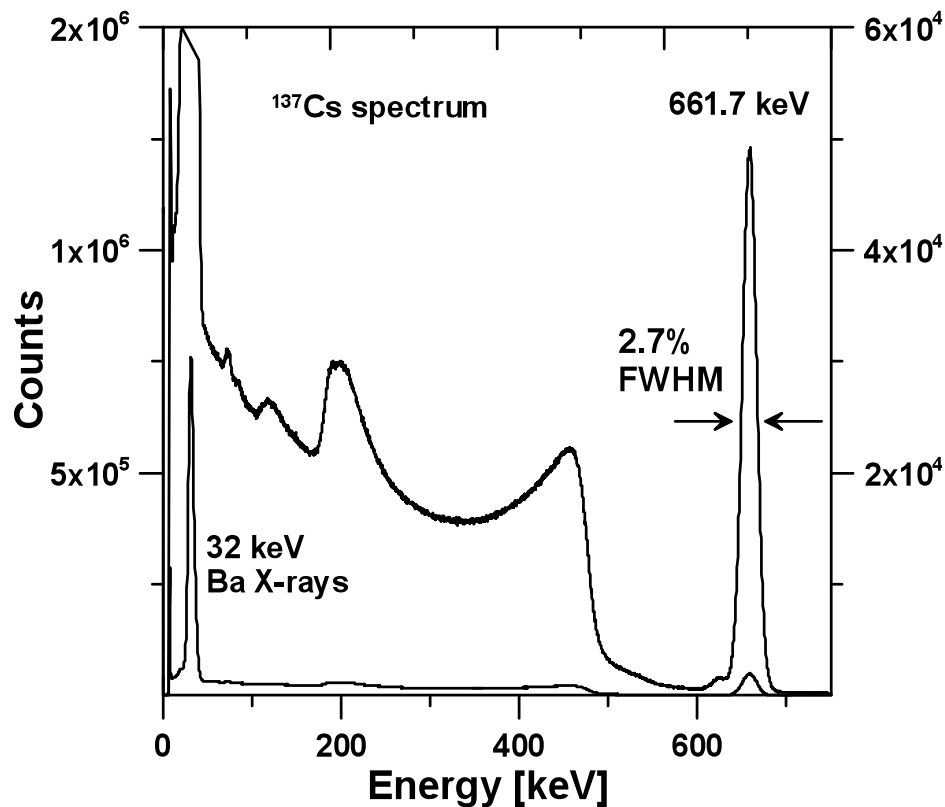
<sup>57</sup>Co spectrum

For comparison, a PMT with QE = 30% and the same crystal would have measured a resolution of 6.6% FWHM (simulated).

# LaBr<sub>3</sub> Spectroscopy Measurements

At higher energies the electronic noise contribution is negligible and we can work at room T.

On the other hand the intrinsic term due to the crystal becomes dominant and the measured energy resolution is heavily affected by the quality of the crystal under test.



The simulated energy resolution with a PMT is 3% FWHM



The effect of the choice of the detector on the measured energy resolution is almost negligible.

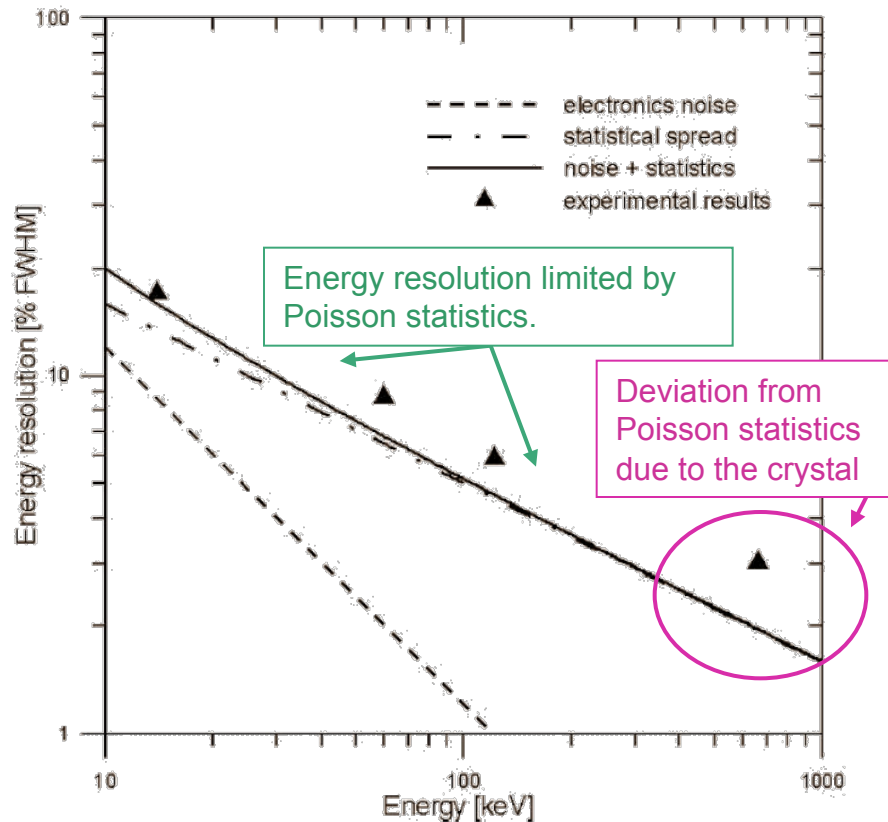
However, a solid state detector like the SDD has a number of practical advantages over a PMT. Moreover, with respect to a solid state device with internal gain, it is much less sensitive to bias voltage variations.

<sup>137</sup>Cs spectrum

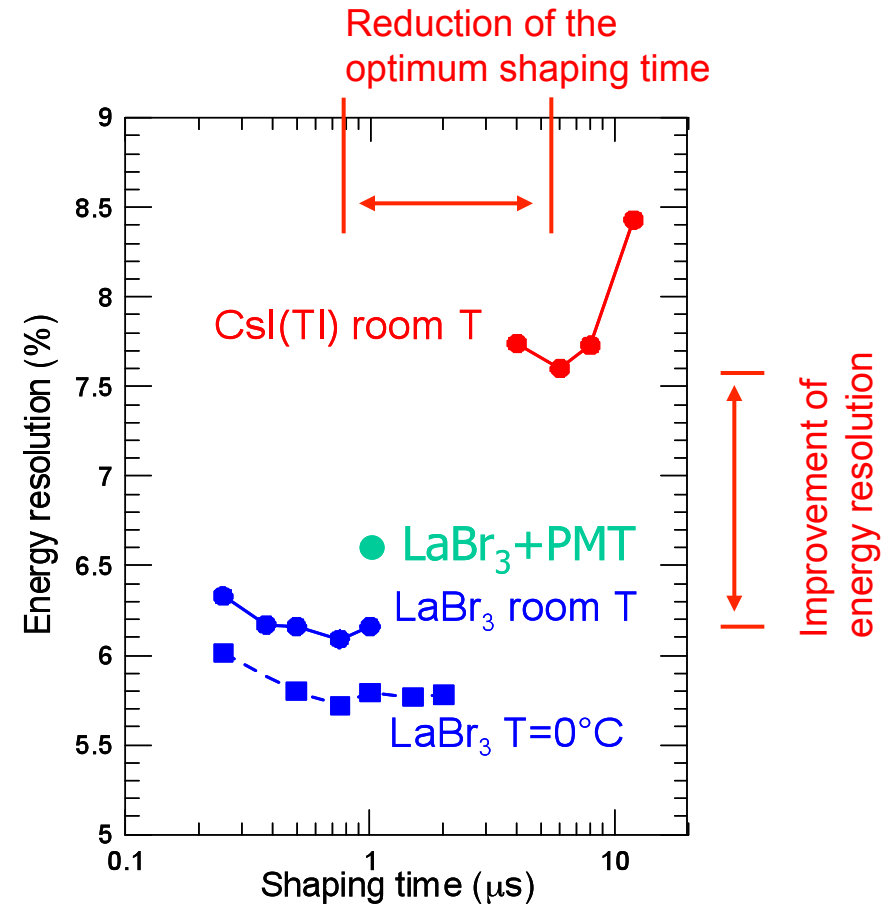
# LaBr<sub>3</sub> Spectroscopy Measurements

Plotting the measured energy resolution vs. the Gama-ray energies we can see that, in the energy range of interest, the SDD acts as an almost noiseless detector (electronic noise).

The statistical term is dominant, but is reduced thanks to a high (very high) QE.



Measured and fitted energy resolution vs. energy for the SDD. The intrinsic term, prevailing at higher energies is not considered.

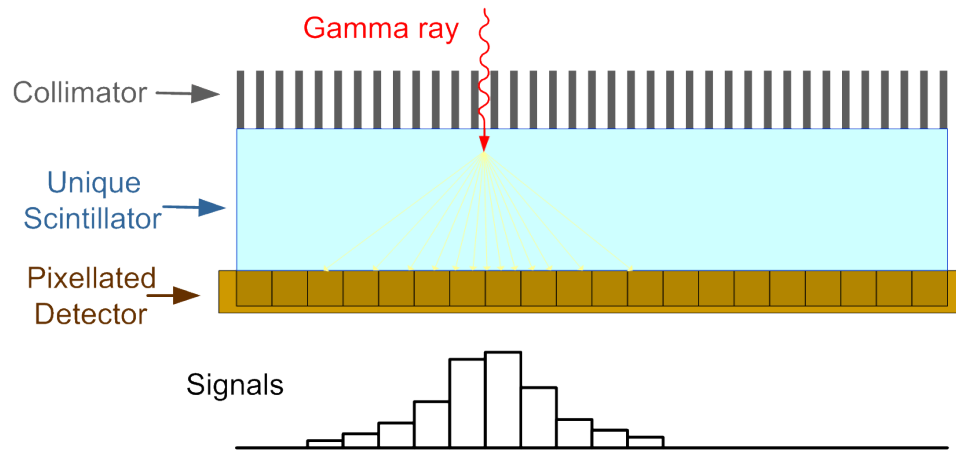


Measured energy resolution vs. shaping time for <sup>57</sup>Co.

# Gamma Camera

Considering the good characteristics of the SDD as a photodetector in the scintillation light readout, the following step is using an array of SDDs for the readout of a Gamma Camera.

→ The position resolution is heavily affected by the precision of the charge (photon) measurement in every pixel of the array.

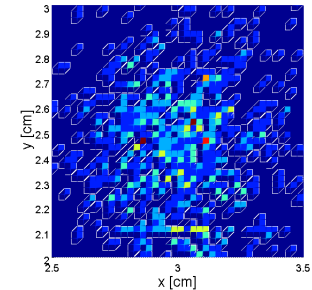


We can say that the final goal of an SDD-based Gamma Camera is to build an imager, whose spatial resolution is affected only by light distribution statistics.

- Lower statistical spread of the light induced signals (high QE, no multiplication)
- Noise spread lower than light statistical spread → to be confirmed, since the signal in every pixel is smaller, due to light sharing.

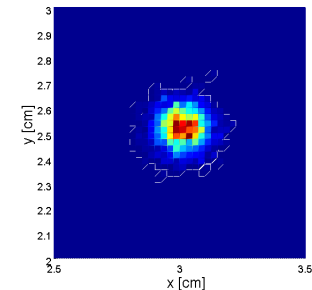
## PIN diode

- Very high electronic noise
- Good QE



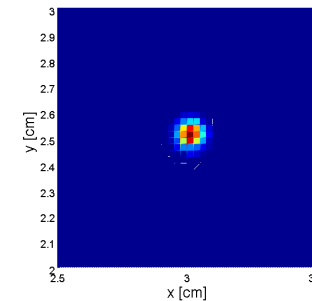
## PMT

- No electronic noise
- Low QE (30% in the simulation)



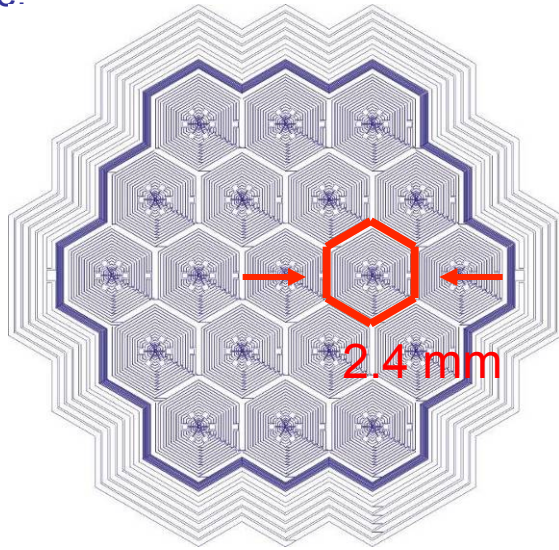
## SDD

- Good QE
- Negligible (??) electronic noise.



# Gamma Camera - Prototype

The study of an SDD-based Gamma Camera was motivated by the good results obtained with a first, small prototype.



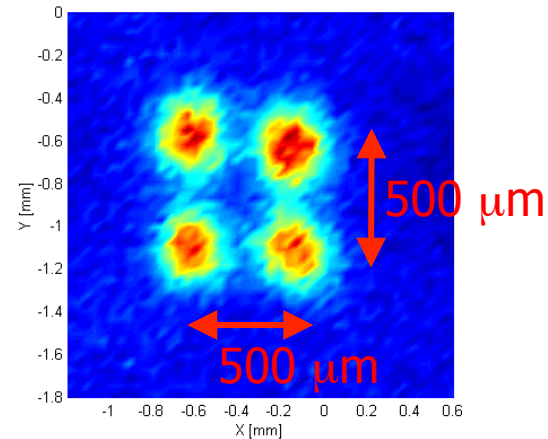
Monolithic SDD array with 19 elements:  
Total active area =  $5 \text{ mm}^2 \times 19 \sim 1 \text{ cm}^2$

CsI(Tl) scintillator: thickness = 3 mm

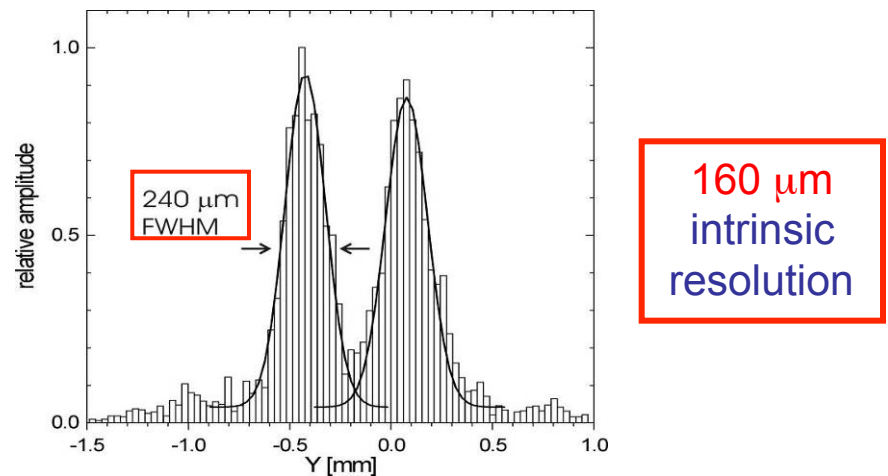
Operating temperature =  $-10^\circ\text{C}$

Collimator hole:  $\varnothing 180 \mu\text{m}$ .

Gamma-ray energy = 122 KeV –  $^{57}\text{Co}$ .



$^{57}\text{Co}$  image, taken through a collimator.



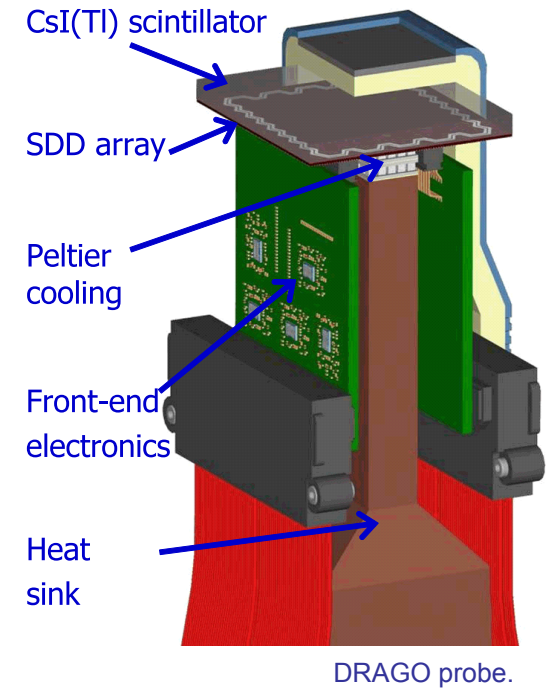
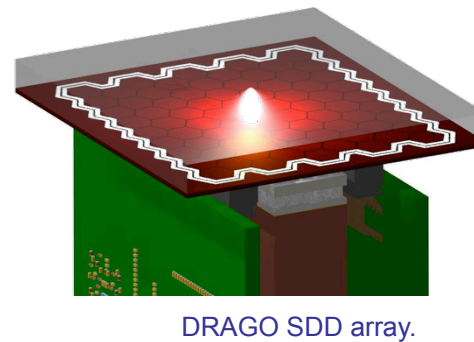
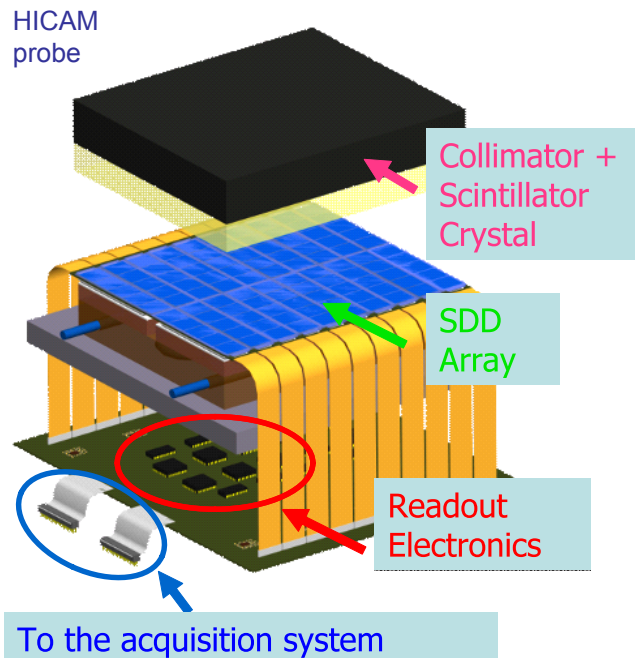
Fitting of the spatial resolution of the system.

# Gamma Camera – Projects

Two different projects have been carried out, focusing on SDD-based Gamma Cameras.

DRAGO project:

- Based on a monolithic array of 77 SDDs, arranged in a honeycomb configuration.
- Total active area: 6.7 cm<sup>2</sup>.
- CsI(Tl) scintillator.
- VLSI readout electronic placed inside the imaging probe.
- Possible applications in preclinical imaging but also for intra-operative probes.

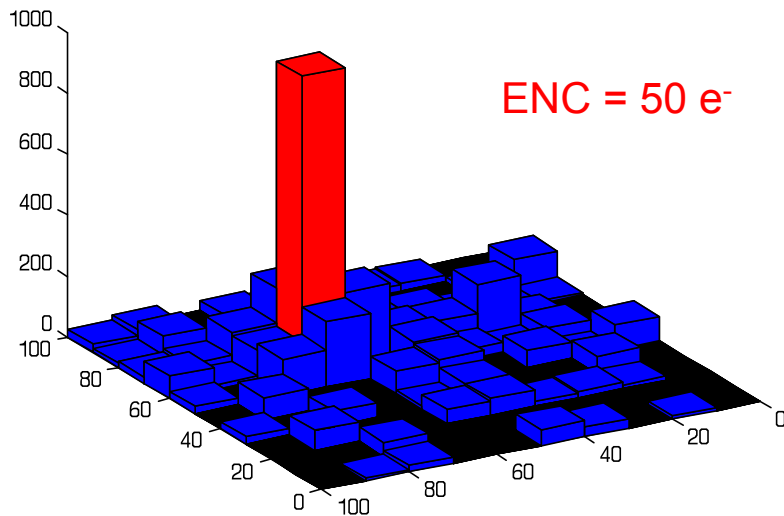
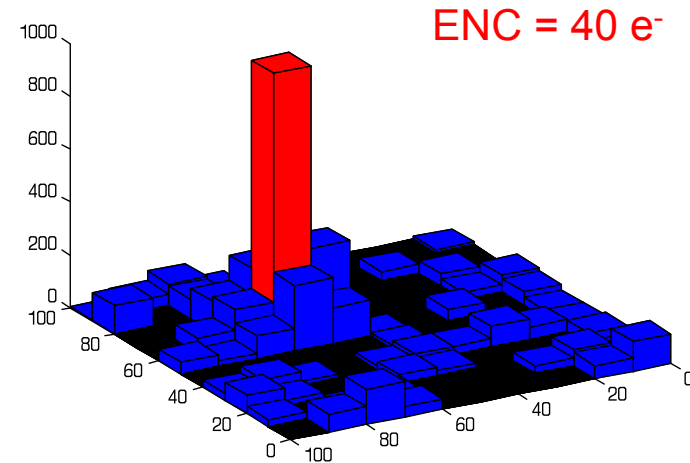
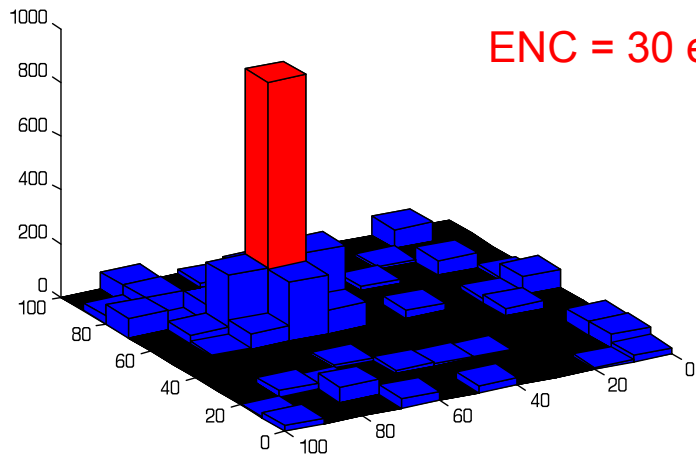


HICAM project:

- Based on several linear arrays of 5 SDDs.
- Total active area: 5x5 cm<sup>2</sup> and 10x10 cm<sup>2</sup>.
- CsI(Tl) scintillator – LaBr<sub>3</sub>(Ce) is an option.
- VLSI readout electronic placed inside the imaging probe.
- Application in preclinical imaging and Human imaging. Tomography.
- Integration with MRI.

# Signal Distribution

Monte Carlo simulation of the response of the signals coming from a Gamma Camera, considering also the electronic noise. The Gamma-ray source is the  $^{99m}\text{Tc}$ .



In order to avoid noise triggering it is desirable to set a relatively high threshold → risk of losing signals from the peripheral detectors hit by the Gamma event.



It is possible to use a system trigger, with a very high threshold: when at least one channel is over threshold, all the channels with a signal are acquired.

→ ASIC implementation

# Energy measurement – Dead Areas

Under the hypothesis of statistical noise only (or dominant statistical noise), the optimal filtering for amplitude measurements is the simple sum of the signals collected by the pixels.

The pixels below a certain threshold, however, are excluded from the sum to avoid the addition of unneeded electronic noise.

$$N_{ph} = k \sum_{V_i > th} V_i$$

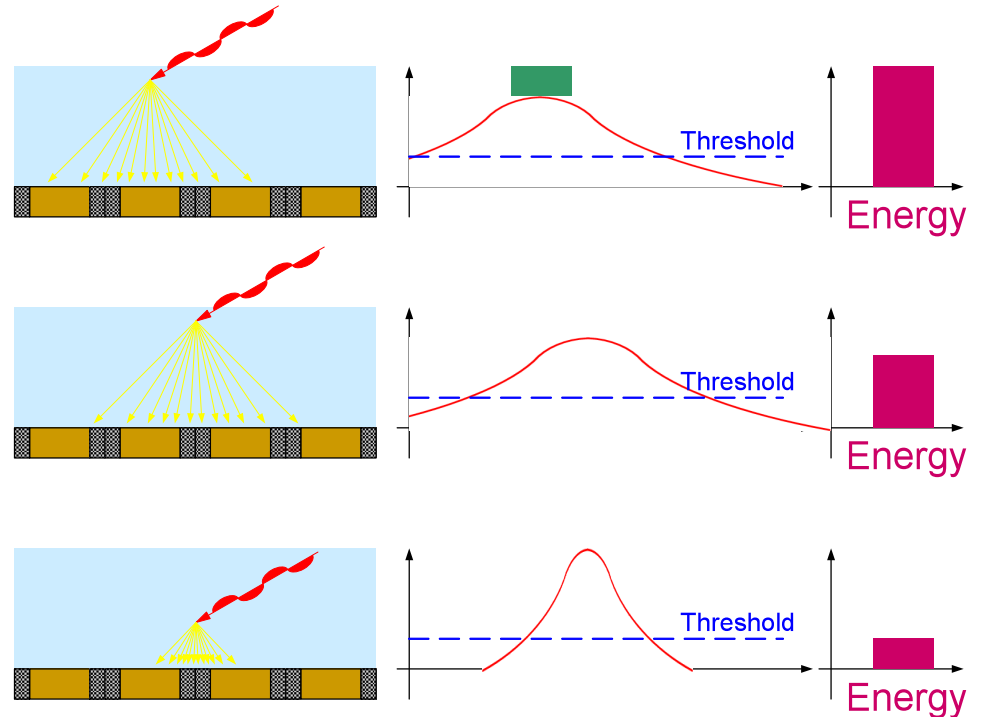
When we consider a real system with dead areas between the detectors, the amount of collected light changes due to:

- The solid angle of the dead areas with respect to the interaction point of the impinging photon.
- The total reflection angle of the ARC –  $\theta_c$ .
- The value of the analog thresholds.



There is a position-dependent signal loss:

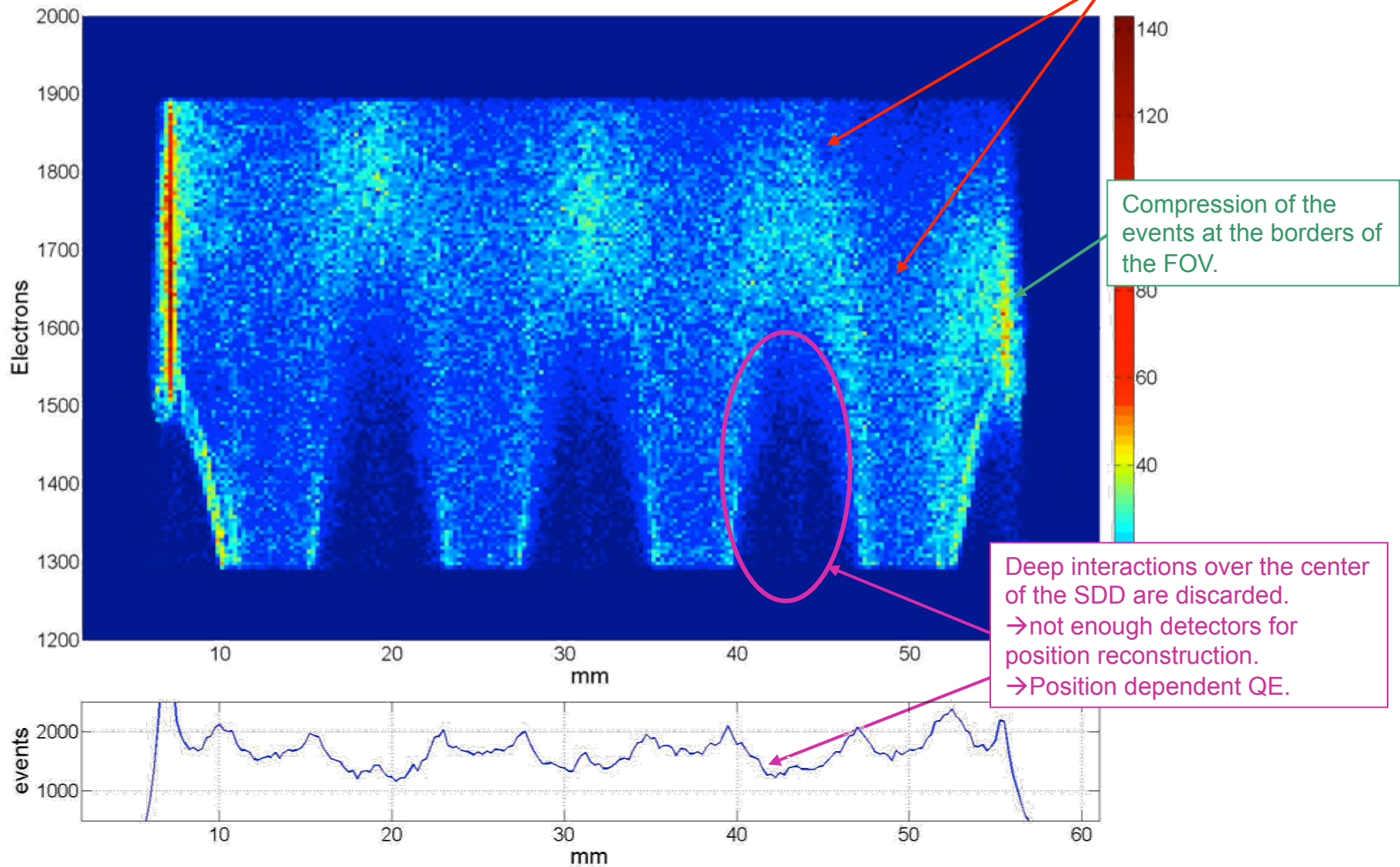
- xy position
- Depth of Interaction



Moreover, in a real system, there are a number of post-processing conditions set to discard noise, interference and generally “bad” events.

→ Position dependent Quantum Efficiency.

# Energy measurement – Dead Areas

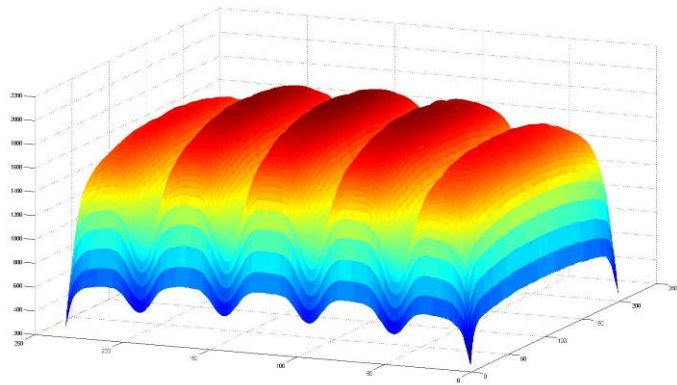


Fermilab – March 25<sup>th</sup>-26<sup>th</sup>, 2010

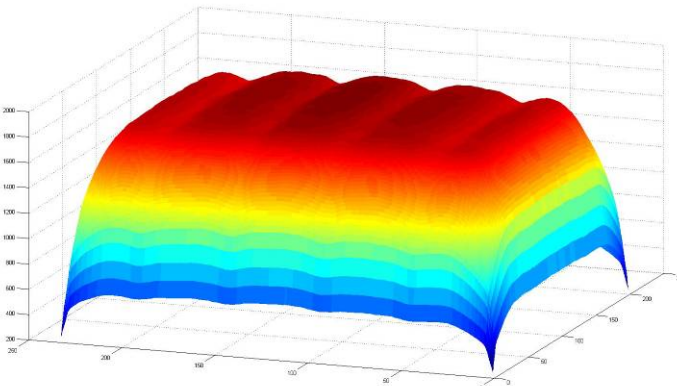
Alberto Gola  
Politecnico di Milano

# Energy measurement – Detector response

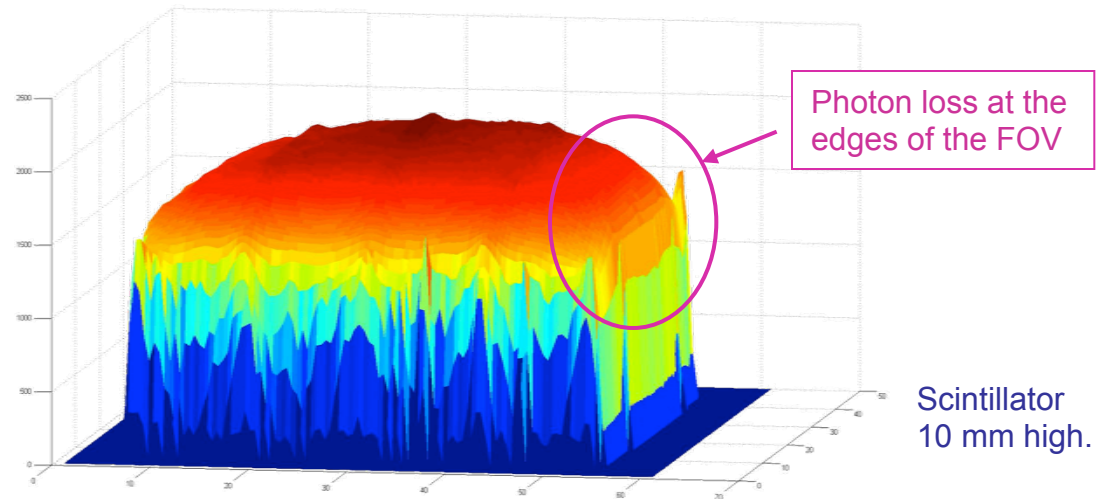
Simulated and measured energy response of a Gamma Camera with dead areas, composed of 5 linear arrays of 5x1 square SDDs, coupled to a 7 and 10 mm high scintillator (SCIDRA custom Monte Carlo code).



Photon interacting at  $h = 2$  mm from photodetector surface. Scintillator 7 mm high.



Photon interacting at  $h = 6$  mm from photodetector surface. Scintillator 7 mm high.



The measured energy response vs. position of interaction can only be averaged over  $z$ , if the position is in the  $xy$  plane.

It can be used for calibrating the energy response of the system.

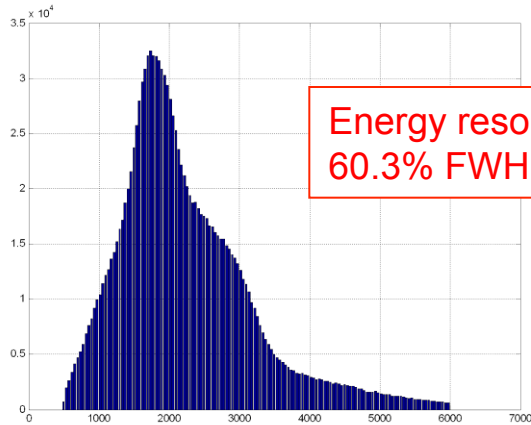
The problem can be mitigated using a thickness of the scintillator dependent of the Gamma-ray energy, because interactions at higher  $z$  feel less the effect of the dead areas, however:

- Tradeoff with position resolution
- Summing signals from more SDDs means more electronic noise is added.

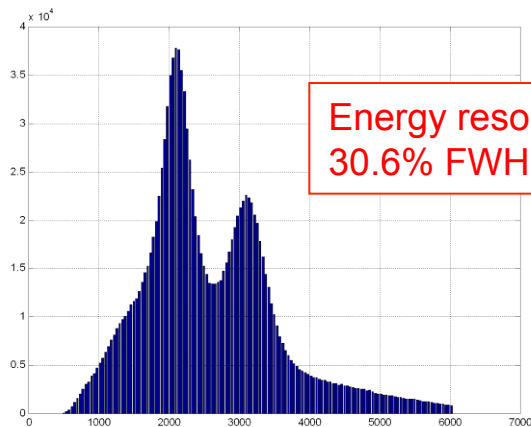
# Energy measurement – Double peak correction

If two Gamma-ray emission lines are available, it is possible to do a full Gain/Offset calibration, pixel-wise.

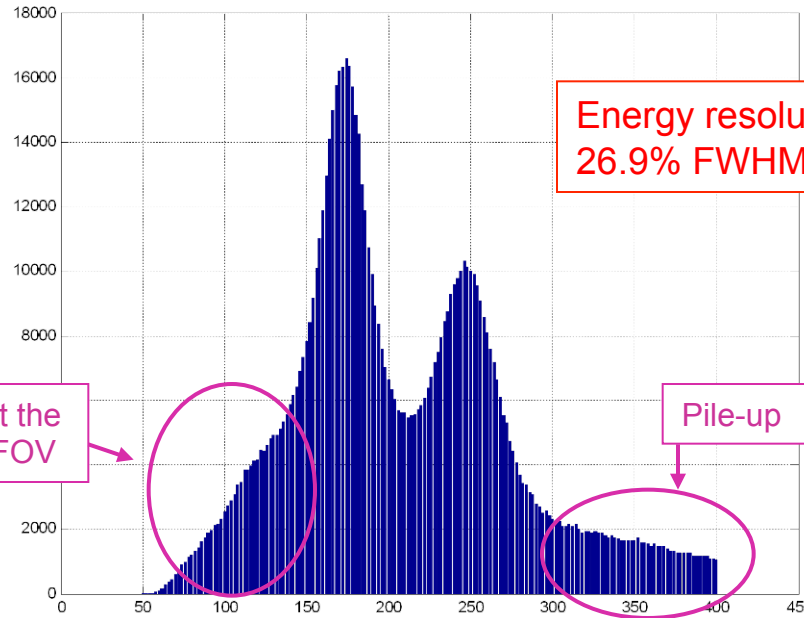
- $^{111}\text{In}$  is a good option, since it is also widely used in pre-clinical imaging, e.g. cell labeling.



Energy not corrected.



Single peak correction.

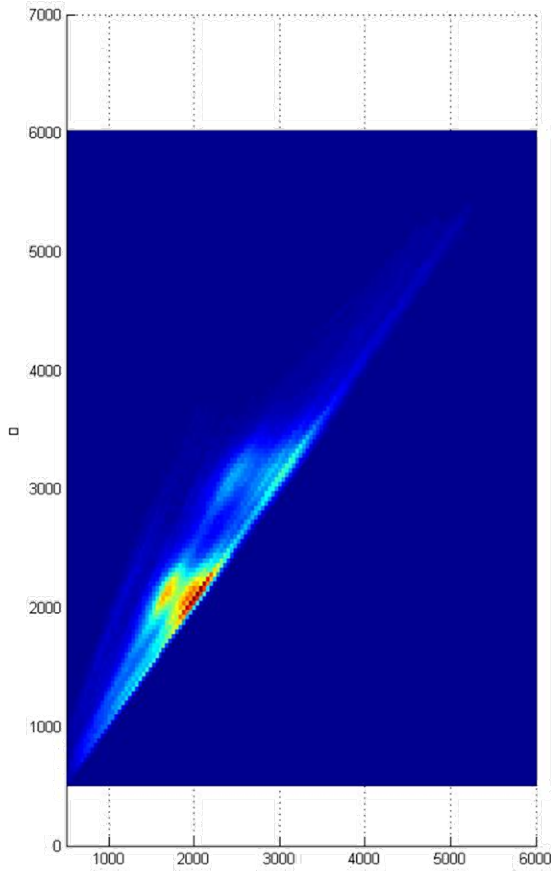


Double peak correction.

The data shown are obtained from a flood image, i.e. without collimator, and summing the energy spectra at every reconstructed position.

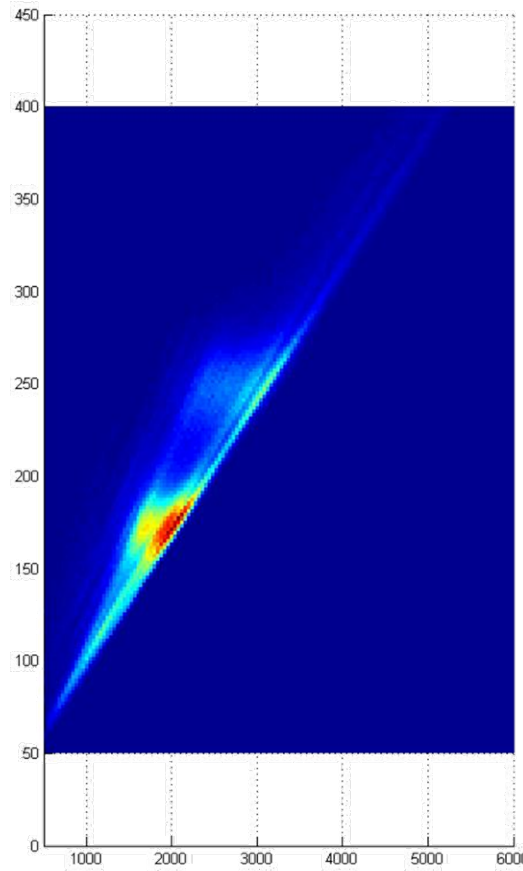
# Energy measurement – Double peak correction

Scatter plot, for the comparison of the single and double peak correction.



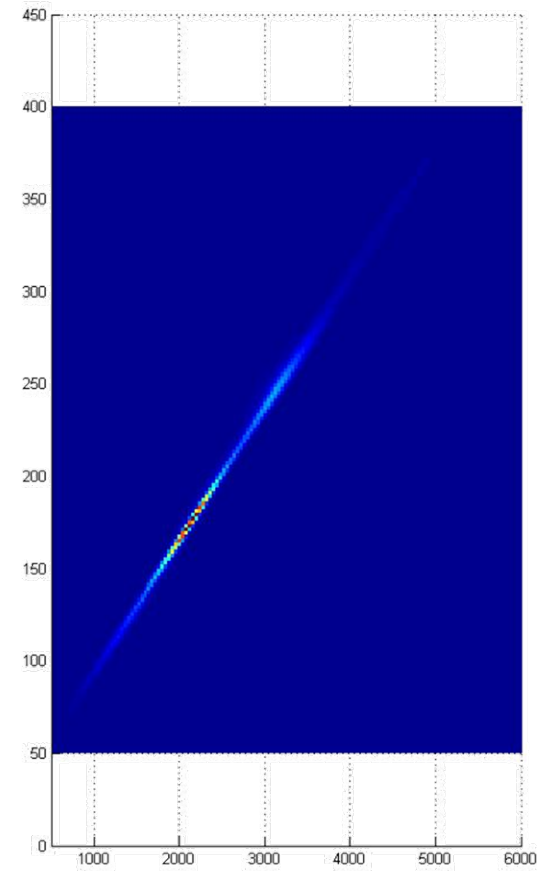
Single peak correction

ADC channels vs. Corrected channels



Double peak correction

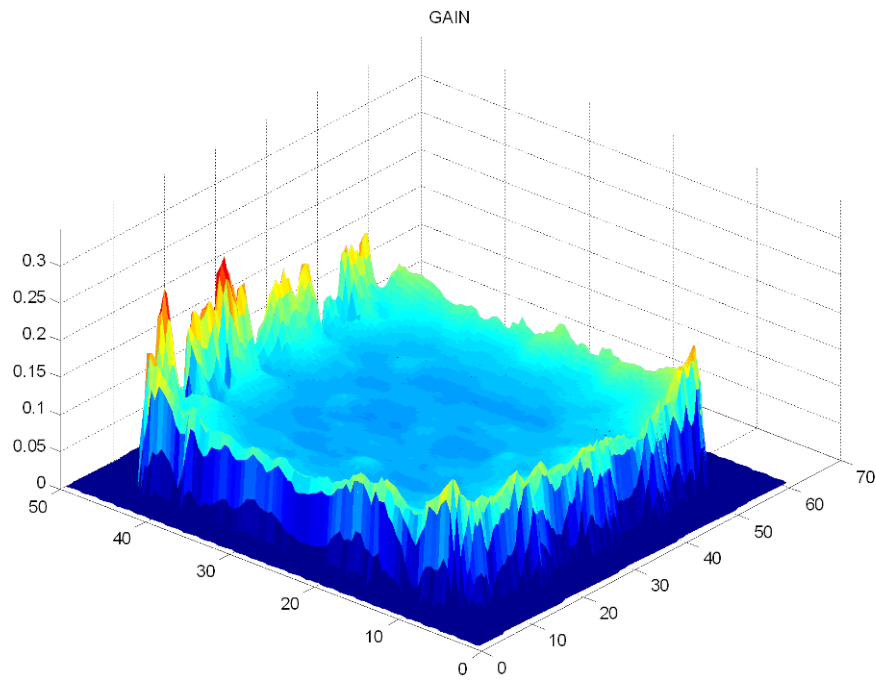
ADC channels vs. Corrected Energy



Correction comparison

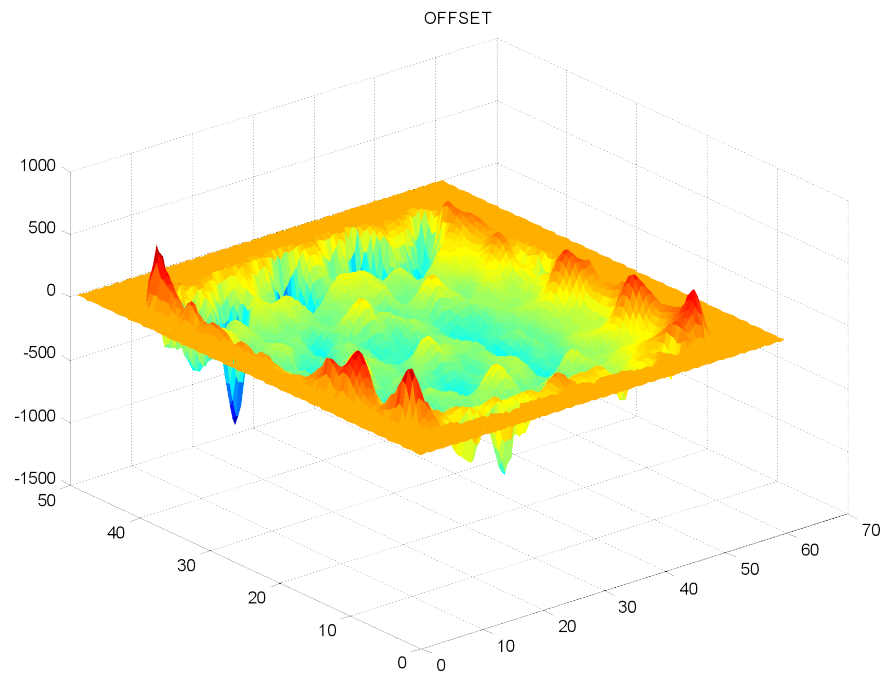
Corrected channels vs. Corrected Energy

# Energy measurement – Double peak correction



Gain

Average energy response.



Offset

Detector pattern.

# Position reconstruction

One of the most simple, yet widely adopted position reconstruction methods is the center of gravity.

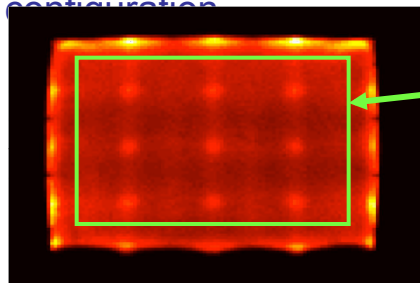
$$\underline{x} = \frac{\sum_i \underline{x}_i \cdot V_i}{\sum_i V_i} = \frac{\sum_i \underline{x}_i \cdot N_i^{ph}}{N_{tot}^{ph}}$$

The method is not optimal and adds geometric distortion to the image.

- Reduction of the FOV and UFOV.
- Need of some correction maps (obtained experimentally).

However the method works reasonably well in many applications, especially when the array of photodetectors is square.

- Not suited for the use with the DRAGO Gamma Camera, which is based on an array of SDDs arranged in a honeycomb configuration



Flood image of <sup>99m</sup>Tc.

UFOV

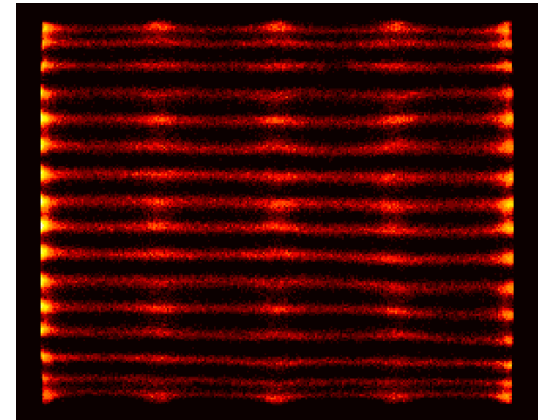


Image obtained using the center of gravity method, the lines have a 2.5 mm pitch.

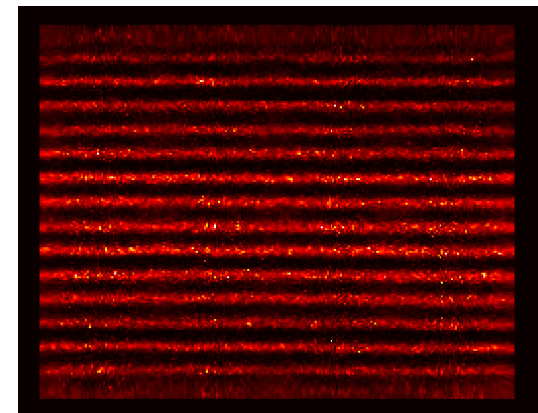
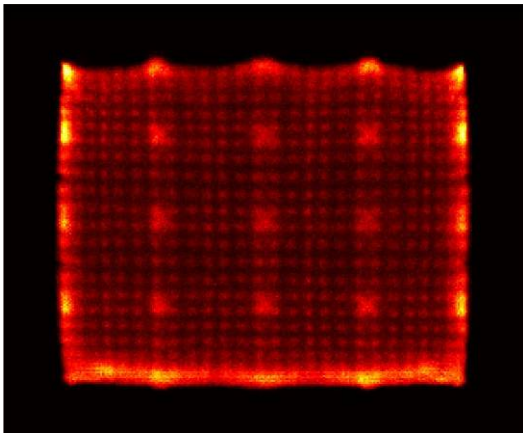
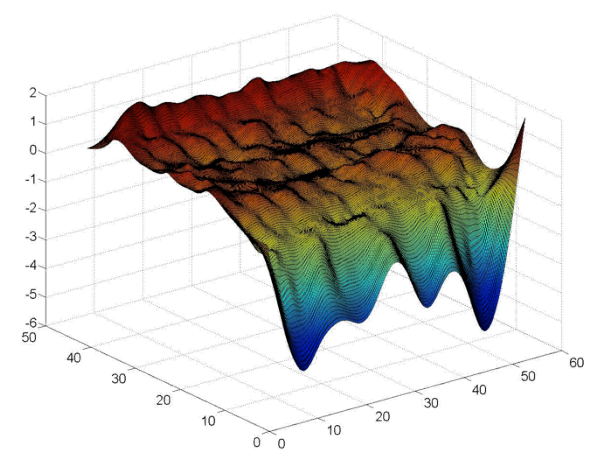
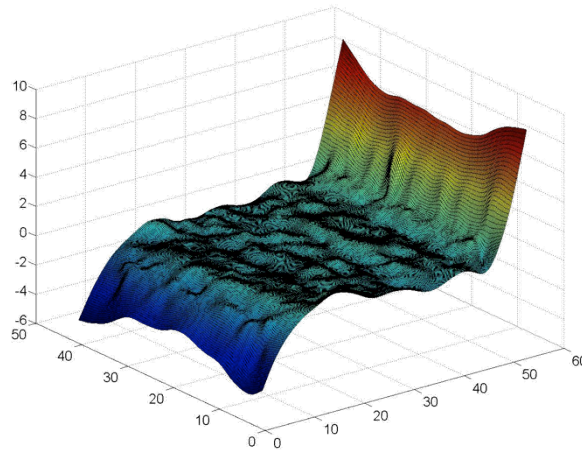
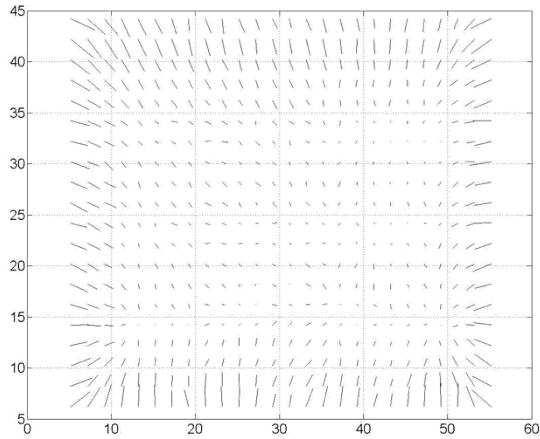


Image obtained after the application of uniformity/geometric corrections.

# Geometric correction

The geometric correction is obtained experimentally, from the image of a grid of points, drilled in a collimator.



Since the number of points in which the xy displacement is measured is much smaller than the number of points of the correction grid, some other condition must be specified.

- continuity of gradient or minimization of laplacian at every grid node.

Once obtained the correction grid, the displacement is applied to the reconstructed position of every single Gamma event.

- The advantage is that no pixel distortion, due to post processing, arises (however the computational cost is high).

# Optimum Position Reconstruction

The *mean* value of the number of photons collected by each photodetector -  $\lambda$  - is a deterministic function of the coordinates of interaction of the Gamma photon with the scintillator -  $\theta$  - and can be obtained from a geometric model or a Monte Carlo simulation of the Gamma Camera.

Under the hypothesis of negligible electronic noise, then the probability distribution function associated to the number of photon measured by each SDD -  $x_i$  - is a Poisson distribution.

Simulation

$$f(x_i | \theta) = \frac{\lambda_{i,\theta}^{x_i} \cdot e^{-\lambda_{i,\theta}}}{x_i!}$$

pdf associated to a single SDD

Independent and identically distributed random variables

Measured small correlation between detectors.

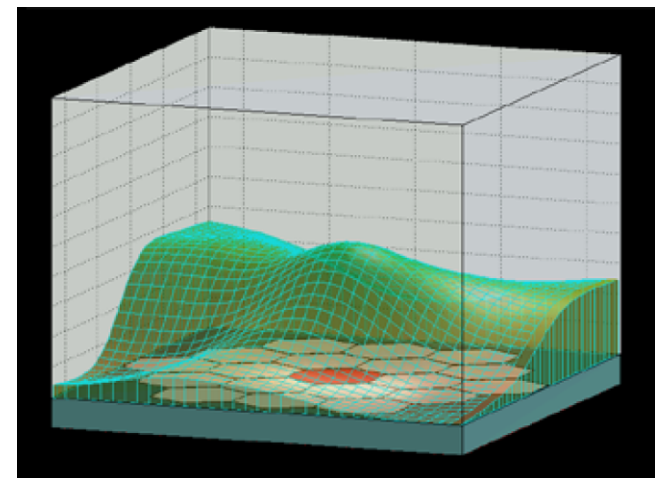
$$f(\underline{x} | \theta) = \prod_i f(x_i | \theta)$$

pdf associated to the SDD array, function of  $\theta$ .

Given a set of observed values  $(x_1, \dots, x_n)$ , the *maximum likelihood estimate* of  $\theta$  is that value of  $\theta$  that maximizes the likelihood function or its logarithm, obtained inverting the roles of  $X$  and  $\theta$ .

$$l(\theta | \underline{x}) = \log(L(\theta | \underline{x})) = \log(f(\underline{x} | \theta))$$

$$l(\theta | \underline{x}) = \sum_i x_i \log(\lambda_{i,\theta}) - \lambda_{i,\theta} - \log(x_i!)$$



Example of likelihood function.

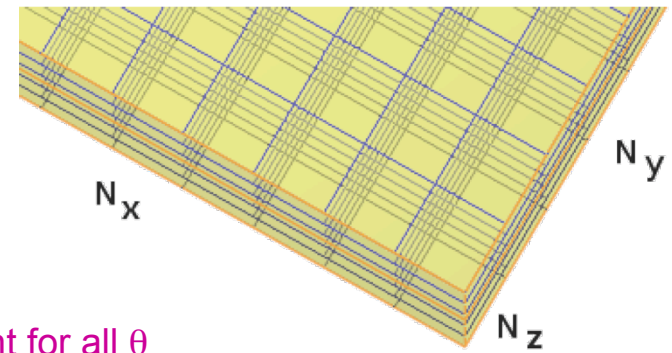
# Optimum Position Reconstruction

The MLE method gives also an estimate of the z coordinate!

The problem can be solved numerically, through the discretization of the solution domain and the use of lookup tables..

Considering the MLE function, some optimizations are possible:

$$l(\theta | \underline{x}) = \sum_i x_i \underbrace{\log(\lambda_{i,\theta})}_{\text{Log calculated off-line}} - \underbrace{\lambda_{i,\theta}}_{\text{Sum calculated off-line}} - \underbrace{\log(x_i!)}_{\text{Constant for all } \theta \rightarrow \text{neglected.}}$$



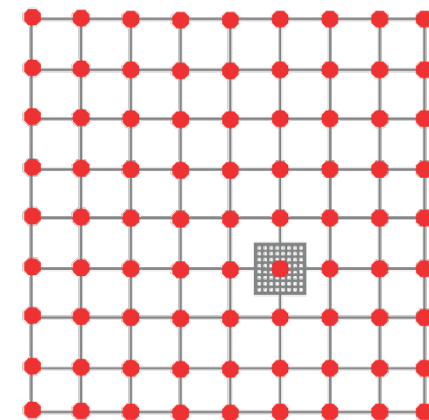
The computational cost of the maximization can be very high:

- Maximum event rate = 100k ev/s
- FOV size = 10x512x512 points (HICAM, with 0.2 mm pixel)

Naïve maximization	26 × 10 <sup>12</sup> FLOPS
Iterative Sampling	112 GFLOPS

Thanks to the smoothness of the Likelihood function it is possible to use efficient search algorithms.

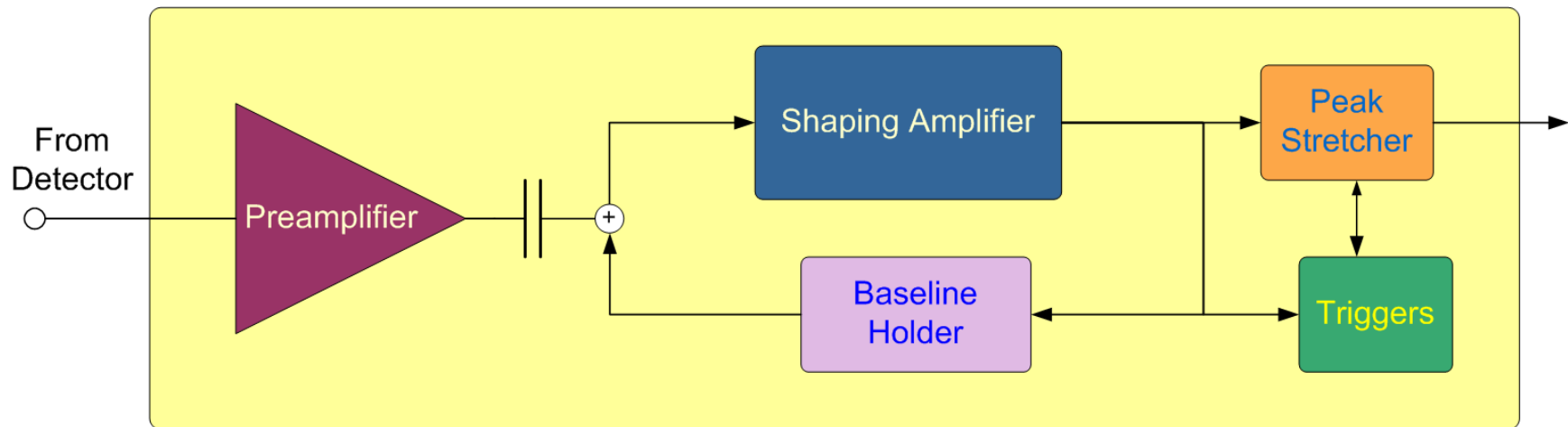
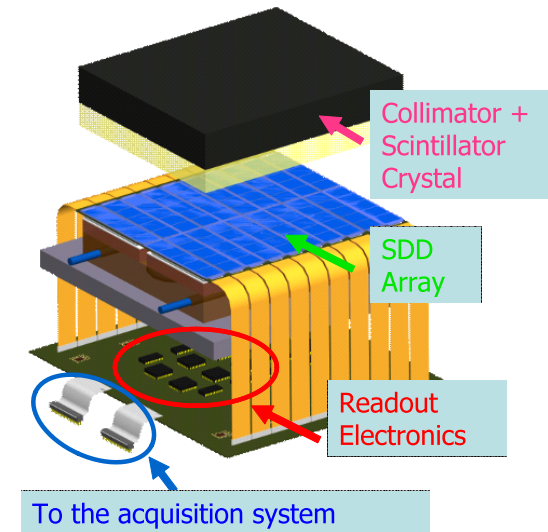
Nevertheless, for real-time operation, HPC is necessary  
 → CUDA from Nvidia is cheap yet powerful option.



# ASIC for SDD

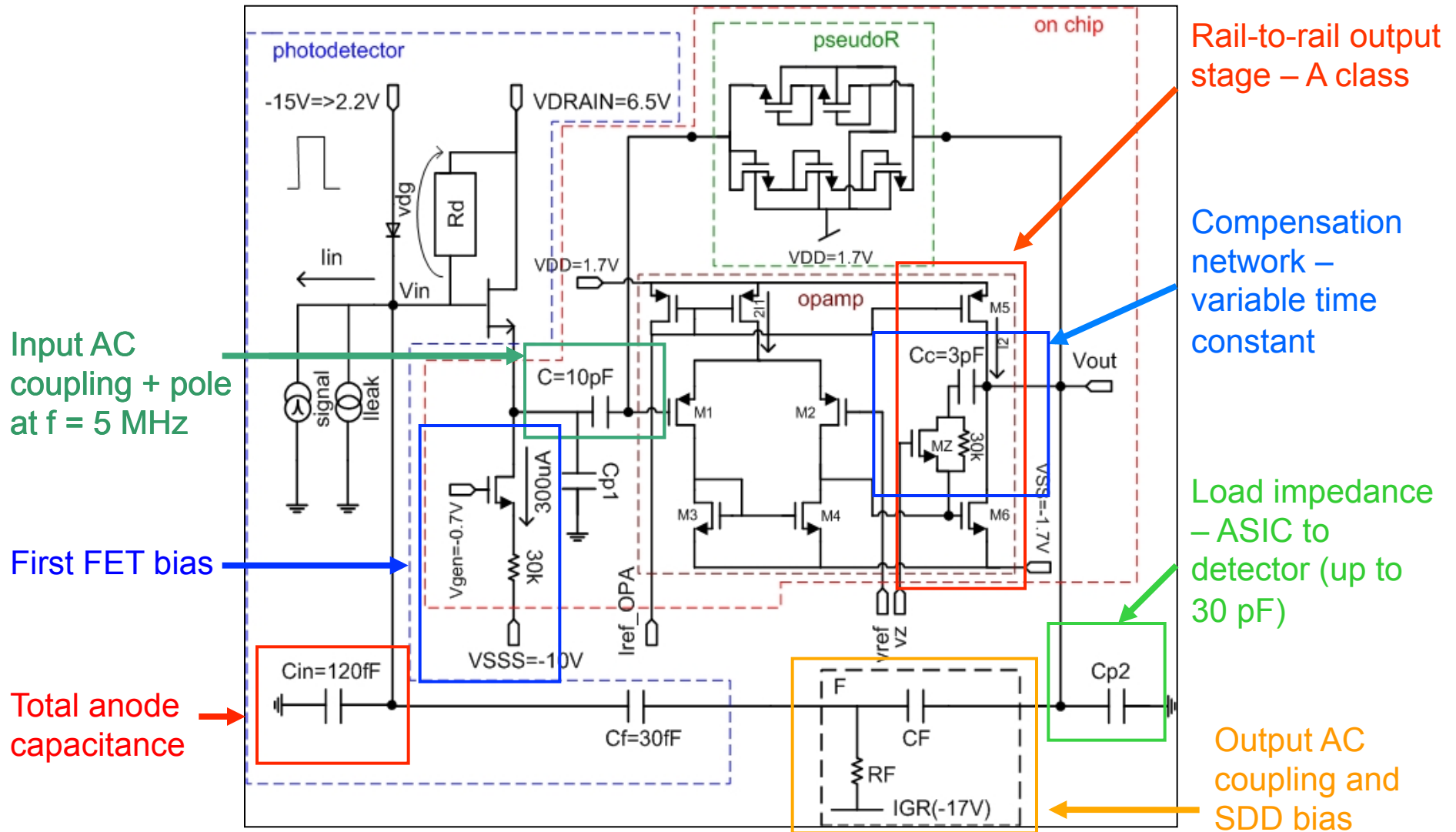
The use of custom integrated circuits is almost mandatory in systems composed of a relatively high number of channels, like an Anger Camera

- Compactness, power consumption, less interference
- Sub-optimal filtering, compared to digital filters

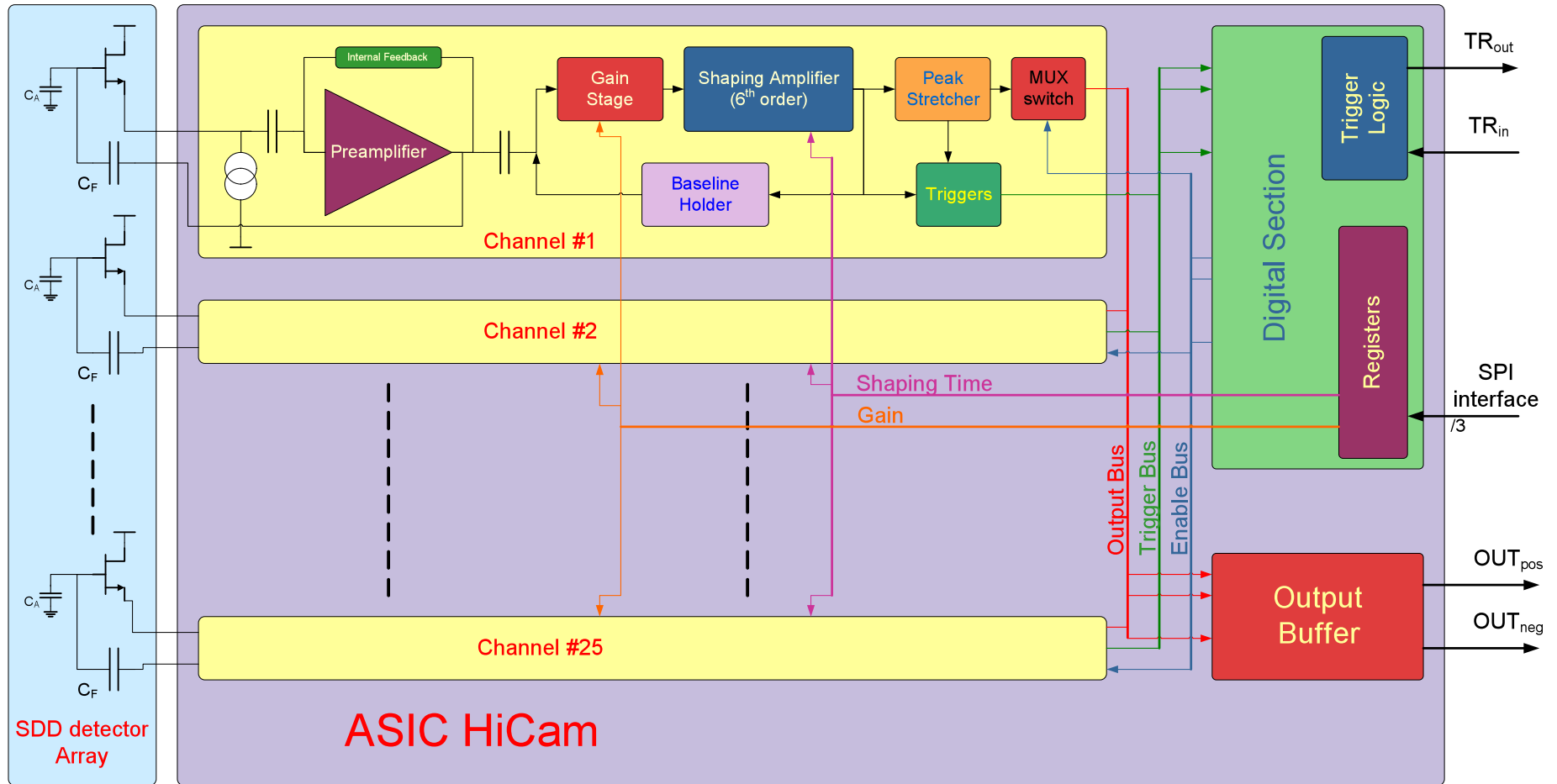


Standards elements composing a single channel of the analog front-end for SDD and for many common detectors.

# Preamplifier



# Complete ASIC for Gamma Camera Readout



# ASIC layout

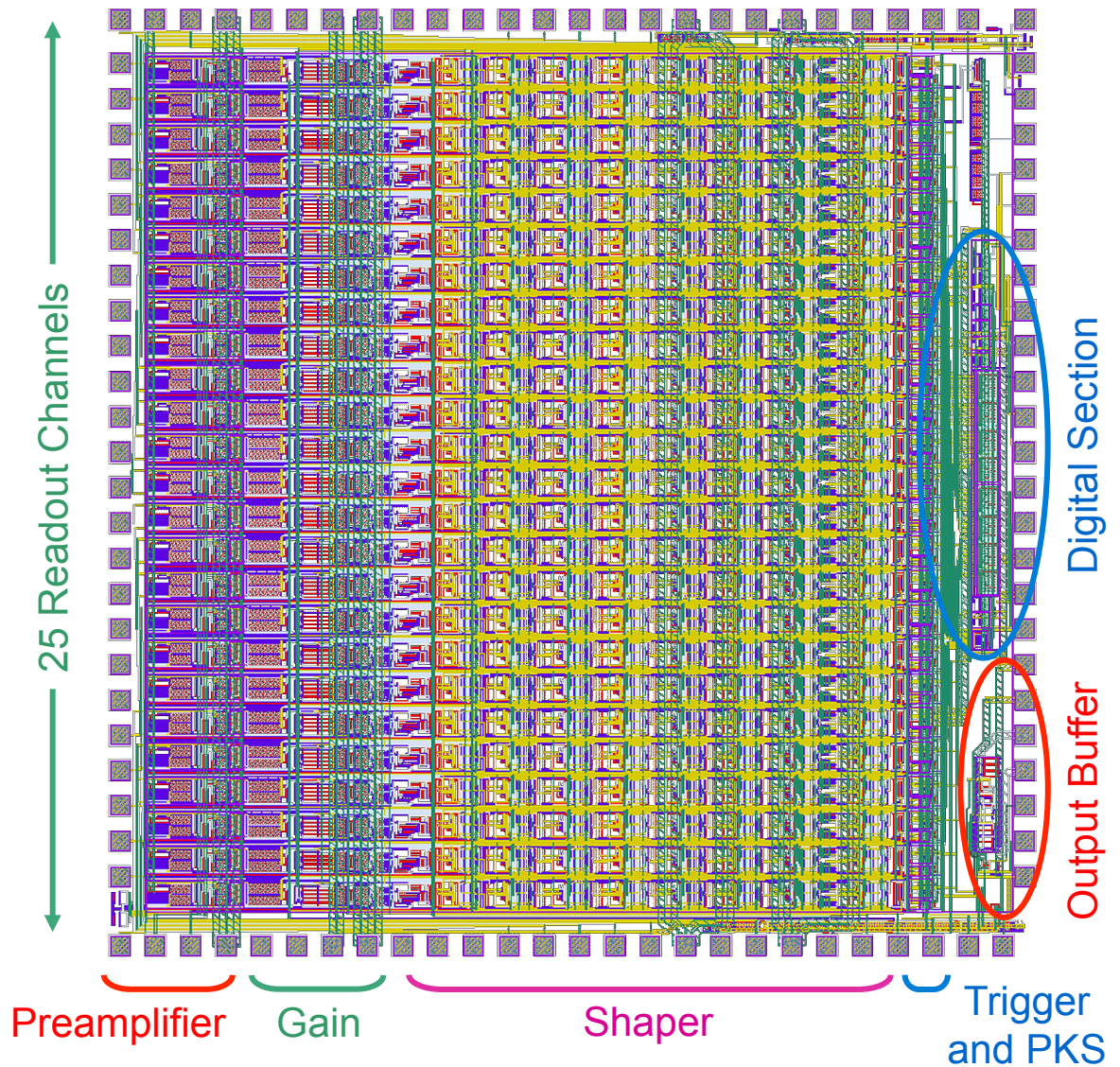
This ASIC has been produced in the **0.35  $\mu\text{m}$ , 3.3V CMOS, AMS** technology

100 pads

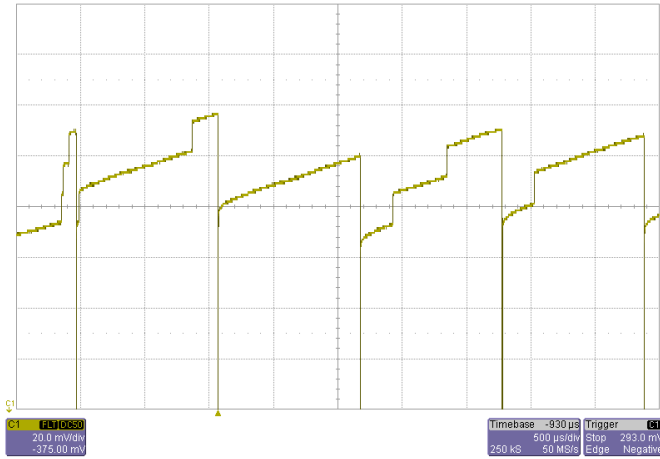
Die size: 4.8 x 4.6 mm<sup>2</sup>

Packaging options:

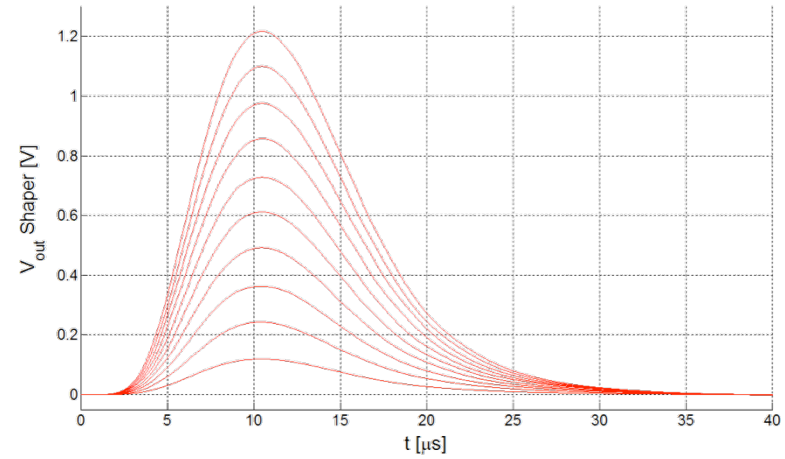
- 100-pin LQFP  $\rightarrow$  20 x 20 mm<sup>2</sup>
- Include the 100-pin MLF, SMD package
- 12 x 12 mm<sup>2</sup>



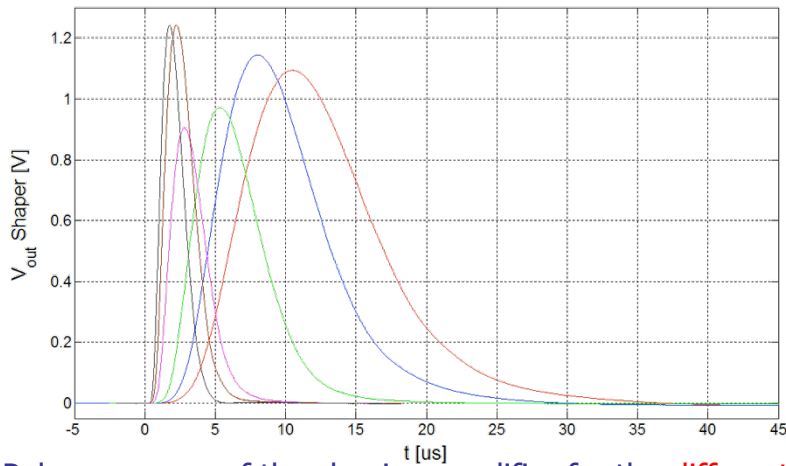
# Example waveforms



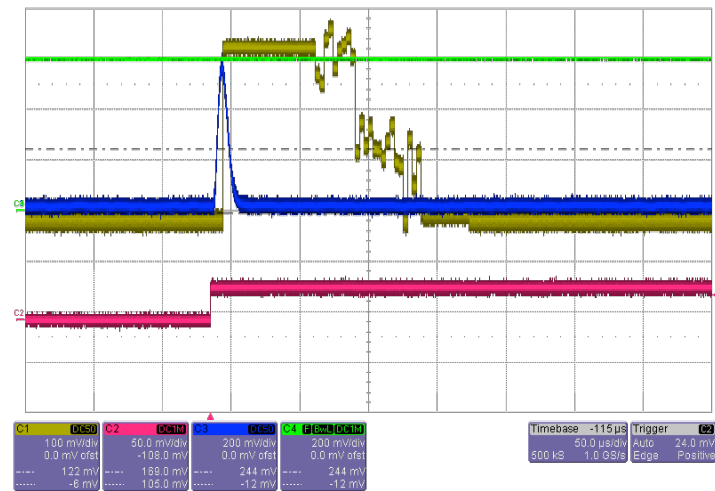
Ramp at the output of the preamplifier, integrating both the leakage and the signals of an X-ray  $^{55}\text{Fe}$  source.



Measured pulse response of the shaping amplifier, for the 11  $\mu$ s peaking time, for different signal amplitudes.



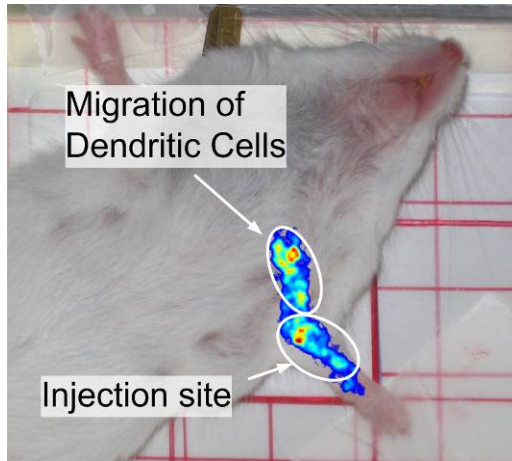
Pulse response of the shaping amplifier for the different shaping times implemented.



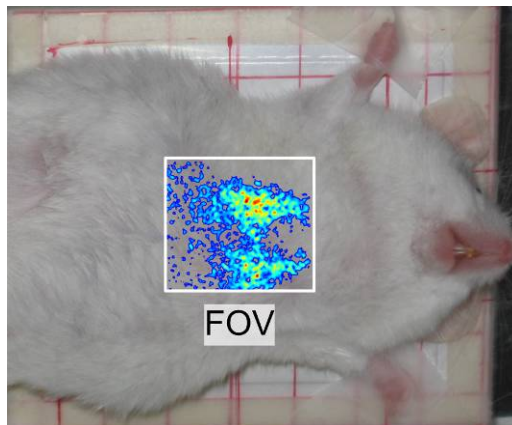
Signals generated by the analog multiplexer, which can work at 5 MHz.

# Gamma Camera - Measurements

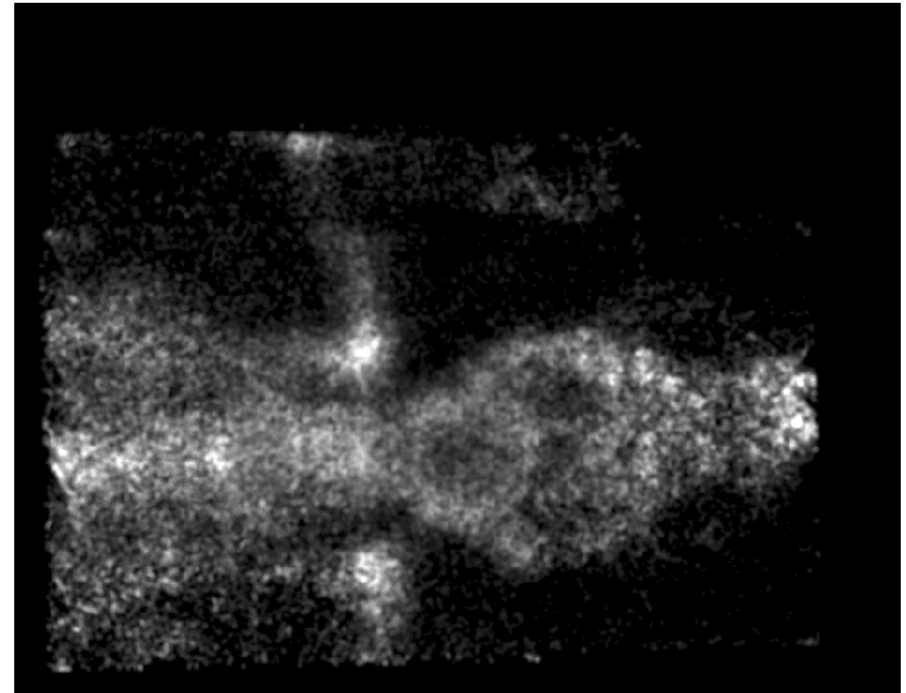
Example images, taken with an SDD-based Gamma Camera during a set of *in-vivo* measurements at the San Paolo hospital, in Milan.



Migration of Dendritic Cells, labeled with 60  $\mu\text{Ci}$  of  $^{111}\text{In}$ -Oxine.



Early lung biodistribution of Neural Stem cells, labeled with 60  $\mu\text{Ci}$  of  $^{111}\text{In}$ -Oxine.



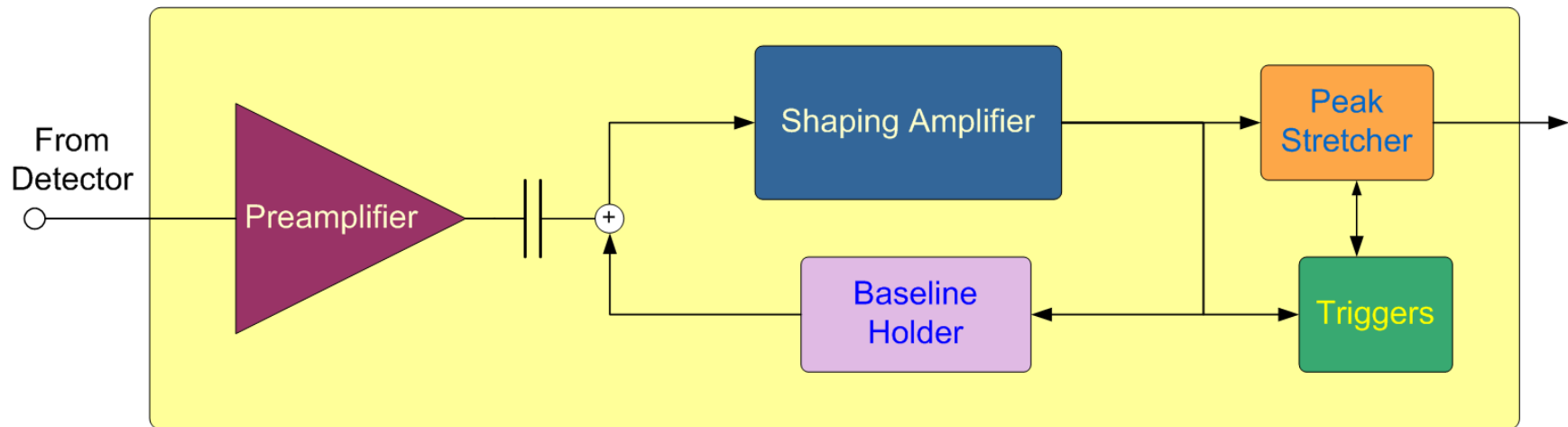
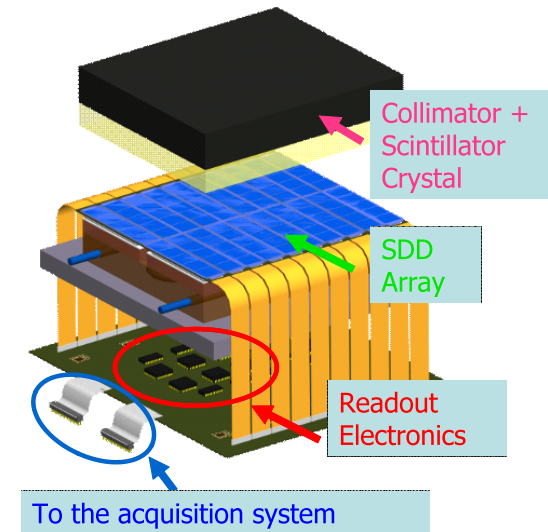
*In-vivo* bones scintigraphy of a mouse, obtained using a parallel holes collimator and the DRAGO detector.  $^{99\text{m}}\text{Tc}$ -MDP was the radiotracer.

# Backup Slides

# ASIC for SDD

The use of custom integrated circuits is almost mandatory in systems composed of a relatively high number of channels, like an Anger Camera

- Compactness, power consumption, less interference
- Sub-optimal filtering, compared to digital filters



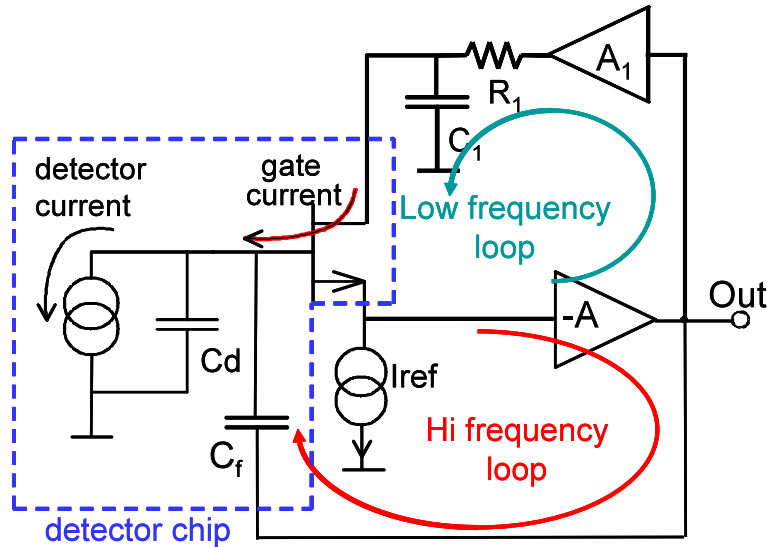
Standards elements composing a single channel of the analog front-end for SDD and for many common detectors.

# Preamplifier

The use of the pulsed reset of the detector has been proposed for reducing the “parallel” noise of the system, by reducing  $I_T$ .

## Continuous reset

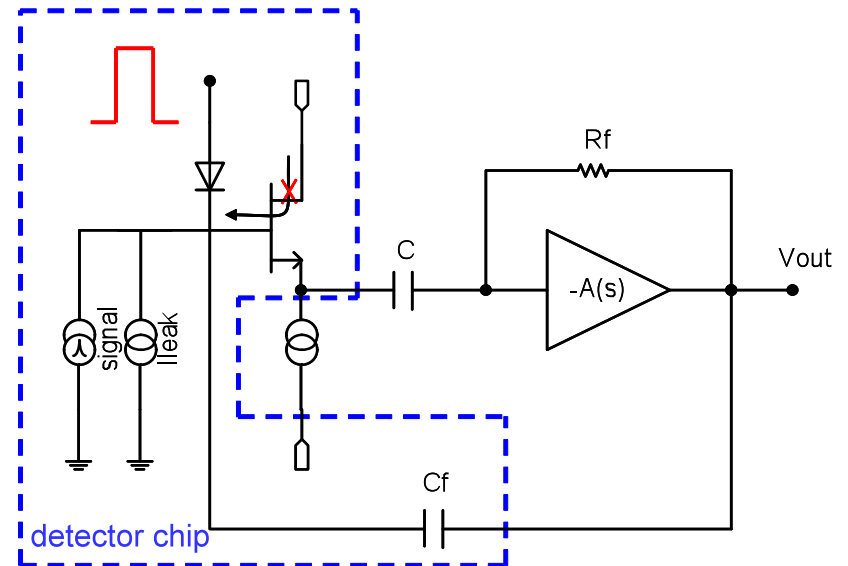
The anode is discharged by a continuous avalanche between Drain and Gate of the FET → noisy



$$I_T = 2 \times I_{leakage} + I_{Signal}$$

## Pulsed reset

A diode periodically resets the anode of the Detector



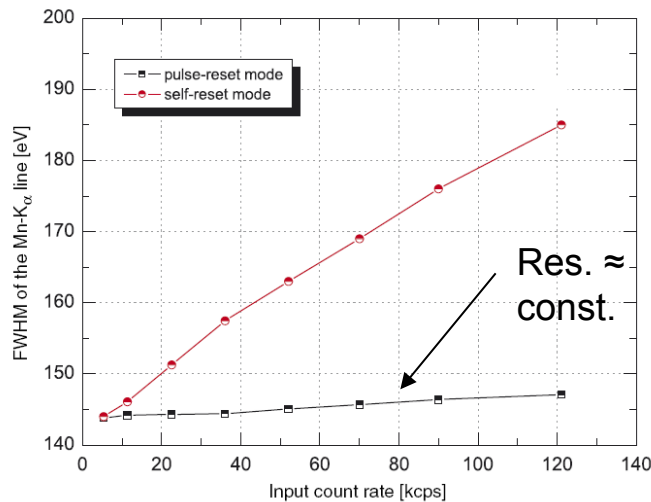
$$I_T = 1 \times I_{leakage} + I_{Signal}$$

# Preamplifier

$$I_T = \underset{\uparrow}{1} \times I_{leakage} + \cancel{I_{Signal}}$$

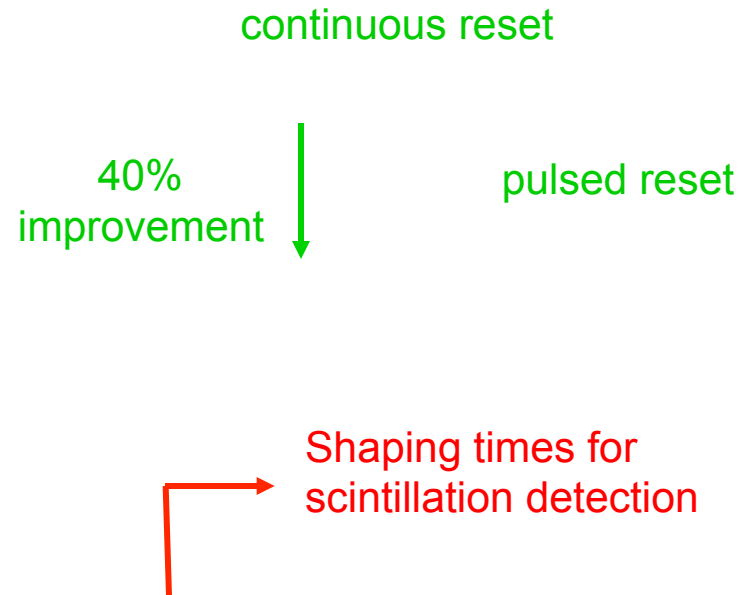
The advantages of the pulsed rest are:

- Almost negligible dependence of the electronic noise on the rate of events
- Reduced dependence of the ENC on  $I_{leakage}$ , which is exp. proportional to the operating Temp.
- Improved energy resolution for same T, or same energy resolution at higher T
- The system can run warmer → reduction of the ballistic deficit of the CsI at higher temperatures.



Energy resolution vs. rate

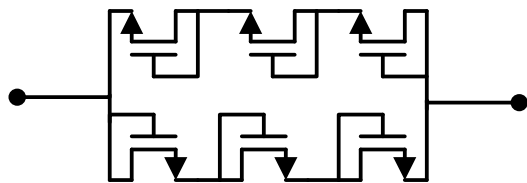
A.Niculae, et al., NIMA, Vol. 568, 2006, pp. 336-342.



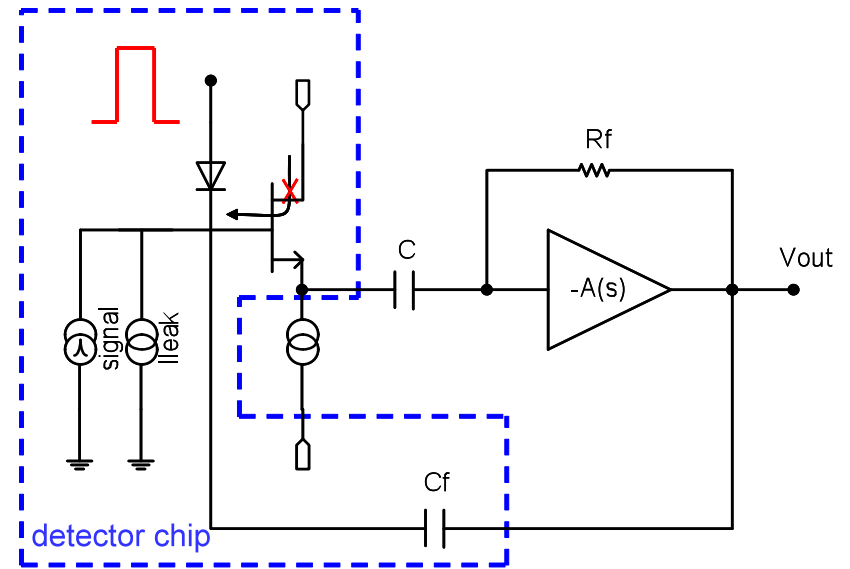
# Preamplifier

The preamplifier is designed in a **charge sensitive configuration**, compatible with the pulsed reset operation.

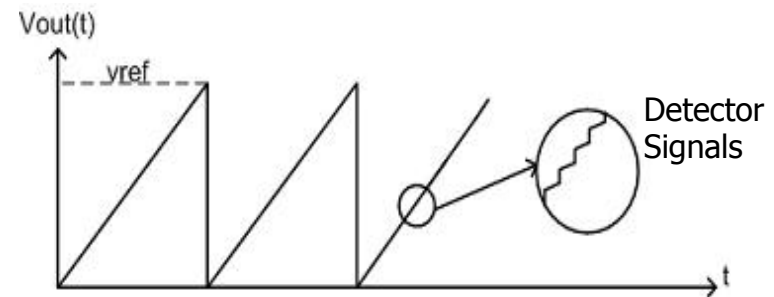
- The feedback capacitor  $C_f$  is **integrated inside the SDD detector**.
- The preamplifier is **AC coupled** to the SDD – more practical than DC coupling.
- A **High-Z feedback element**, controlling the DC bias of the preamplifier, is obtained with the series of small, under-threshold transistors.
- The time constant of the AC coupling has been sized in order to **integrate both signal and leakage**.
- The **reset is synchronous** for all the readout channels, for minimizing the combined dead time of the system.
- 2 pads per channel



High-Z feedback element of the inner loop.

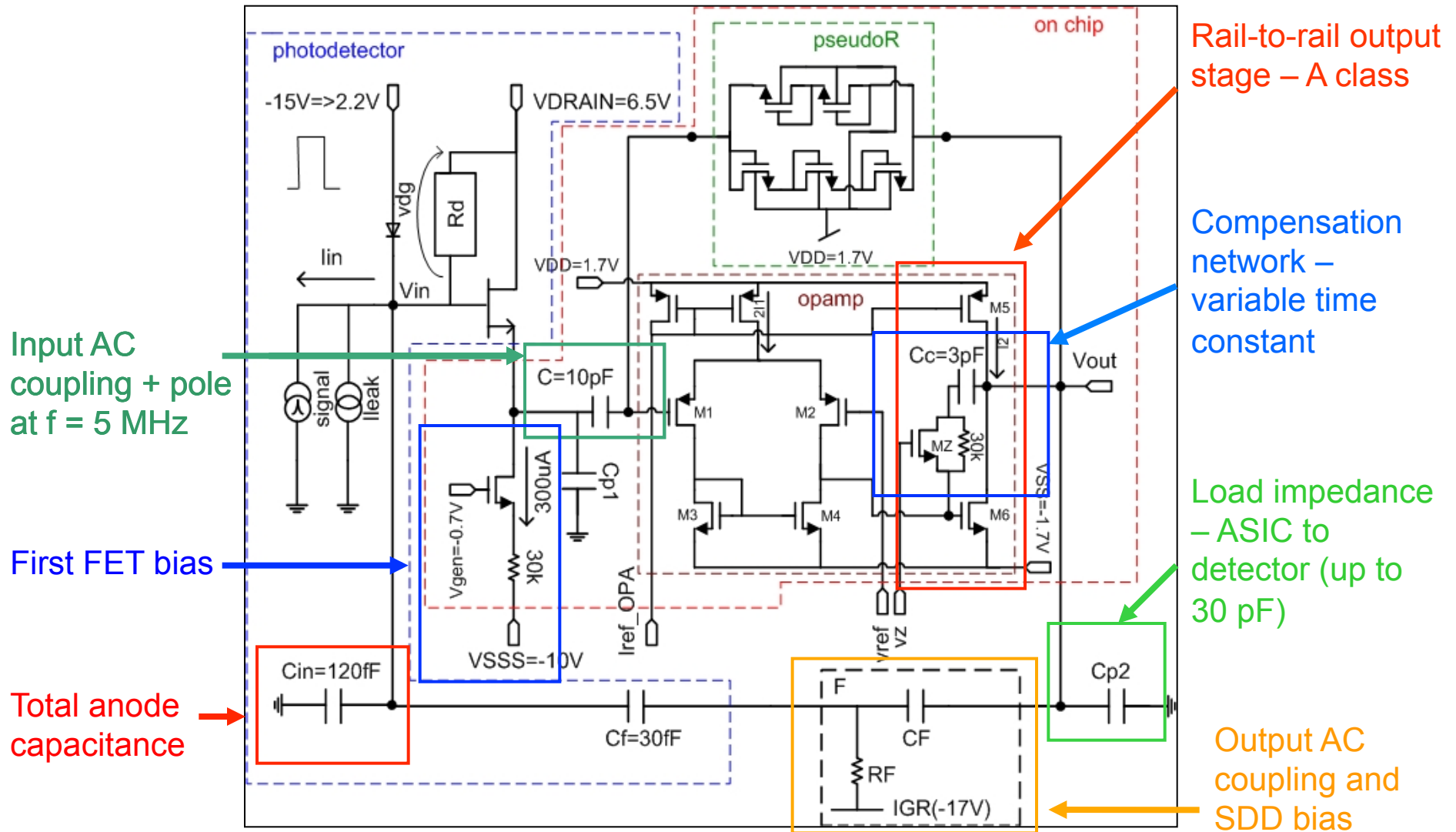


Schematic of the preamplifier, together with the SDD detector.

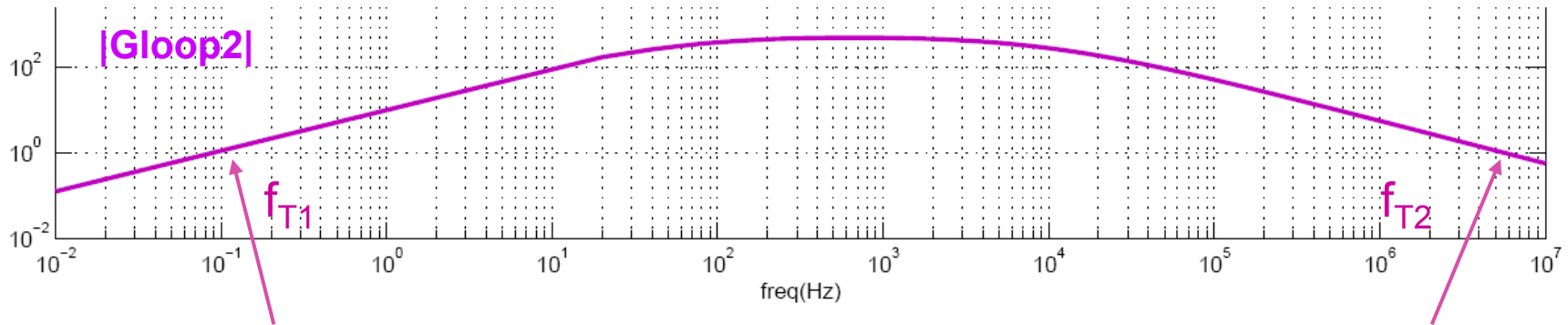


Drawing of the output of the preamplifier.

# Preamplifier



# Preamplifier



The integration of the leakage current is guaranteed by  $f_{T1} < 1$  Hz.

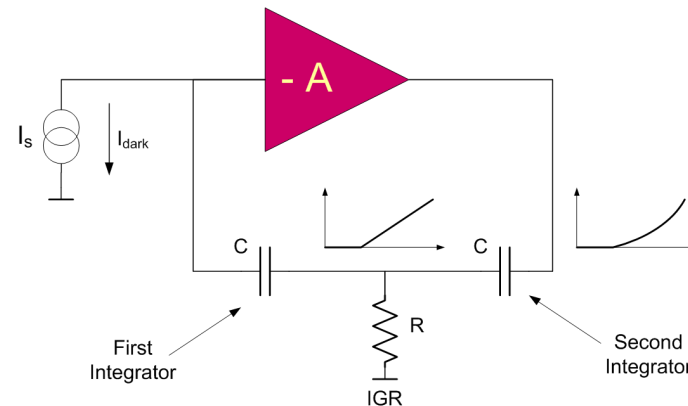
Closed-loop pole = 6 Mhz  $\rightarrow \tau_{rise} = 60$  ns (10-90%)

However, due to the output AC coupling we have a double integrator for  $\tau_{signal} > \tau_{AC}^{OUT}$ .

The zero of the compensation is needed to cancel the input-coupling pole (in the signal band)

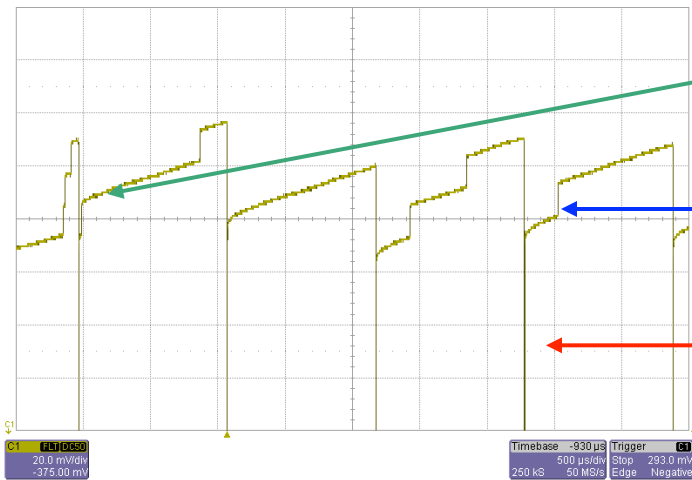
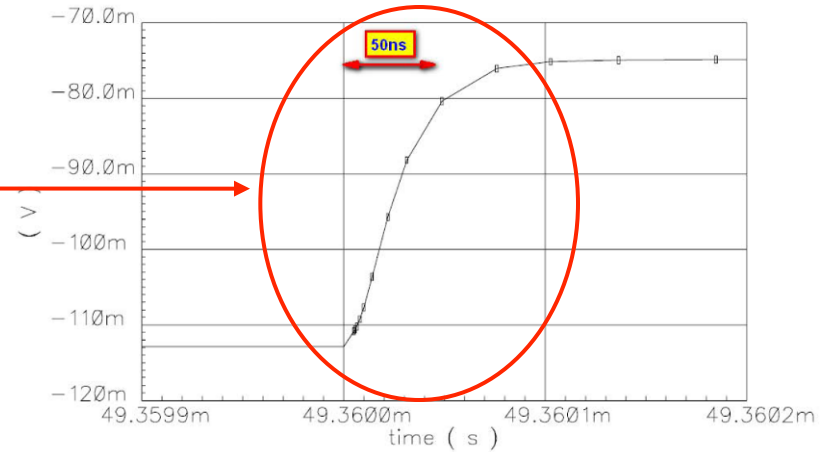
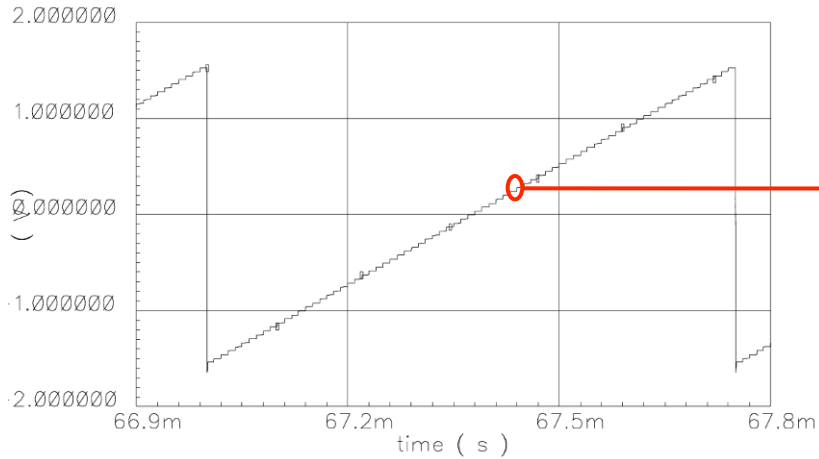
- The linearity of the ramp is critical, because, after being derived, constitutes the baseline of the shaper.
  - not completely compensated by the BLH
  - after reset dependent on quality of detector (surface currents)
- $t_{AC}^{OUT}$  must be consequently large, but  $R_{IGR}$  can't be very high due to the leakage of the IGR
- $R_{IGR}$  is also needed to decouple the different detectors in a multi-channel system – e.g. SDD array

- The second pole of the OPA is uncompensated, careful study of the phase margin is necessary.



# Preamplifier

Simulated and measured response of the preamplifier to the leakage current and to X-ray signals.



Deviation from linear behavior after reset

Signal pulses, superimposed to leakage integration

Periodic reset of the detector

Ramp at the output of the preamplifier, integrating both the leakage and the signals of an X-ray  $^{55}\text{Fe}$  source – roughly 1640  $e^-$ .

# Shaping Amplifier

The function of the shaping amplifier is to enhance the S/N ratio of the signal measured from the detector, and is of maximum importance in case of detectors with no internal charge multiplication.

Its most important design characteristics are:

- Noise coefficients → optimized considering the noise parameters of the detector and the signal shape.
- Return to zero time → reduced pile-up.
- Ease of implementation (multi-channel ASICs)

Considering a system with only series, 1/f and parallel noise, the input-referred noise can be expressed as the Equivalent Noise Charge, in electrons:

$$ENC^2 = C_T^2 \left( \underbrace{A_1 \alpha \frac{4kT}{g_m} \frac{1}{\tau_s}}_{\text{Series noise}} + \underbrace{A_2 2\pi A_f}_{1/f \text{ noise}} \right) + \underbrace{A_3 2qI_l \tau_s}_{\text{Parallel noise}}$$

E. Gatti et al.: "Suboptimal filtering of 1/f-noise in detector charge measurements".

# Shaping Amplifier

The coefficients  $A_1$ ,  $A_2$  and  $A_3$  depend only on the “shape” of the shaping amplifier and not on the duration of its pulse response, expressed by  $\tau_s$ .

- $\tau_s$  is the shaping time and is optimized according to the noise parameters of the system.

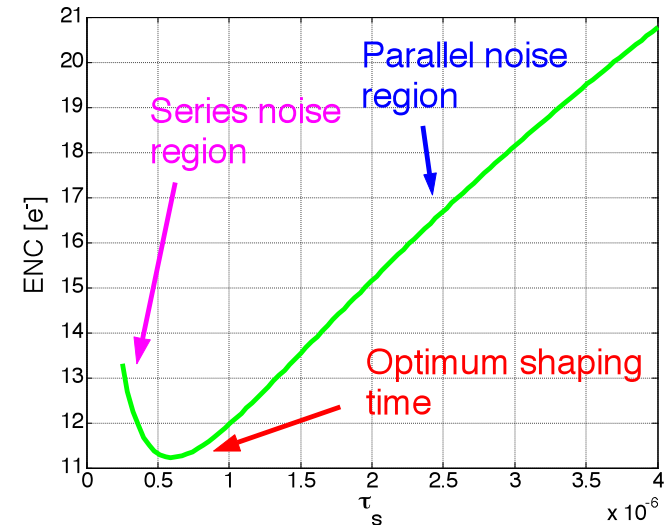
Meaning of the shaper coefficients, if  $h(t)$  is the pulse response of the shaping amplifier:

$$A_1 = \int_{\Re} |h'(\tau)|^2 d\tau$$

$$A_3 = \int_{\Re} |h(\tau)|^2 d\tau$$

$$A_2 = \int_{\Re} |\omega| |H(j\omega)|^2 \frac{d\omega}{2\pi}$$

← Fractional derivative of  $h(t)$



Simulated ENC of a 30 mm<sup>2</sup> SDD device vs. shaping time, proportional to the duration of the shaper pulse response.

For a rational  $H(f)$ , the integrals are finite if:

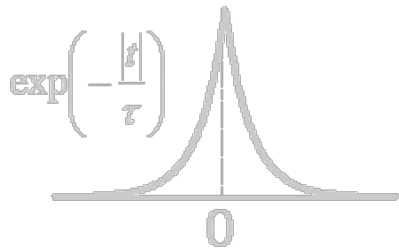
$$n_{poles} \geq n_{zeros} + 2 \Rightarrow A_i < \infty$$

# Shaping Amplifier

Different kinds of shaping amplifiers and related  $A_i$  coefficients:

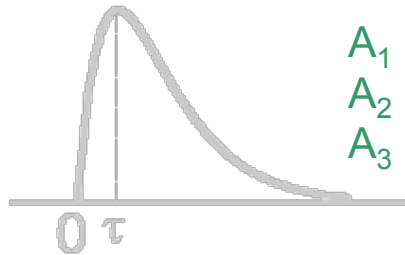
## Indefinite Cusp

Optimal filter for white noises



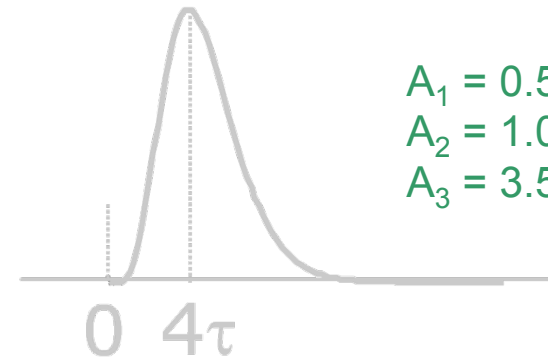
$$\begin{aligned} A_1 &= 1 \\ A_2 &= 2/\pi \\ A_3 &= 1 \end{aligned}$$

## RC-CR



$$\begin{aligned} A_1 &= 1.85 \\ A_2 &= 1.18 \\ A_3 &= 1.85 \end{aligned}$$

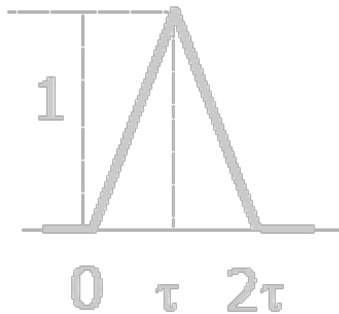
## Pseudo Gaussian (4° order)



$$\begin{aligned} A_1 &= 0.51 \\ A_2 &= 1.04 \\ A_3 &= 3.58 \end{aligned}$$

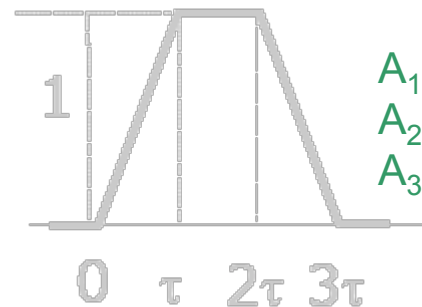
## Triangular

Optimal filter for white voltage noise and finite duration.



$$\begin{aligned} A_1 &= 2 \\ A_2 &= 4\ln \\ & (2)/\pi \\ A_3 &= 2/3 \end{aligned}$$

## Trapezoidal

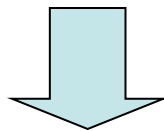


$$\begin{aligned} A_1 &= 2 \\ A_2 &= 1.38 \\ A_3 &= 5/3 \end{aligned}$$

# Optimal Shaping

In presence of only series and parallel white noise it is easy to calculate the optimal filter for AMPLITUDE MEASUREMENTS, which is the indefinite cusp.

$$\left(\frac{S}{N}\right)^2 = \frac{Q^2 (\max[h(t)])^2}{ENC^2} = \frac{Q^2}{a C_T^2 \int_{\Re} |h'(t)|^2 dt + b \int_{\Re} |h(t)|^2 dt}$$

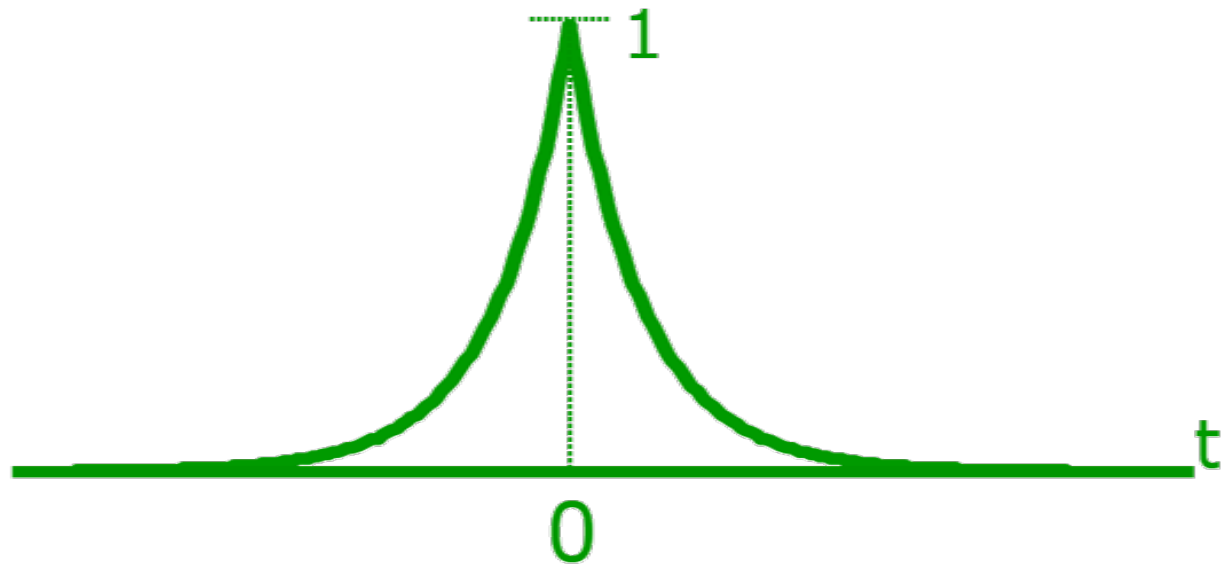


Variational Method

$$h_{opt}(t) = \exp\left(-\frac{|t|}{\tau_c}\right)$$

$$ENC_{opt} = \sqrt[4]{ab C_T^2}$$

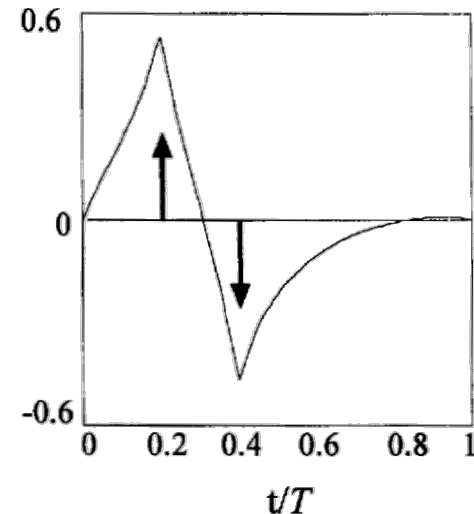
$$\tau_c = C_T \sqrt{\frac{a}{b}}$$



# Optimal Shaping

During the years a quite complete and interesting theory has been developed, for the synthesis of the optimal filter, with arbitrary constraints and noise (DPLMS):

- $1/f$  and colored noise.
- Finite duration.
- Amplitude or timing measurements.
- Arbitrary pulse shapes  $\rightarrow$  Scintillator.
- Known interference suppression.
- Automatic synthesis basing upon the noise measurement.



Optimal weighting function, with finite duration, for a zero-area signal pulse, composed of two delta-like pulses of opposite sign.

Due to their quite complex shape, the implementation of such filters is limited to digital signal processing.

In multi channel systems, i.e.  $> 100$ , the use of an analog circuit is still preferred, because of compactness, power consumption, .. at an acceptable performance cost.

# Analog Shaping Amplifiers

There are different analog shaping amplifiers try to approximate the pulse response of the optimal filter with lumped parameters circuits.

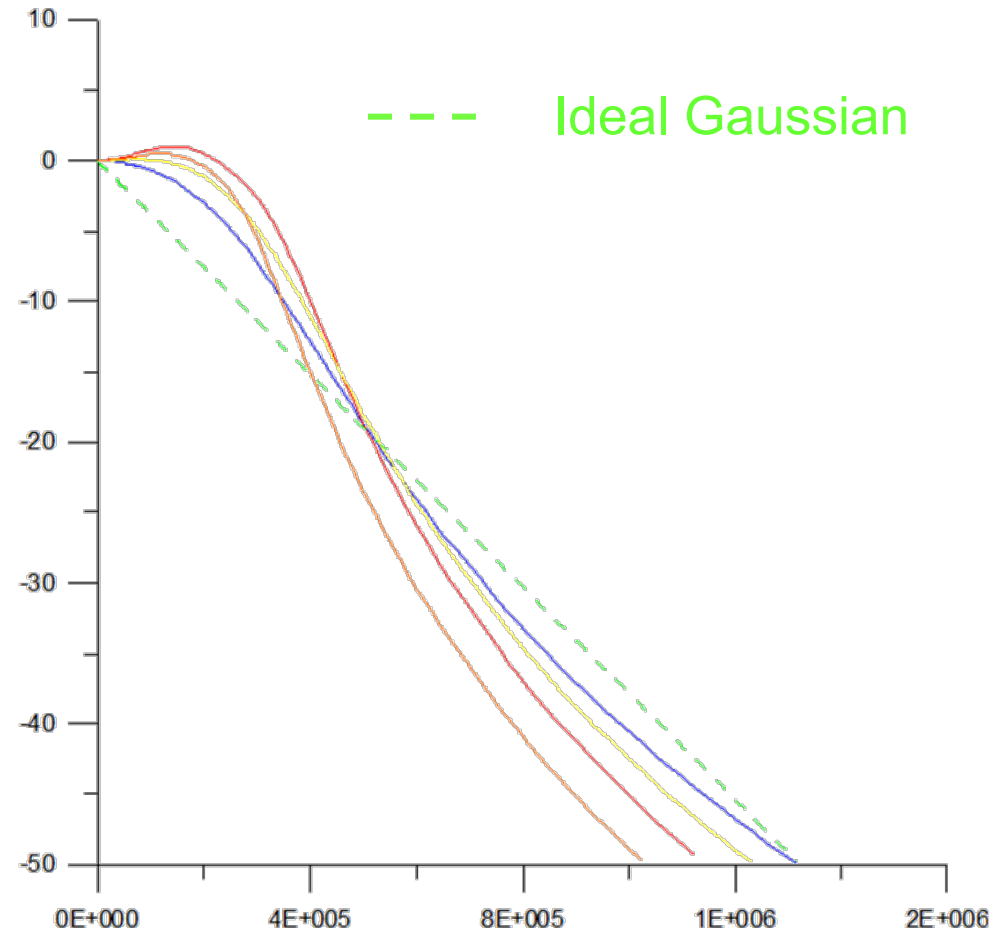
$$FoM = \frac{SNR_{shaper}}{SNR_{opt}}$$

Considering also the importance of the return-to-zero time, in high rate applications, usually a symmetric pulse-response is preferred.

→ Approximation of the frequency response of a Gaussian waveform with rational functions, i.e. with poles and zeros (with linear phase).

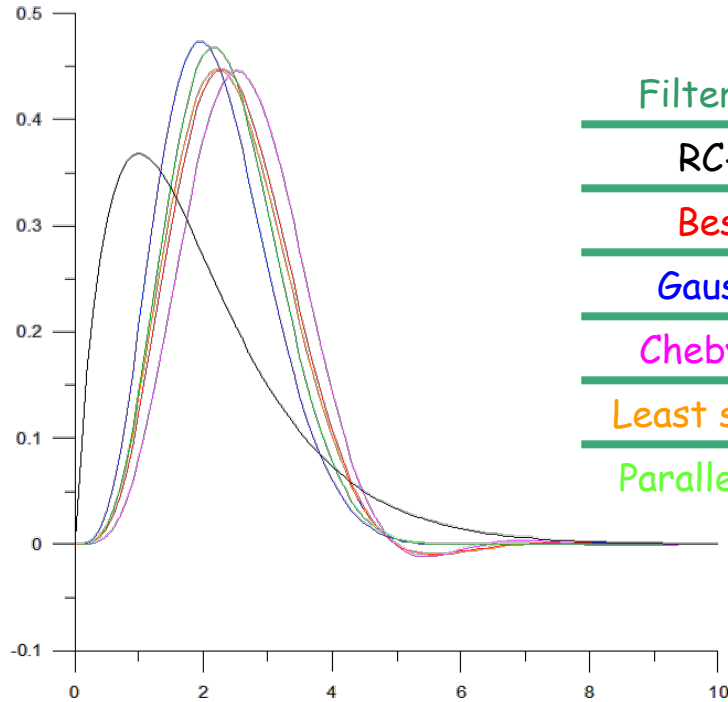
→ Different implementations are possible, with different characteristics with respect to FoM and return to zero.

S. Ohkawa et al.: "Direct synthesis of the gaussian filter for nuclear pulse amplifiers".

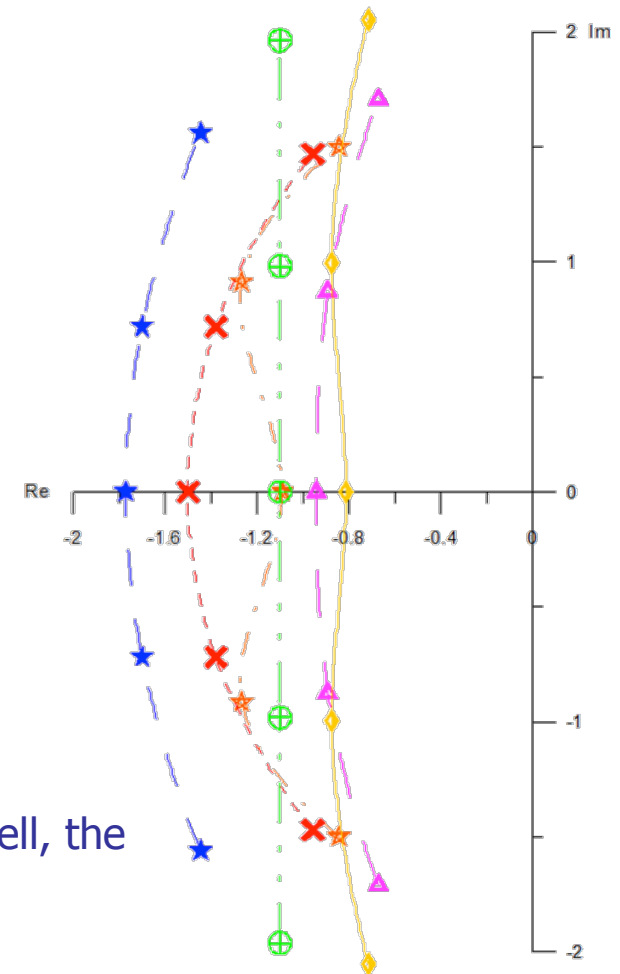


# Analog Shaping Amplifiers

There are different analog shaping amplifiers try to approximate the pulse response of the optimal filter with lumped parameters circuits.



Filter type	FoM @ opt
RC-CR	0.736
Bessel	0.867
Gaussian	0.868
Chebyshev	0.868
Least squares	0.867
Parallel poles	0.873



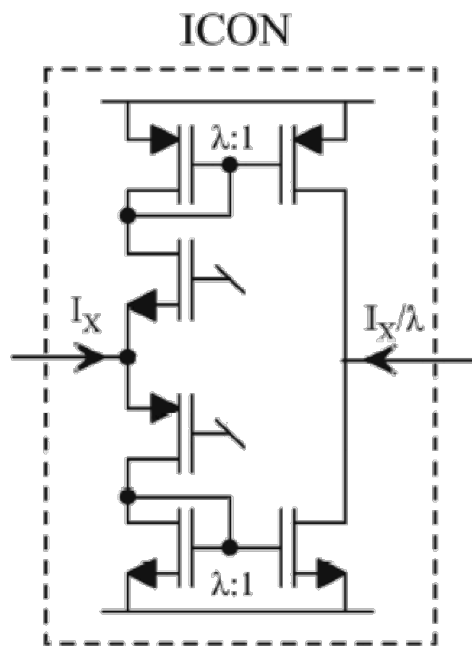
The FoM have no big variation with higher order filters.

Considering that it is less sensitive to the GBPW of the shaping cell, the Semigaussian shaping is often preferred.

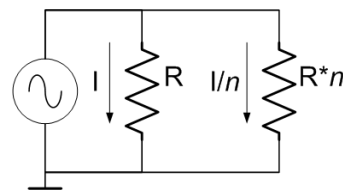
# Integration of the Shaper

Considering the ENC curve of a typical SDD, the optimal shaping time is of the order of  $10 \mu\text{s}$  when used coupled to a scintillator.

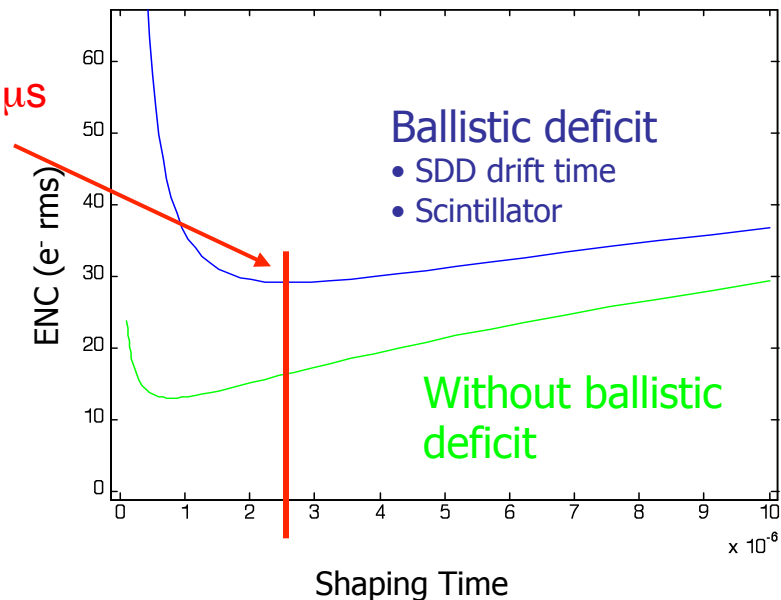
The corresponding time constants are difficult to integrate  $\rightarrow$  resistor multiplication mechanism through the ICON cell.



Peaking time =  $7 \mu\text{s}$



$$R_{eq} = n R$$

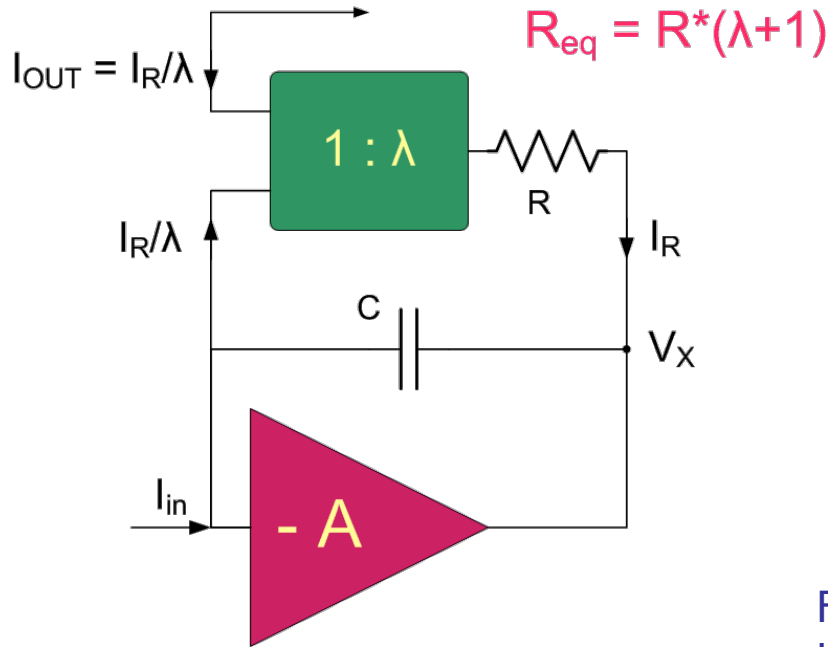


Simulated ENC for a  $30 \text{ mm}^2$  SDD coupled to a CsI scintillator at  $-10^\circ\text{C}$ .

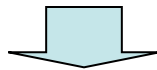
R. L. Chase et al.: "8-channel CMOS preamplifier and shaper with adjustable peaking time and automatic pole-zero cancellation".

$$\tau_p = 1 \mu\text{s} \Rightarrow C = 1 \text{ pF}; R = 1 \text{ M}\Omega$$

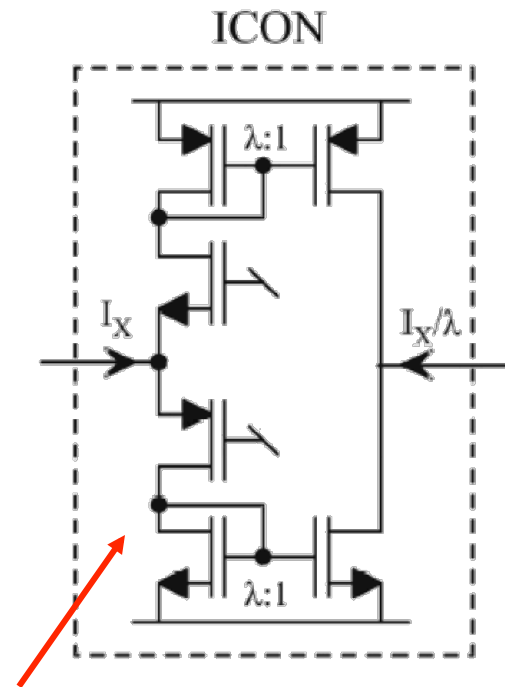
# ICON cell



The current mirrors must be biased at low current, due to noise constraints.  
The input impedance is high.



Signal-dependent time constant.

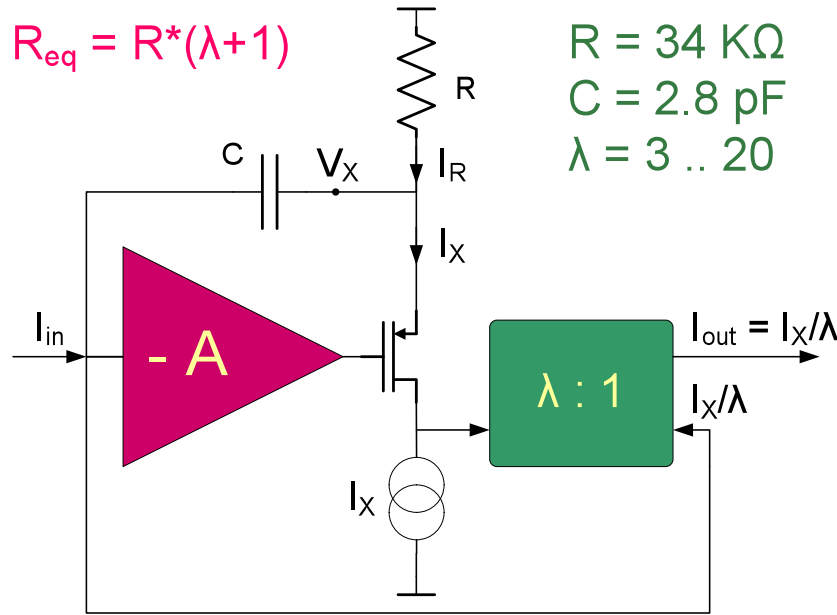


For precise mirror matching, the transistors in the read and output branch of the mirror are based on the same finger size.

$\lambda$  limited only to rational (integer) values

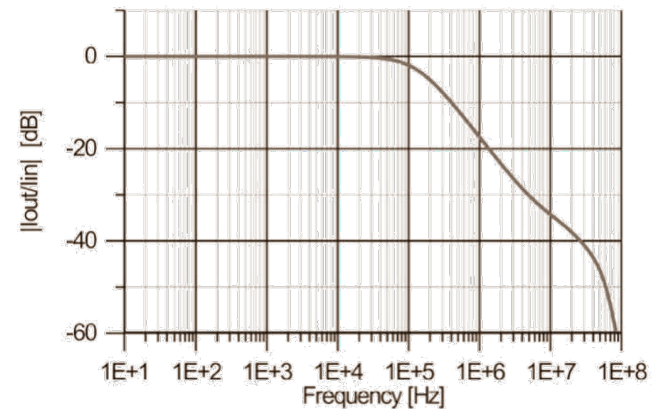
$$\lambda = \frac{n_{read}}{n_{output}}$$

# Linearized ICON cell



The cell provides high linearity and stability of the implemented time constants, thanks to the feedback loop.

$$I_{out} = I_{in} \frac{1 + sCR}{1 + sCR(\lambda + 1)}$$

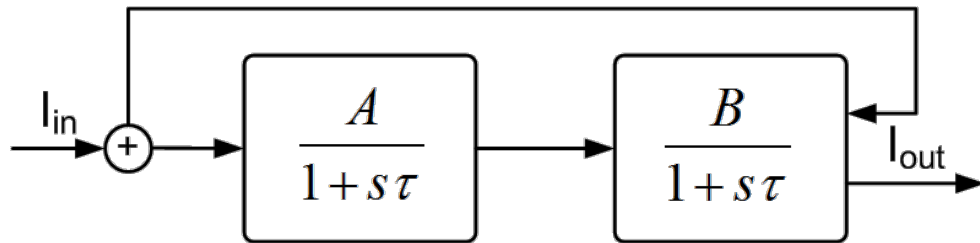


- The different shaping times are obtained by changing the multiplication coefficient – switching on/off transistors of the mirror.
- Unwanted zeros at higher frequencies  
 → important for lower  $\lambda$  – short shaping times.  
 → it is better to switch the capacitor values.

C. Fiorini and M. Porro: "Integrated RC Cell for Time-Invariant Shaping Amplifiers".

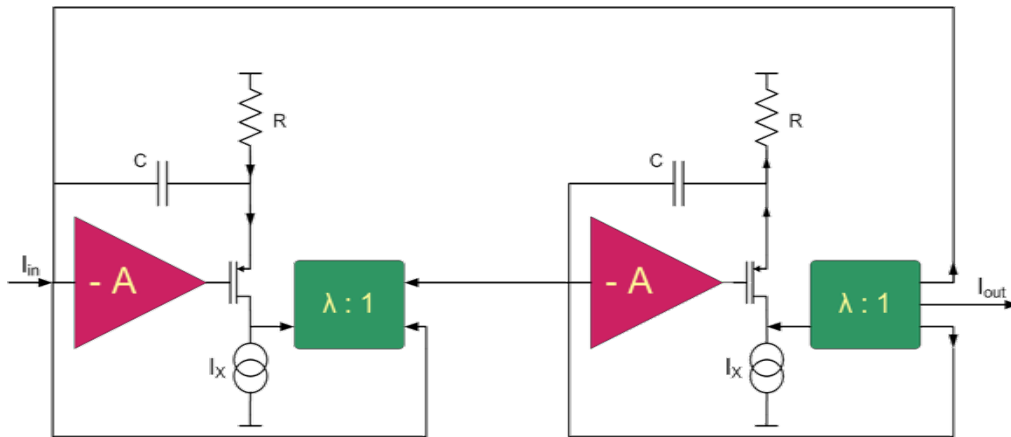
## Modification if the ICON for complex poles

It is possible to realize a couple of complex-conjugate poles starting from two single real-pole cells.



$$I_{out} = I_{in} \frac{AB}{(1+s\tau)^2 + AB}$$

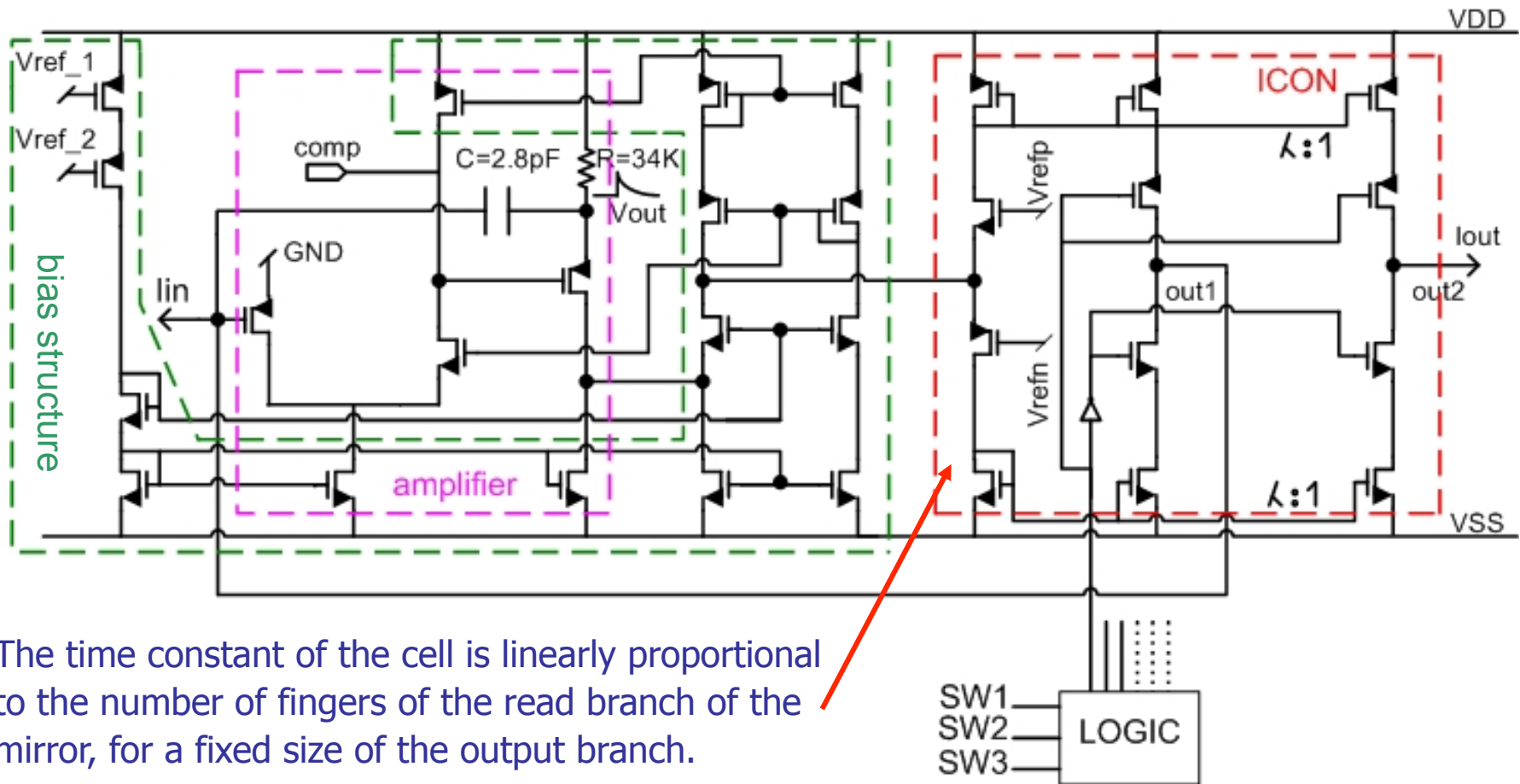
Block diagram of the connection of two real-poles cells for synthesizing complex-conjugate poles.



ICON implementation of complex conjugate poles.

The advantages of the complex-conjugate poles shaping amplifier, with respect to a real-poles one, is the shorter return to zero time (more symmetric pulse response).

# Circuit implementation of the ICON cell – real poles

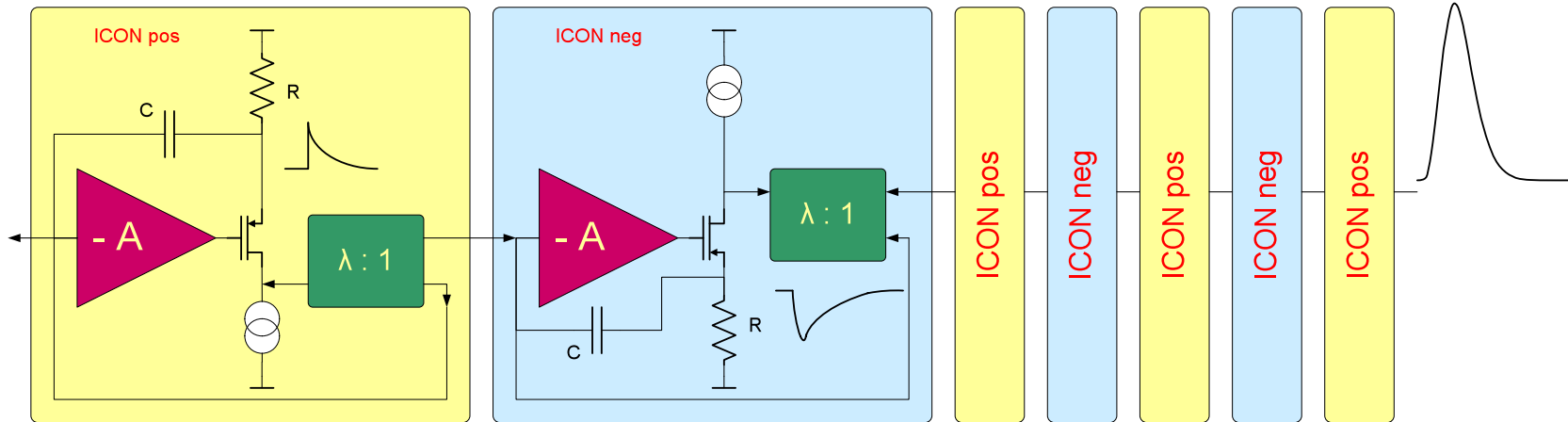


The time constant of the cell is linearly proportional to the number of fingers of the read branch of the mirror, for a fixed size of the output branch.

Grouping the fingers of the read mirror according the powers of 2, it is possible to implement a "DAC" for time constants.

$$\tau = n_{read} RC$$

# Shaping Amplifier - Example

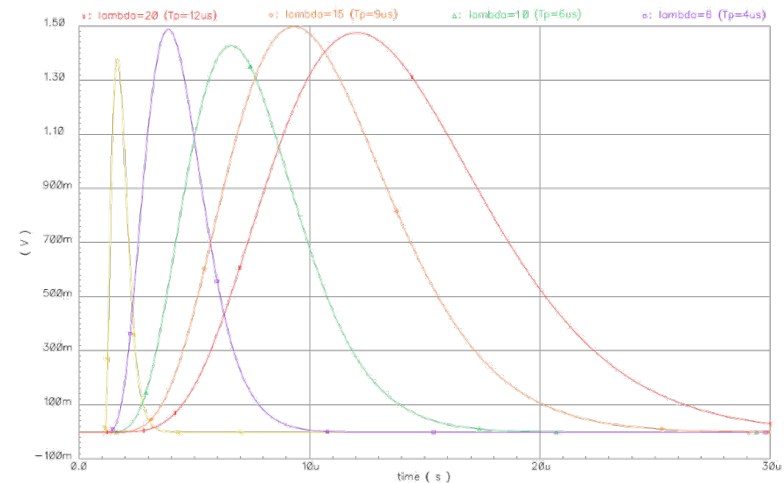


6<sup>th</sup> order, real poles, semi-Gaussian shaping amplifier:

- Modular structure, based on a cascade of single real pole cells: the ICON cells.

$$\frac{V_{out}(s)}{I_{in}(s)} \cong \frac{G_{Sh}R\lambda}{[1 + sRC(\lambda + 1)]^7}$$

$$V_{out}(t) = Q \cdot G_{Sh}R\lambda \cdot \frac{1}{720} \frac{t^6}{[RC(\lambda + 1)]^7} \cdot \exp\left(\frac{-t}{[RC(\lambda + 1)]}\right) u(t)$$



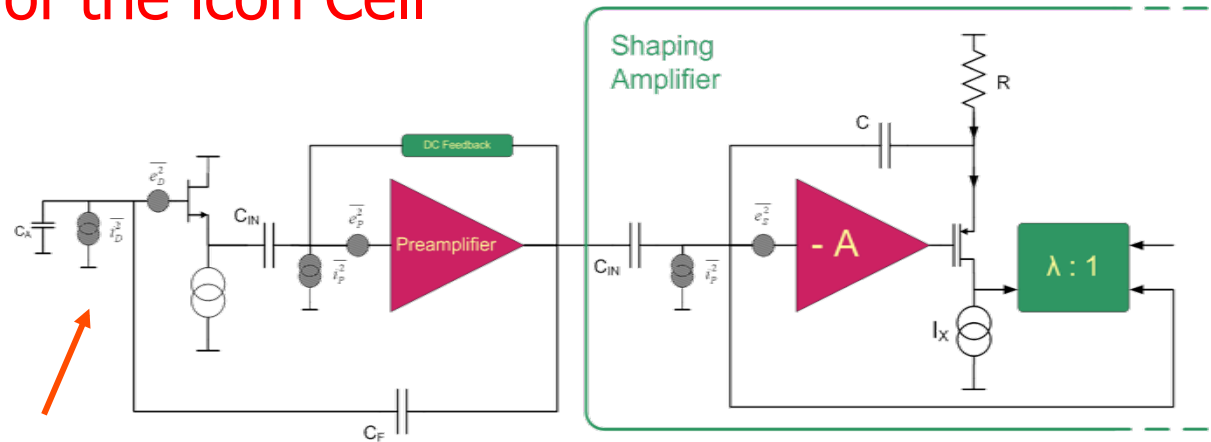
Simulated pulse response of the shaping amplifier, for different time constants

# Noise of the icon Cell

Being biased in A class, the ICON cells increase the parallel noise of the system.

There is a current gain between the ICON cells, so that the contribution of the first one is dominant.

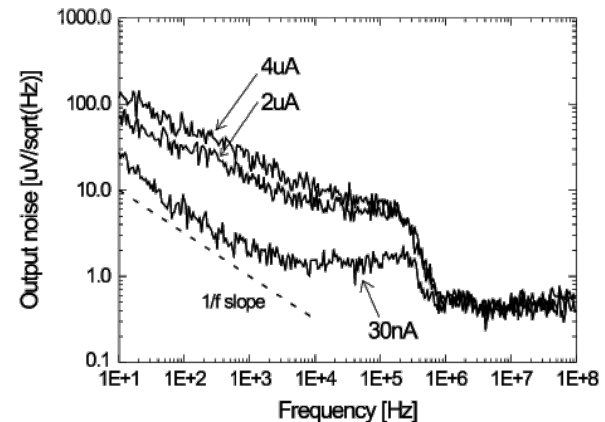
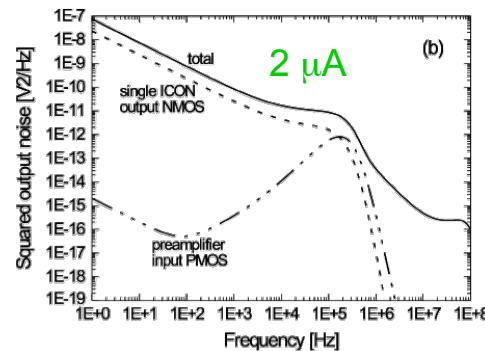
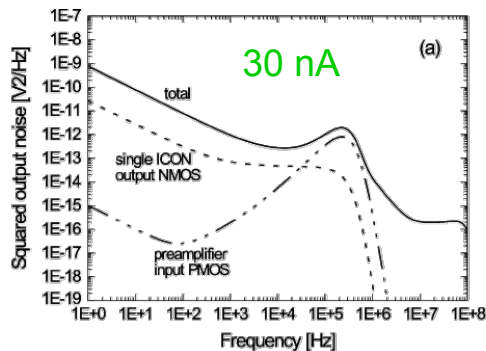
The cells cannot be biased with too small current to avoid signal distortion.



$$\overline{i_{Tot}^2} \cong \overline{i_D^2} + \frac{\overline{i_S^2}}{G_I^2}$$

Current Gain

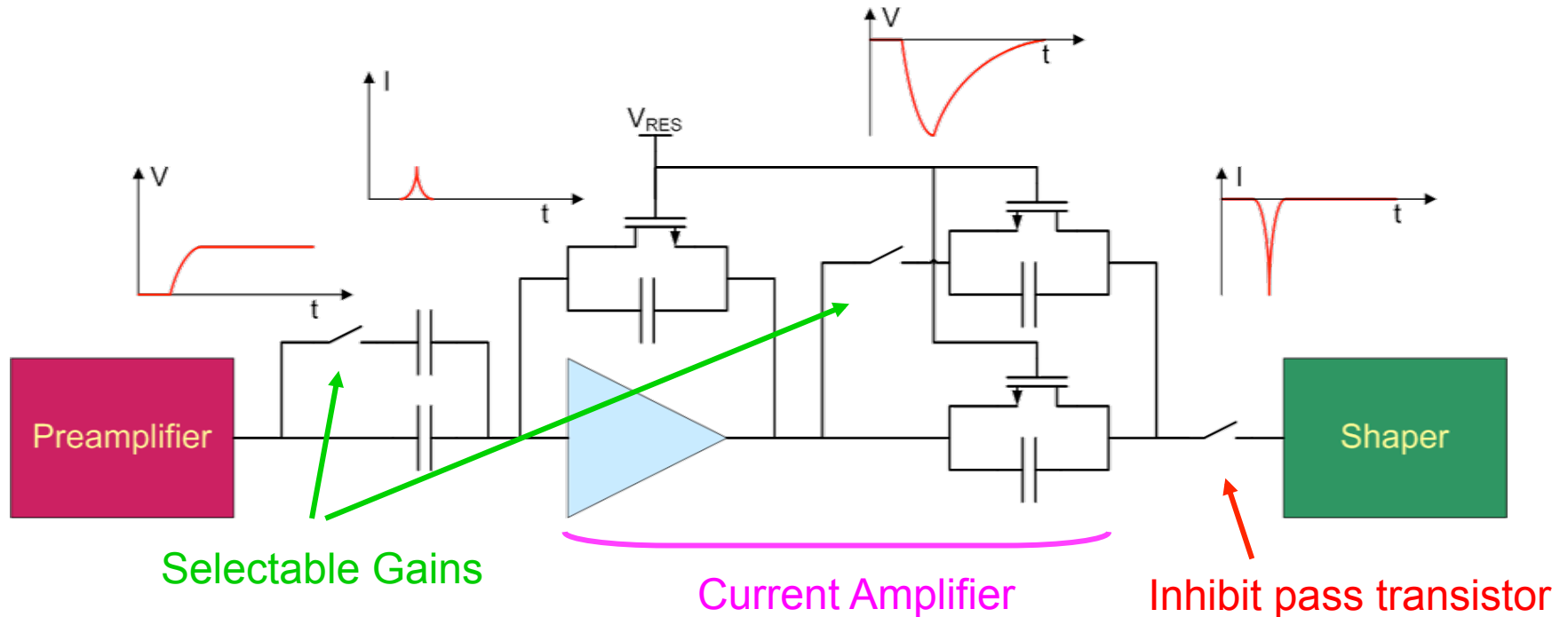
$$G_I = \frac{C_{IN}}{C_F}$$



Simulated output voltage noise of a readout channel composed of a voltage preamplifier and a 5<sup>th</sup> order, real-poles shaping amplifier, for different bias currents of the ICON cell

Measured output voltage noise of the same channel

## Gain Stage + Inhibit



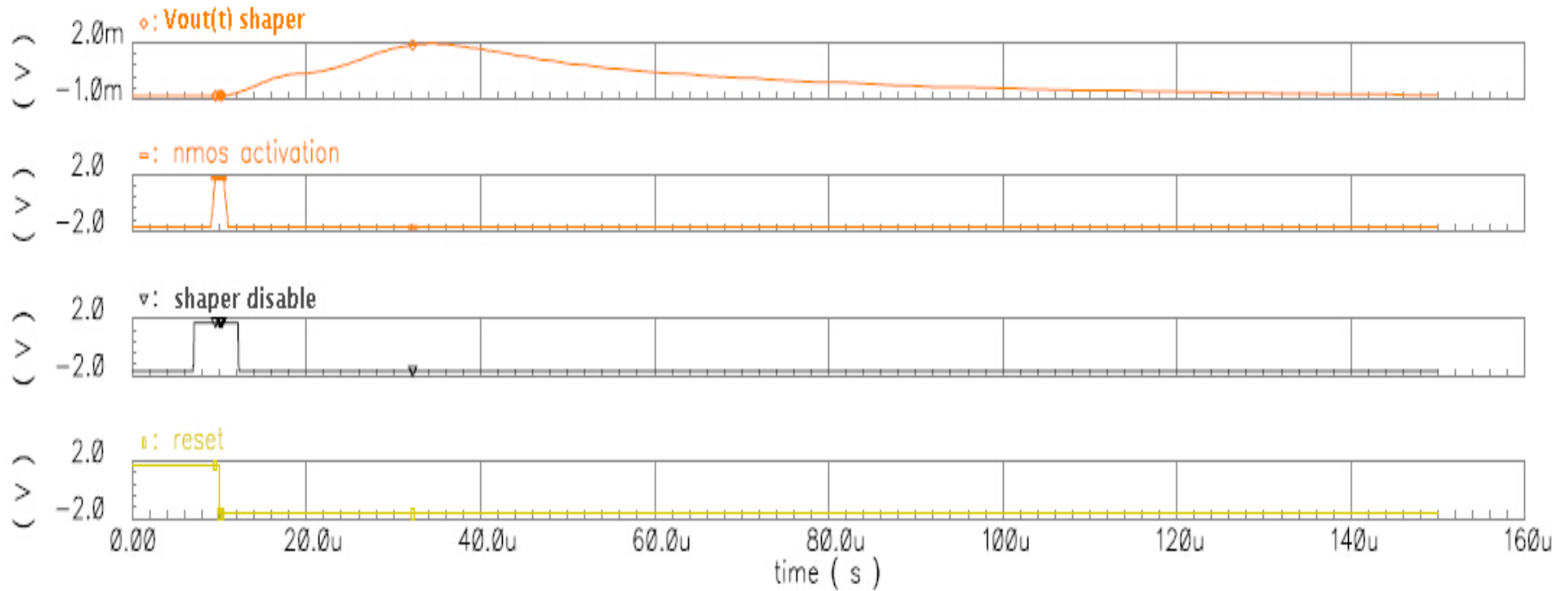
The current amplifier is based on a fully compensated continuous reset mechanism:

- Provides additional gain, necessary for reducing the input-referred current noise of the ICON cells.
- The shaper input is disconnected during the reset of the detector, when the output of the preamplifier saturates to the power supply  $\rightarrow$  reduce the shaper recovery time, potentially very slow  $> 3 * \tau_{shaping}$ .
- A set of pass transistors provide adjustable gain.
- The possible saturation of the amplifier dynamic is a critical issue in high rate applications.

G. De Geronimo and P. O'Connor: "A CMOS detector leakage current self-adaptable continuous reset system: Theoretical analysis"

# Gain Stage + Inhibit

Simulated waveform of the shaping amplifier during detector reset

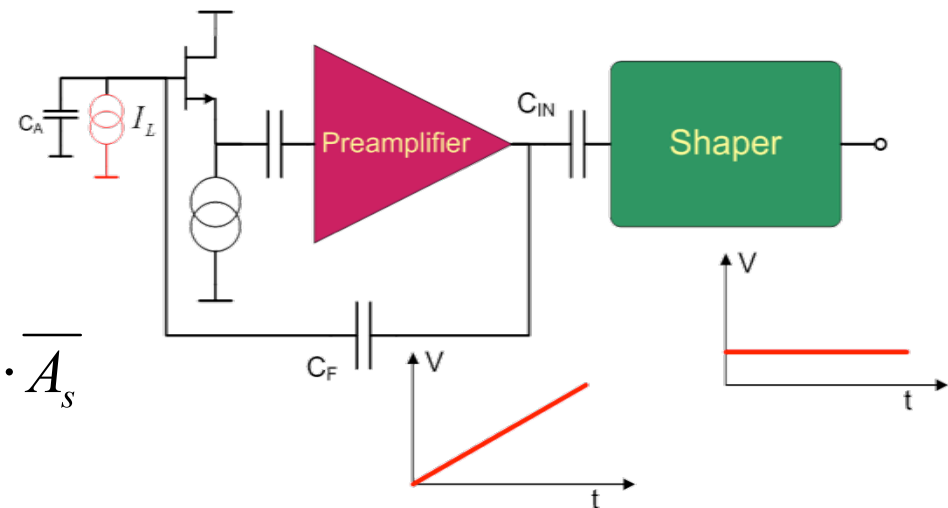
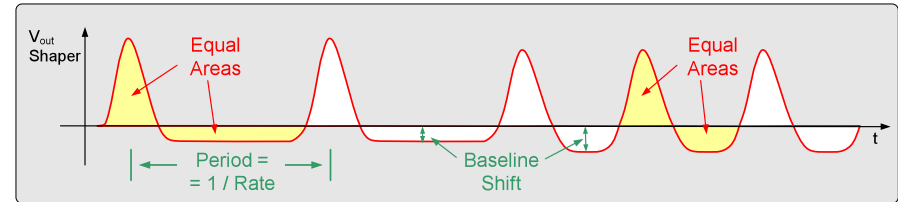


# Baseline Holder

The BLH block is used for the stabilization of the baseline of the shaping amplifier.

The baseline changes because of:

- Leakage current of the detector, which is integrated by the preamplifier, and derived before the shaper, generating a constant signal.
- In a multi-channel ASIC there are variations among the channels, due to mismatch of the integrated components.
- Variations in the rate of the incoming events due to the AC coupling of the circuit to the detector.



$$V_{DC}^{OS} = I_L \cdot \underbrace{G_I \cdot R_{DC}^{shaper}}_{> 2 \text{ G}\Omega, \text{ for } \tau_s = 12 \mu\text{s}} \pm \Delta V_{mismatch} - f_s \cdot A_s$$

Up to 1 nA  
@ room T

> 2 GΩ, for  
 $\tau_s = 12 \mu\text{s}$

Up to 500 mV

Under the hypothesis that:  $\tau_{AC} \gg \frac{1}{f_s}$

# Baseline Holder

The BLH introduces a low-frequency loop for cutting the DC transfer function of the shaping amplifier.

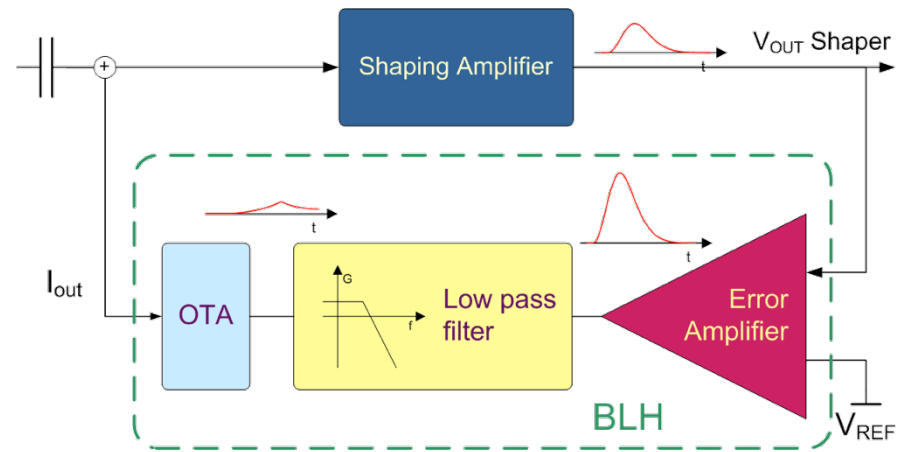
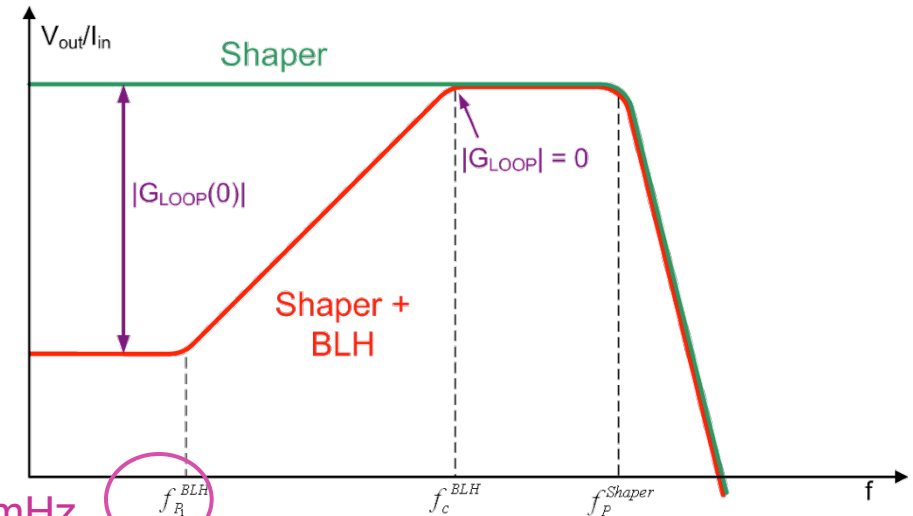
$$H(s) = \frac{S(s)}{1 - S(s) \cdot B(s)} \xrightarrow{s \rightarrow 0} -\frac{1}{B(0)} \approx 0$$

The position of first pole of the BLH is critical, because we need  $f_c^{BLH} \ll f_P^{Shaper}$

- Avoid distortion of the pulse response of the shaping amplifier
- Have a good phase margin  $\rightarrow$  stability of the BLH loop
- With the proposed ICON topology the DC gain of the shaping amplifier is proportional to the shaping time.
- For longer shaping times it becomes harder to implement, because of a quadratic relationship with the shaping time.

For a fixed DC response of the shaper:

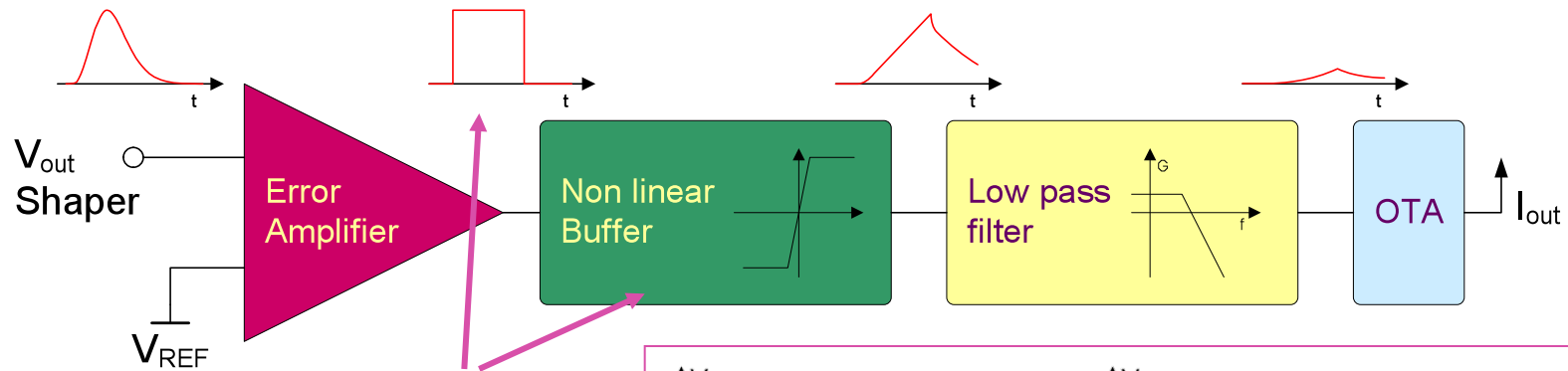
$$\tau_{P_1}^{BLH} = \frac{G_{DC}^{Shaper}}{G_{DC}^{opt}} \cdot K \cdot \tau_s = \frac{K}{G_{DC}^{opt}} \alpha \cdot \tau_s^2$$



G.De Geronimo et al.: "A CMOS baseline holder (BLH) for readout ASICs".

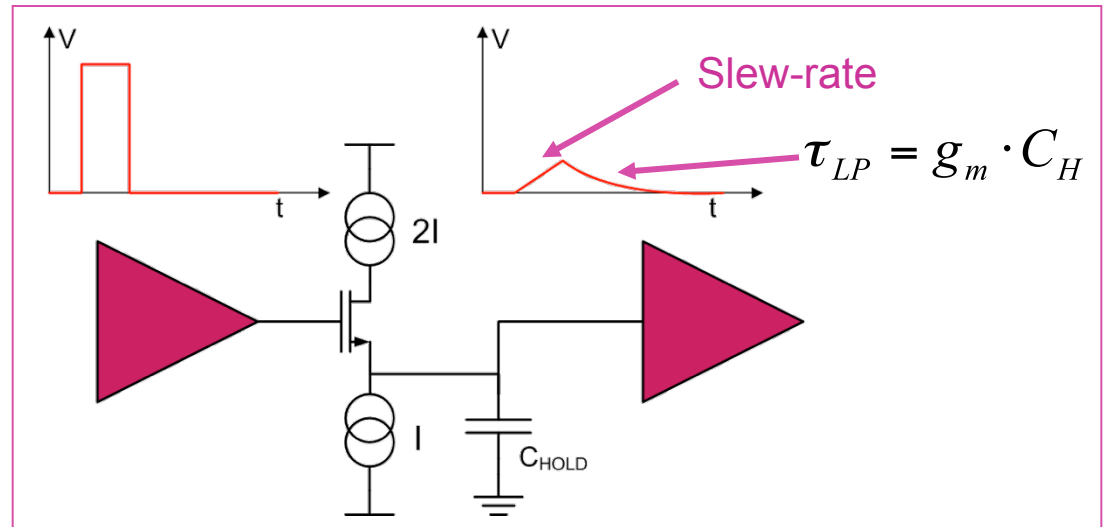
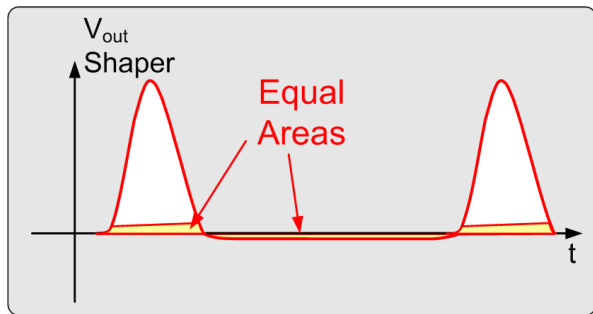
# Baseline Holder

Since the described topology is linear, it compensates for  $\Delta V_{\text{mismatch}}$  and  $I_L$ , but it acts like an AC copuling  $\rightarrow$  rate-dependent baseline shift.



Non-linearity

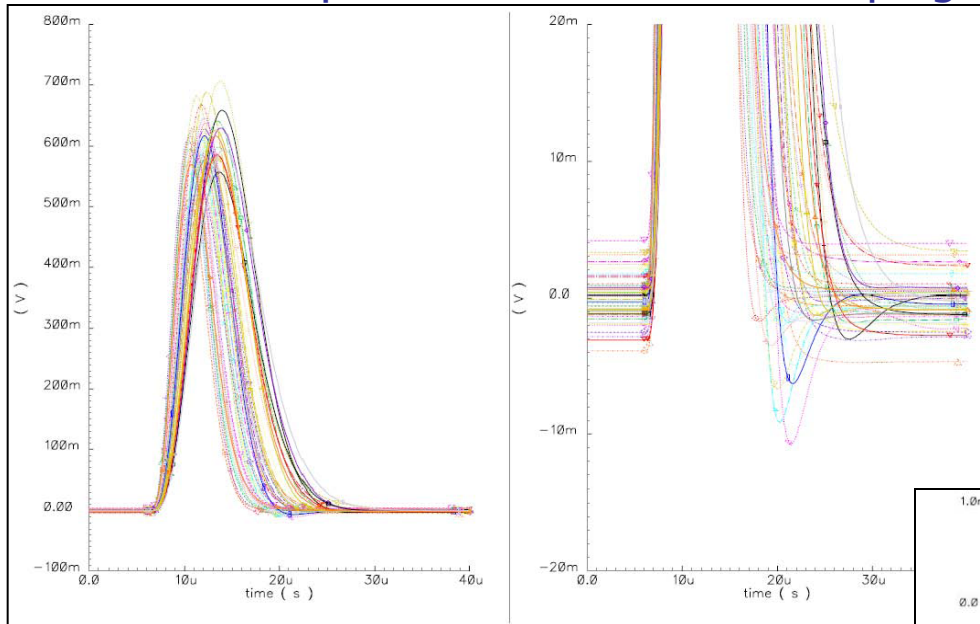
$$V_{DC}^{OS} = -f_s \cdot A_{eff}$$



Single stage implementing both the non linear buffer and the low-pass filter

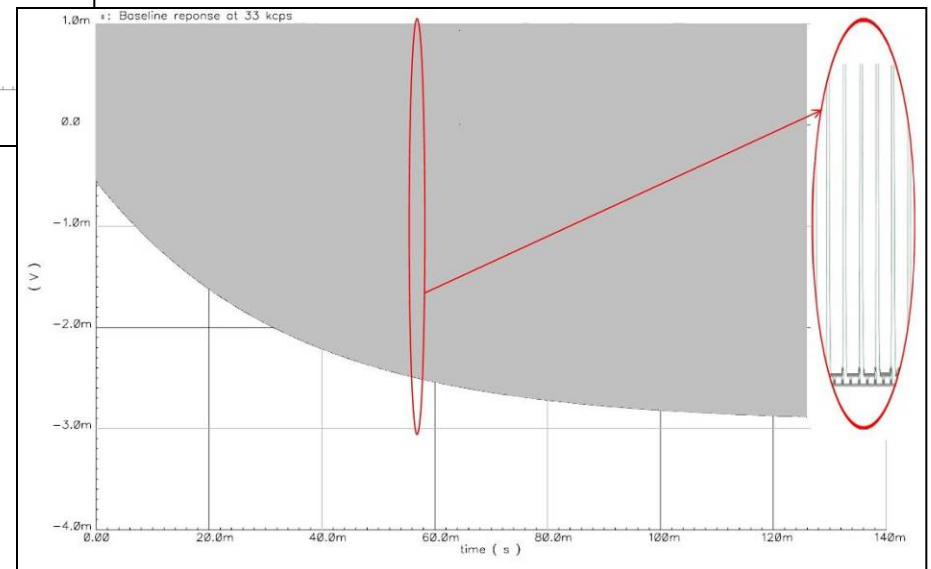
# Baseline Holder

Simulated output waveforms of the Shaping amplifier with the BLH.



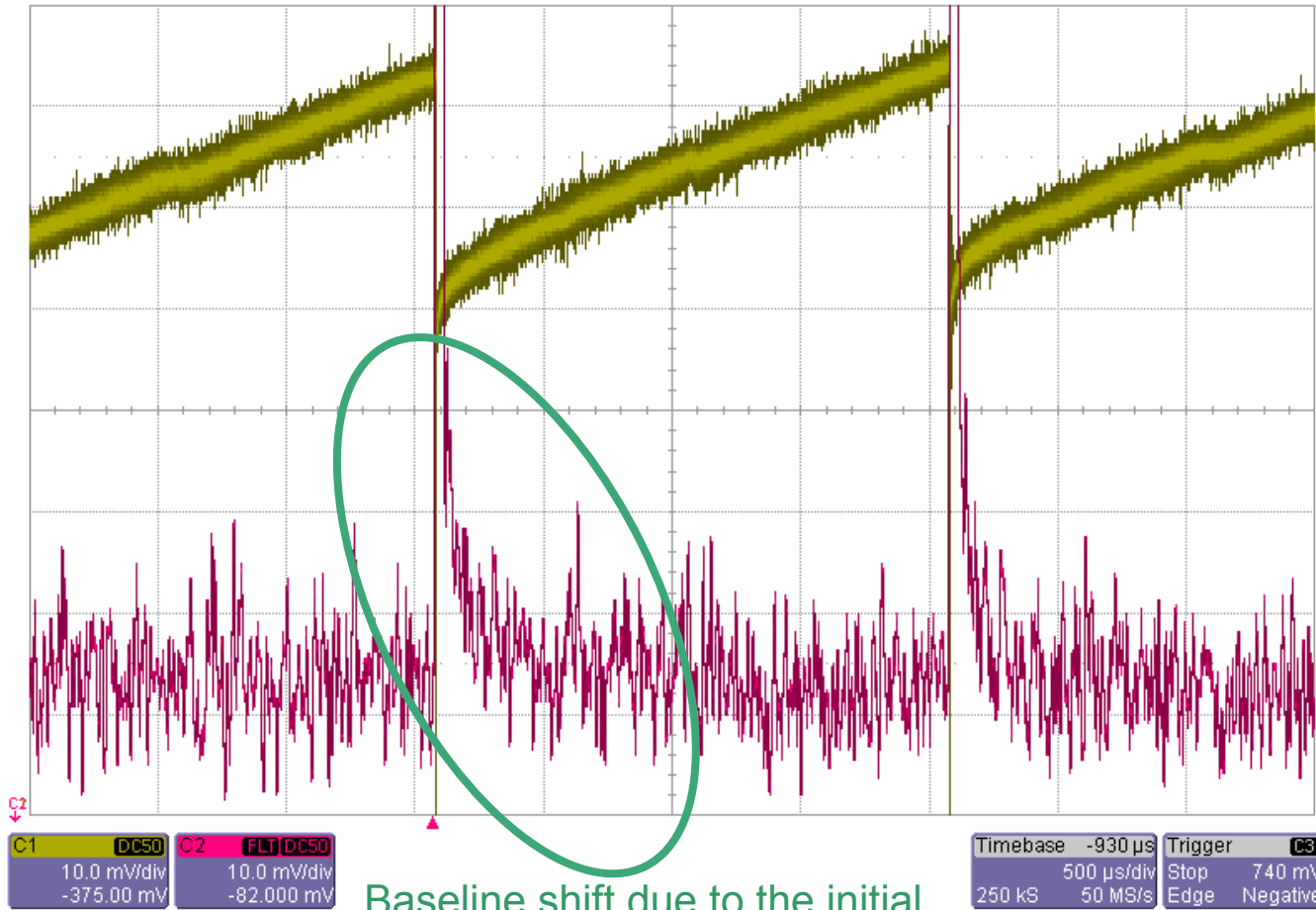
Even with the BLH, there is a residual rate-dependent baseline shift. However it is a design parameter, function of  $C_{\text{HOLD}}$ ,  $I$ ,...

Monte Carlo simulation of the residual offsets between different channels of a multi-channel ASIC due to mismatch of the components.



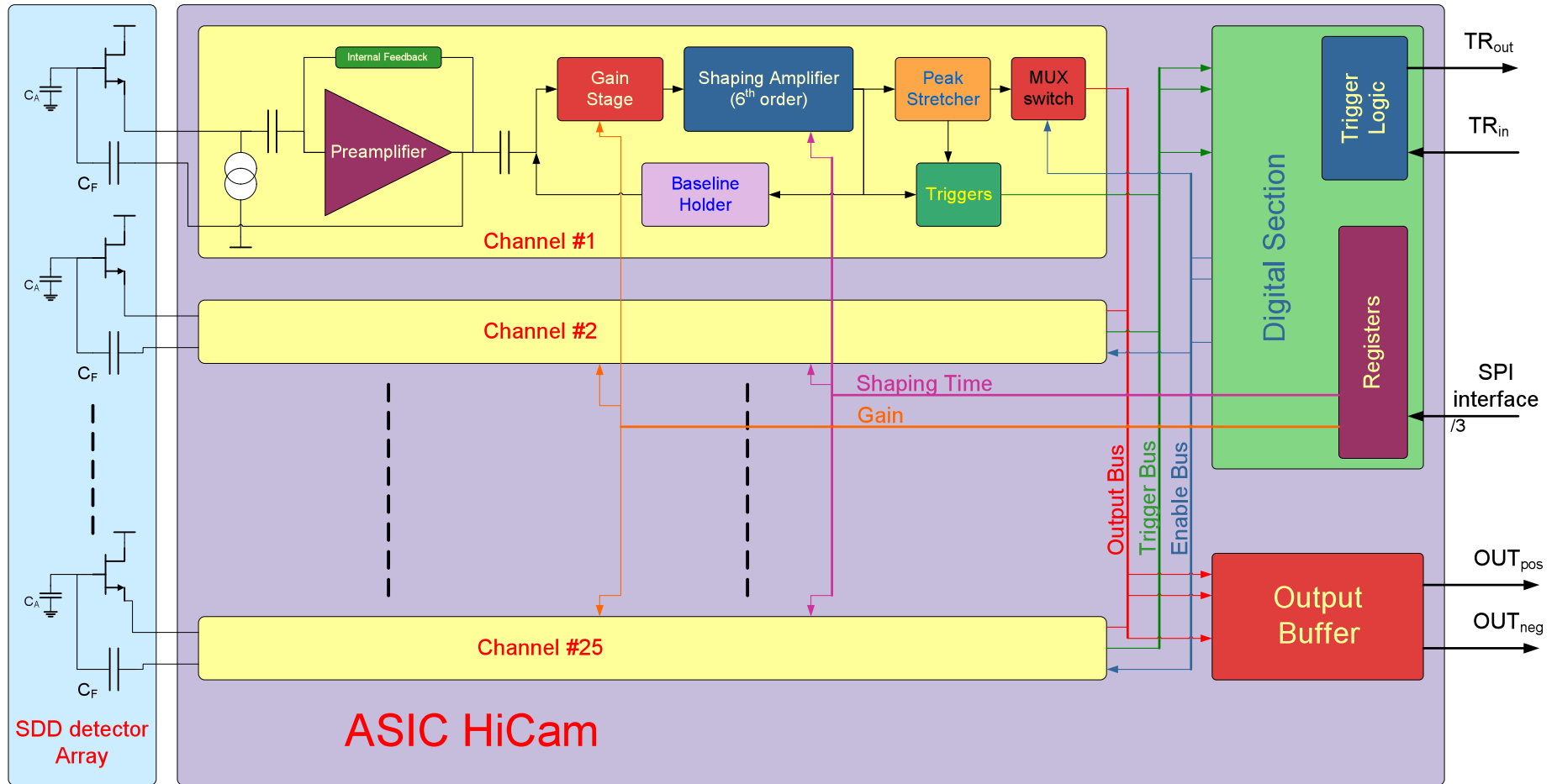
# Baseline Holder

Measured baseline shift on a prototype circuit



Baseline shift due to the initial non-linearity of the ramp (detector)

# Complete ASIC for Gamma Camera Readout



# ASIC layout

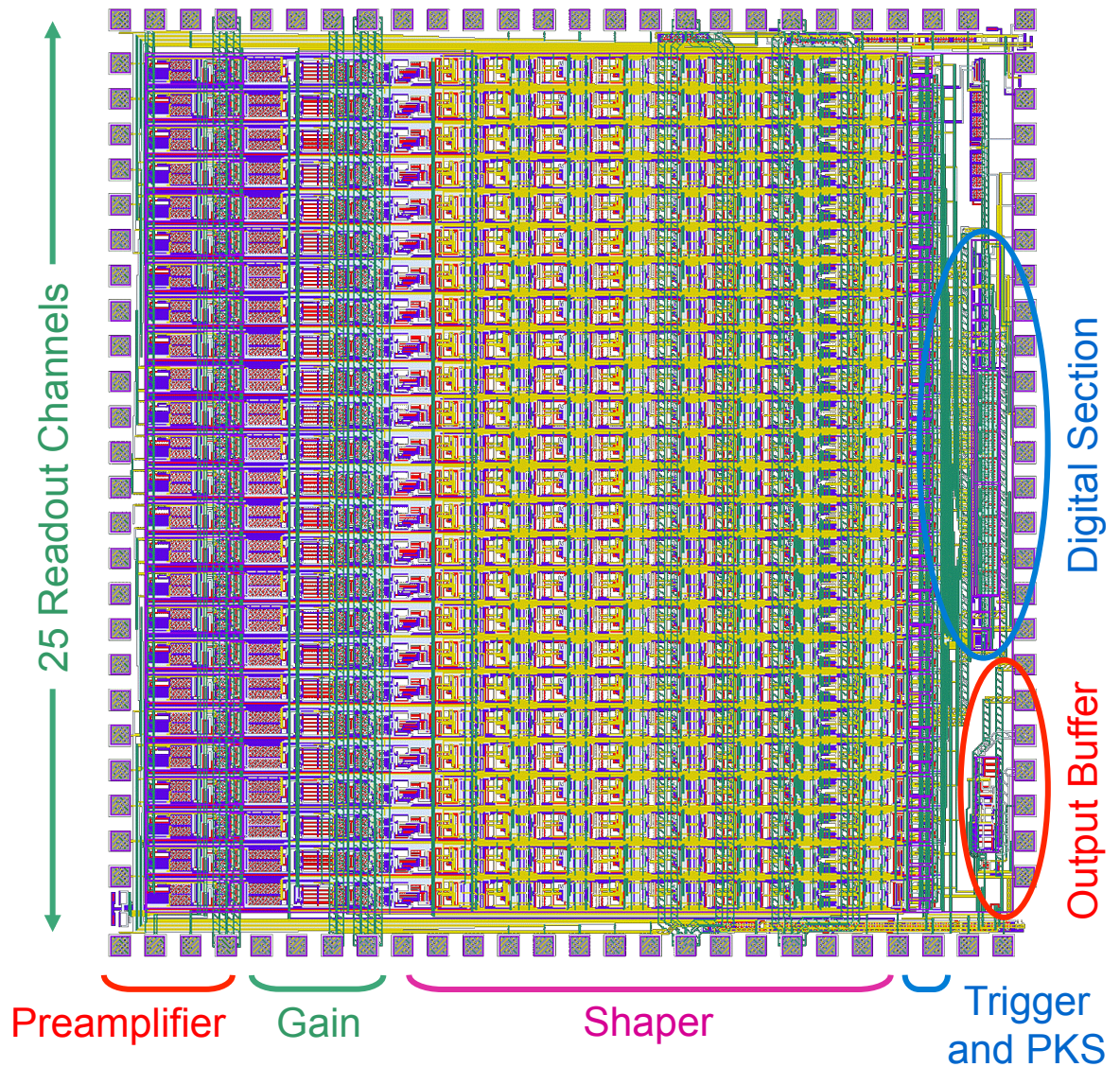
This ASIC has been produced in the **0.35  $\mu\text{m}$ , 3.3V CMOS, AMS** technology

100 pads

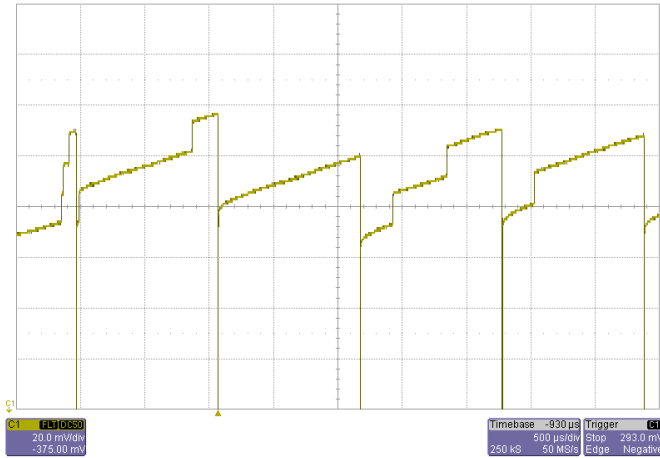
Die size: 4.8 x 4.6 mm<sup>2</sup>

Packaging options:

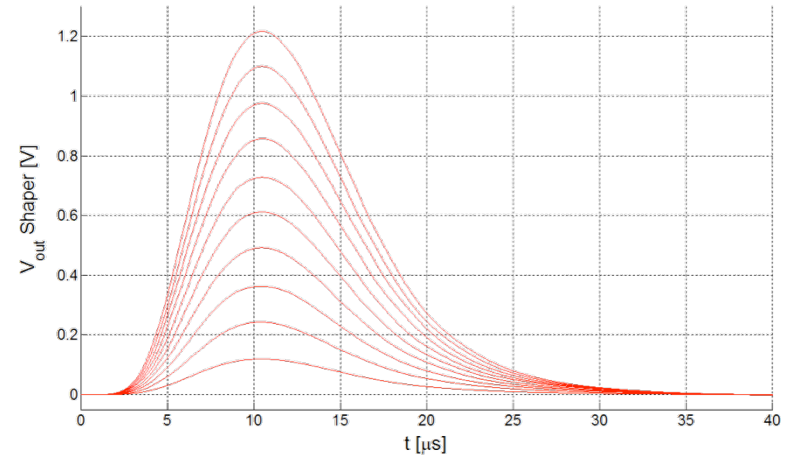
- 100-pin LQFP  $\rightarrow$  20 x 20 mm<sup>2</sup>
- Include the 100-pin MLF, SMD package
- 12 x 12 mm<sup>2</sup>



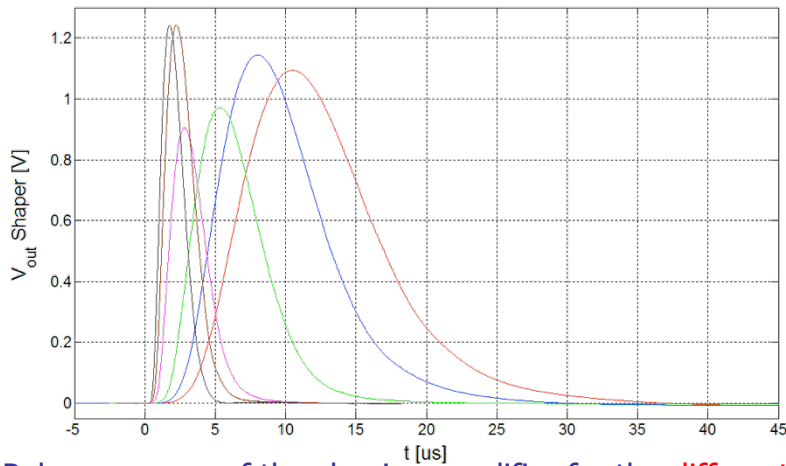
# Example waveforms



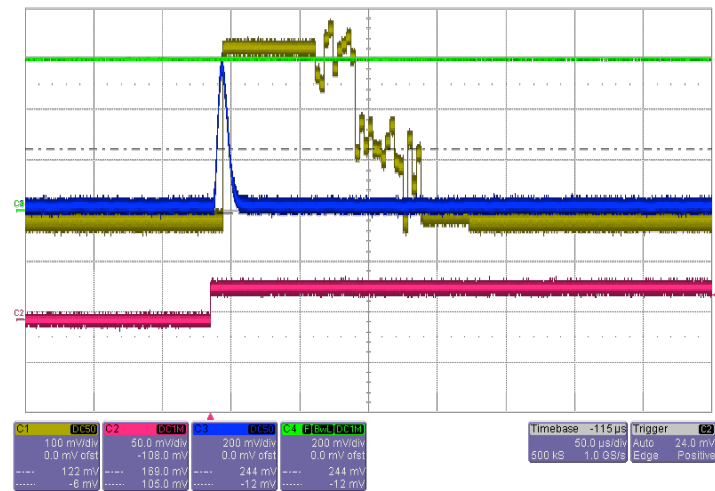
Ramp at the output of the preamplifier, integrating both the leakage and the signals of an X-ray  $^{55}\text{Fe}$  source.



Measured pulse response of the shaping amplifier, for the 11  $\mu\text{s}$  peaking time, for different signal amplitudes.



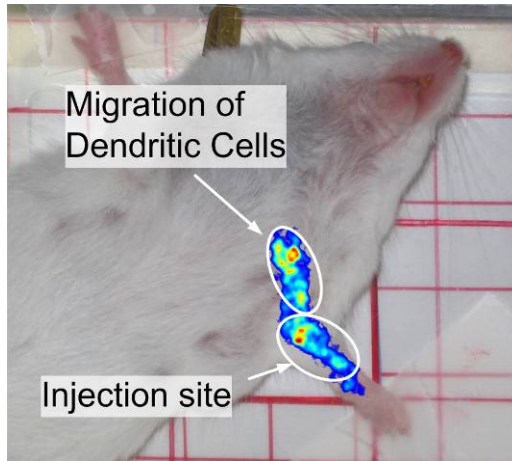
Pulse response of the shaping amplifier for the different shaping times implemented.



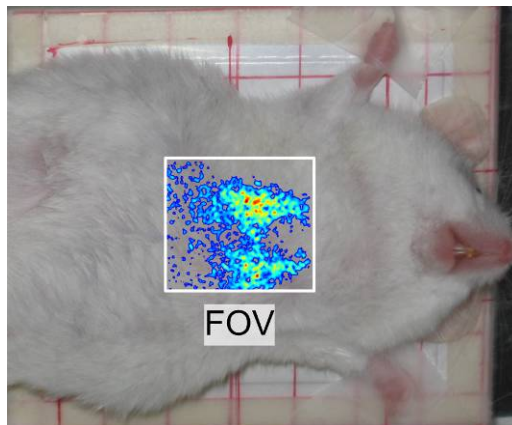
Signals generated by the analog multiplexer, which can work at 5 MHz.

# Gamma Camera - Measurements

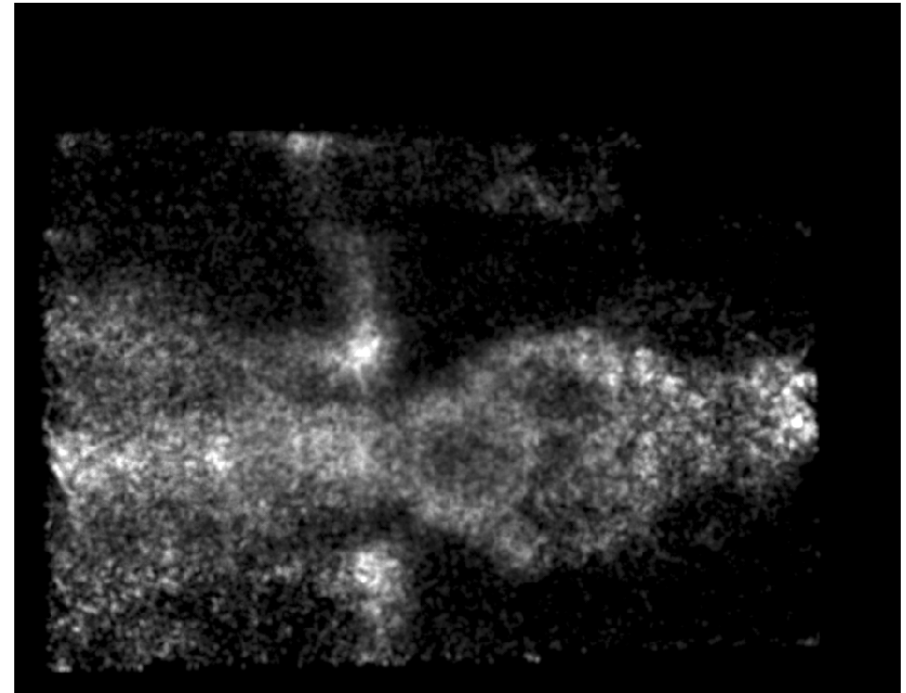
Example images, taken with an SDD-based Gamma Camera during a set of *in-vivo* measurements at the San Paolo hospital, in Milan.



Migration of Dendritic Cells, labeled with 60  $\mu\text{Ci}$  of  $^{111}\text{In}$ -Oxine.



Early lung biodistribution of Neural Stem cells, labeled with 60  $\mu\text{Ci}$  of  $^{111}\text{In}$ -Oxine.



*In-vivo* bones scintigraphy of a mouse, obtained using a parallel holes collimator and the DRAGO detector.  $^{99\text{m}}\text{Tc}$ -MDP was the radiotracer.